Jurassic paleogeography of the Tian Shan: An evolution driven by far-field tectonics and climate

Julien Morin, Marc Jolivet, Cécile Robin, Gloria Heilbronn, Laurie Barrier, Sylvie Bourquin, Yingying Jia

Jurassic paleogeography of the Tian Shan: An evolution driven by far-field tectonics and climate

Julien Morin, Marc Jolivet, Cécile Robin, Gloria Heilbronn, Laurie Barrier, Sylvie Bourquin, Yingying Jia

PII: S0012-8252(18)30327-1
DOI: doi:10.1016/j.earscirev.2018.10.007
Reference: EARTH 2712

To appear in: *Earth-Science Reviews*

Received date: 25 May 2018
Revised date: 4 September 2018
Accepted date: 9 October 2018

Please cite this article as: Julien Morin, Marc Jolivet, Cécile Robin, Gloria Heilbronn, Laurie Barrier, Sylvie Bourquin, Yingying Jia , Jurassic paleogeography of the Tian Shan: An evolution driven by far-field tectonics and climate. Earth (2018), doi:10.1016/j.earscirev.2018.10.007

JURASSIC PALEOGEOGRAPHY OF THE TIAN SHAN: AN EVOLUTION DRIVEN BY FAR-FIELD TECTONICS AND CLIMATE

Julien Morin[1], Marc Jolivet[1], Cécile Robin[1], Gloria Heilbronn[2], Laurie Barrier[3], Sylvie Bourquin[1], Yingying Jia[4]

[1] Univ Rennes, CNRS, Géosciences Rennes, UMR 6118, CNRS – F-35000 Rennes, France.

[2] CASP, West Building, Madingley Rise, Madingley Road, Cambridge, CB3 0UD, United Kingdom.

[3] Institut de Physique du Globe de Paris, Sorbonne Paris Cité, Université Paris Diderot, UMR 7154 CNRS, Paris, France.

[4] University of Chinese Academy of Sciences, No. 19A Yuquan Road, Beijing 100049, China.

ABSTRACT

The strongly intracontinental Tian Shan region, in Central Asia represents a key area to understand the long term evolution of continents in general and Asia in particular. If its Paleozoic and Cenozoic geodynamics are well understood, its Mesozoic evolution remains poorly constrained. In order to decipher the paleogeographic and large-scale tectonic evolution of the Tian Shan area during the Jurassic, we compiled, detailed field analyses of sedimentary rocks acquired within and around the Chinese Tian Shan region together with previously published data. We present three paleogeographical maps corresponding to the late Early – early Middle Jurassic, late Middle – early Late Jurassic and Late Jurassic - Early Cretaceous transition periods. We provide a large - scale picture of the Jurassic paleogeographic and climatic evolution of the Tian Shan region and discuss the geological

evolution of the range together with the possible driving mechanisms. During the Early to early Middle Jurassic, the topographic evolution of the Tian Shan Range was dominated by progressive planation of late Paleozoic to early Mesozoic relief, locally interrupted by short-lived tectonic uplift. Throughout the region, contemporaneous sedimentation was characterized by alluvial to lacustrine strata deposited under humid conditions. During this period, recurrent limited deformation events associated with strike-slip and compressive tectonics occurred that cannot be explained by far field effect of the Qiangtang collision but could instead be associated to the coeval subduction-related extension affecting the Caspian - Turan domains. During the late Middle to early Late Jurassic, the planation of the Paleozoic – early Mesozoic Tian Shan Range then continued. A shift to more semi-arid conditions during the Late Jurassic is also recorded in the sedimentary series all over the region. At that time, few evidences of deformation exists in the Tian Shan or within the Caspian – Turan domains. We propose that the late Middle – early Late Jurassic corresponded to a period of relative tectonic quiescence in the area. Finally, the Late Jurassic – Early Cretaceous transition was marked by a tectonic reactivation leading to the inversion of the Yarkand – Fergana Basin and to localized relief building in the Tian Shan. This renewed transpressive deformation phase could be mainly related to the coeval accretion of the Helmand block to the south-west, and possibly to the onset of the accretion of the Lhasa Block along the southwestern margin of Eurasia. Finally, this period was also characterized by the climax of aridification which played a major role on the emplacement of extensive alluvial fan systems in the basins surrounding the range.

KEYWORDS: Jurassic, Tian Shan, Paleogeography, Climate, Tectonics

1. INTRODUCTION

The long-term geodynamic evolution of Asia is characterized by a succession of orogenesis driven by accretion of continental blocks along the southern margin of the continent (e.g., Jolivet, 2017). These collisional orogenic events succeeded one another from the Paleozoic, with the final accretion of the Central Asian Orogenic Belt during the Permian (e.g., Windley et al., 2007; Wilhem et al., 2012), the Permian-Triassic Indosinian orogeny and the closure of the paleo-Tethys ocean (e.g., Roger et al., 2010, 2011), the Mesozoic accretion of the various blocs that form the Tibetan and South Caspian domains (e.g., Zonenshain and Le Pichon 1986; Thomas et al., 1999; Brunet et al., 2003), the Cretaceous closure of the Mongol-Okhotsk ocean in Siberia (e.g., Enkin et al., 1992; Zorin, 1999; Cogné et al., 2005; Jolivet et al., 2017b), and finally the Cenozoic collision of India (e.g., Allègre et al., 1984; Tapponnier et al., 2001). These successive events bring the idea of a continent essentially affected by compressive deformation and largely characterized by the growth of large mountain ranges. Within this largely compressive geodynamic setting, the Jurassic period corresponds to a peculiar time span comprised between two major orogenic events: 1) the Cimmerian orogeny which began during the late Paleozoic and ended during the Triassic – Jurassic transition (e.g., Sengör, 1979; Watson et al., 1987; Mattauer et al.1992; Roger et al., 2010; Metcalfe, 2013) and 2) the Cenozoic Himalayan orogeny (e.g., Molnar and Taponnier, 1975; Yin, 2009). During the Jurassic, the Eurasian continent was mostly surrounded by subduction zones leading to late Early – Middle Jurassic extension within the Caspian – Turan domains (e.g., Zonenshain and Le Pichon 1986; Nikishin et al. 1998; Thomas et al., 1999; Brunet et al., 2003, 2017; Robert et al., 2014; Mordvintsev et al., 2017) and to Late Jurassic – Cretaceous extension within the Siberian - Mongolian domains (e.g., Zorin 1999; Graham et al., 2001; Johnson et al., 2004; Daoudene et al., 2009; Donskaya et al., 2008; Ritts et al. 2010). However, the Jurassic paleogeographic and kinematic evolution of the probable relay

zone corresponding to the Tian Shan region in Central Asia is yet to be fully understood. Some studies indicate that during its Jurassic evolution, this area was dominated by progressive planation of the Tian Shan relief (Dumitru et al., 2001; Jolivet et al., 2010) while others propose that the region underwent recurrent periods of relief building (e.g., Allen et al., 1991; Hendrix et al., 1992; Yang et al., 2015). Recurrent tectonic activity did occur during that period but the kinematics and driving mechanisms of these events are highly debated. Some consider that the Tian Shan region was dominated by strike-slip and transtensive tectonics in a rather quiescent geodynamic setting (Jolivet et al., 2013) whereas others propose that the Tian Shan was rather under a compressional setting related to far-field collisions (e.g., Hendrix et al., 1992; Eberth et al., 2001; Vincent et al., 2001; Greene et al., 2001; Yang et al., 2013; Liu et al., 2013; Yang et al., 2015).

Finally, a Late Jurassic – Early Cretaceous tectonic reactivation has been recorded by low-temperature thermochronology data within the Kyrgyz Tian Shan, although to the east, in the Chinese Tian Shan, the same type of data only suggest slow cooling (Dumitru et al., 2001; Jolivet et al., 2010; De Grave et al., 2007, 2012, 2013; Glorie and De Grave., 2016; Nachtergaele et al., 2018). At the same period, extensive alluvial fan systems have been deposited in several basins surrounding the Tian Shan Range. These alluvial fans were inferred to have been formed in response to renewed tectonic activity (Hendrix et al., 1992; Sobel et al., 1999; Vincent et al., 2001; Yang et al., 2015). Moreover, a rapid transition from humid conditions that prevailed during the Middle Triassic to Middle Jurassic to a semi-arid/arid climate that developed during the Late Jurassic – Early Cretaceous period also occurred in the Tian Shan area (Hendrix et al., 1992; Eberth et al., 2001; Shao et al., 2003; Jolivet et al., 2017a). This change in climatic conditions is thought to have had a major impact on the paleogeographical evolution of this region by controlling the emplacement of the extensive Late Jurassic – Early Cretaceous alluvial fan systems (Jolivet et al., 2017a). However, available descriptions of the Jurassic paleogeography or tectonic evolution of the

Tian Shan Range usually address too restricted areas and/or stratigraphic intervals to fully understand the impact of far-field deformation within this peculiar period in Central Asia history (e.g., Shao et al., 2003; Bian et al., 2010; Feng et al., 2015; Yang et al., 2015; Jolivet et al., 2017a; Gao et al., 2017).

Therefore, in order to better understand the paleogeographic and large-scale tectonic evolution of the Tian Shan area, we compiled, our own detailed field analyses of sedimentary rocks in various basins associated with the range and previously published data to construct three paleogeographic maps for the periods of to the late Early – early Middle Jurassic, late Middle- early Late Jurassic and Late Jurassic - Early Cretaceous transition. We provide a large - scale picture of the Jurassic paleogeographic and climatic evolution of the Tian Shan region and discuss the kinematic evolution of the range together with the possible driving mechanisms.

2. GEOLOGICAL SETTING

2. 1. LATE PALEOZOIC LITHOSPHERIC STRUCTURES AND MESO-CENOZOIC REACTIVATIONS:

The lithospheric structure of the Tian Shan results from the late Paleozoic amalgamation of continental blocks and magmatic arcs along the southern margin of the Central Asian Orogenic Belt (CAOB; Sengör et al., 1993; Windley et al., 2007; Charvet et al., 2011; Alexeiev et al., 2017b). Subsequently, the Tian Shan Range underwent transpressive deformation during the Permian – Early Triassic in response to the oblique convergence between Siberia and Baltica (Bazhenov et al., 1999; Van der Voo et al., 2006). This induced dispersed rotations and motion along numerous strike-slip faults such as the Talas – Fergana fault, the Nikolaev line or the North Tian Shan fault (Fig. 1) (e.g., Allen et al., 1991; Laurent-

Charvet et al., 2002; Buslov et al., 2004; Van der Voo et al., 2006 and references therein; Rolland et al., 2013). An alternative model proposed that counterclockwise rotation of the Yili – West Junggar blocks with respect to Tarim and Siberia induced large strike-strike slip motions along the previously mentioned lithospheric faults, resulting in about 1160 ± 380 km lateral displacement in the Tian Shan belt (Wang et al., 2007a). Independently to the tectonic model, thermochronology data recorded a strong Permian-Triassic cooling- exhumation phase within the Tian Shan Range implying the build-up of a major topography during that period (Dumitru et al., 2001; Jolivet et al., 2010).

During the Meso-Cenozoic, the Paleozoic faults played a major role in localizing the deformation during the successive tectonic episodes that affected the Tian Shan Range (Allen et al., 1991, 2001; Hendrix et al., 1992; Sobel et al., 1999; Dumitru et al., 2001; Jolivet et al., 2010; Rolland et al., 2013; Alexeiev et al., 2017). From the Triassic to the Cretaceous, several accretion-collision events (generally known as the Cimmerian Orogeny) took place along the southern Eurasian margin including the collision of the Qiangtang (Late Triassic-Early Jurassic), Lhasa (Late Jurassic-Early Cretaceous) and the Kohistan-Ladakh (Late Cretaceous) blocks (Matte et al., 1996; Kapp et al., 2007; Roger et al., 2010). These events induced the reactivation of the Palaeozoic structures, which led to crustal deformation in the Tian Shan area (Hendrix et al., 1992; Allen et al., 2001; Dumitru et al., 2001; De Grave et al., 2007; Jolivet et al., 2010; Glorie and De Grave., 2016). Finally, tectonic reactivation related to far-field effects of the India-Asia collision initiated during the late Oligocene – Miocene and led to the growth of the present-day Tian Shan Range (e.g., Molnar and Taponnier, 1975; Thomas et al., 1999; Sobel et al., 1999; Macaulay et al., 2014; Jia et al., 2015).

2. 2. LATE PALEOZOIC – EARLY CRETACEOUS EVOLUTION OF THE TIAN SHAN SEDIMENTARY BASINS

2. 2. 1. The Junggar Basin

The Junggar (Fig. 1) is an intracontinental basin bordered by the Tian Shan Range to the south, the Halaalate mountains to the west, and the Altai Range to the north-east. This basin preserves, in its thickest part, around 16 km of late Paleozoic to Quaternary sediments. The formation of the Junggar Basin followed the southward subduction of the North Tian Shan Ocean underneath the Yili block and its subsequent Late Carboniferous – Early Permian closure (e.g.,Gao et al., 1998; Wang et al., 2006; Charvet et al., 2011). Depending on the authors, the Junggar Basin initiated either during the Late Carboniferous in a post-collisional extensional setting (Qiu et al., 2005; Yang et al., 2013; Liu et al., 2015) or during the Permian as a response to a transtensional tectonics (Allen et al., 1991) associated with magmatism (Carrol et al., 1995; Wang et al., 2009).

In this basin, the Upper Carboniferous strata consist of interbedded marine mudstone, siltstone and rare clayey limestone units followed upward by thick units of sandstone (Novikov, 2013). The Lower Permian then marks the end of marine sedimentation with the deposition of a regressive sequence representing the final retreat of the sea from the South Junggar and the onset of continental sedimentation (Carroll et al., 1990, 1995). The top of the Permian sequence consists of conglomerates, sandstones, siltstones and mudstones interpreted as alluvial plain and lacustrine deposits (Carroll et al., 1995; Bian et al., 2010; Yang et al., 2013).

During the Triassic, the Junggar Basin evolved either as a foreland basin (Hendrix et al., 1992; Bian et al., 2010) or as a transtensional basin (Allen et al., 1995). Lower and Middle Triassic units consist of conglomerates, sandstones and red to brown siltstones typical of

continental sediments deposited in alluvial fan and alluvial plain environments. They are locally associated to caliche beds indicating deposition in seasonal semi-arid to arid conditions (Hendrix et al., 1992; Bian and al., 2010; Nivokov, 2013). Finally, the Upper Triassic sedimentary rocks consist of interbedded conglomerates, sandstones and grey siltstones interpreted as deposited in alluvial fan to alluvial plain environments under humid conditions (Hendrix et al., 1992; Ashraf et al., 2010; Bian et al., 2010; Nivokov, 2013). Subsequently, the Junggar Basin is thought to have evolved either as a flexural depression (Bian et al., 2010; Yang et al., 2012; Feng et al., 2015) or as a transpressional basin (Dengfa et al., 2008; Gao et al., 2017) during the Jurassic period. The contemporaneous conglomeratic to sandy and silty deposits are mainly related to alluvial to lacustrine environments (Hendrix et al., 1992; Eberth et al., 2001; Bian et al., 2010; Feng et al., 2015; Yang et al., 2015). The occurrence of widespread coal deposits in the Lower to Middle Jurassic series suggests humid conditions (e.g., Hendrix et al., 1992; Eberth et al., 2001; Vincent et al., 2001). Upper Jurassic series are then characterized by the disappearance of coal and by the formation of calcareous paleosols indicative of semi-arid conditions (Hendrix et al., 1992; Eberth et al., 2001; Vincent et al., 2001; Jolivet et al., 2017a). Finally, the Jurassic-Cretaceous transition is characterized by the emplacement of well-developed conglomerates thought either to mark a tectonic reactivation of the Tian Shan Range (Hendrix et al., 1992; Yang et al., 2015) or to be mostly driven by climate (Jolivet et al., 2017a).

2. 2. 2. The intra-mountain basins

Several intra-mountain basins such as the Yili, Bayanbulak, and Turfan basins are preserved within the interior of the Tian Shan Range (Fig. 1).They formed concurrently to the Junggar Basin and are associated to the same late Paleozoic post-orogenic phase of extensive

or transtensive deformation (Wang et al., 2006, 2009; Charvet et al., 2007; Jolivet et al., 2010; Xia et al., 2012).

The Yili Basin is bordered by the Borohoro Range (North Tian Shan) to the north and by the Narat Range (South Tian Shan) to the south. In its thickest part, this basin preserves around 5 km of Permian to Quaternary sediments. Its Permian series consist of marine sediments followed by the emplacement of volcanics and volcanoclastics deposits during the Upper Permian (Li et al., 2015). These series are uncomformably overlaid by the Triassic sediments, implying tectonic deformation at least up to the Lower Triassic (Li et al., 2015). Jurassic series consist of alluvial, lacustrine delta and lake deposits containing extensive coal beds that indicate humid conditions (Li et al., 2014). However this basin does not contain Upper Jurassic - Lower Cretaceous sediments (AGMCA, 2008).

The Bayanbulak Basin is located between the Narat Range to the north, the South Tian Shan Range to the south, and the Erbin Shan Range to the east. It preserves Mesozoic and Cenozoic sediments but its late Paleozoic to Mesozoic evolution is poorly known.

The Turfan Basin is a flexural basin containing in its deepest part around 7 km of Permian to Quaternary sediments (Shao et al., 1999). It is located between the Bogda Shan-Barkhol Tagh ranges to the north and the Chöl Tagh mountain range to the south. Its Lower Permian strata consist of continental and marine deposits interbedded with volcanic and volcanoclastic series (Shao et al., 1999; Wartes et al., 2002). During the Late Permian – Early Cretaceous, the Turfan Basin then evolved as a compressive basin (Hendrix et al., 1992; Allen et al., 1993; Shao et al., 1999; Wartes et al., 2002). Its Upper Permian to Early Cretaceous series are entirely continental and consist of alluvial to lacustrine deposits (Hendrix et al., 1992; Shao et al., 1999; Greene et al., 2001; Wartes et al., 2002).

In the Kyrgyz Tian Shan, the Issyk-Kul, Naryn, Aksai and Ming-Kush basins are intra-mountain depressions containing Jurassic to Quaternary sediments (Fig. 1) (Lasovskiy and Mozolev, 1961; VNIGNI and Beicip Franlab, 1992; Macaulay et al., 2014; De Pelsmaeker et

al., 2018). In the Issyk-Kul Basin, these sedimentary rocks consist mainly of alluvial to shallow lacustrine deposits containing numerous coal beds and plant fragments indicating humid conditions but they also contain caliche - type paleosols more typical of semi-arid conditions (De Pelsmaeker et al., 2018). The Ming-Kush Basin is a narrow transpressive depression containing 100-680m thick Jurassic deposits resting unconformably on Paleozoic basement rocks (Lasovskiy and Mozolev, 1961; De Pelsmaeker et al., 2018). They mainly consist of alluvial plain, fan delta and shallow lacustrine deposits associated with coal-rich layers and plant fragments indicating humid conditions (Lasovskiy and Mozolev, 1961; De Pelsmaeker et al., 2018). Finally, Jurassic sedimentary rocks consisting mainly of coal-bearing continental deposits resting unconformably on Paleozoic rocks occur in both the Naryn and Aksai basins (VNIGNI and Beicip Franlab, 1992; AGMCA, 2008).

2. 2. 3. The Tarim Basin

The Tarim Basin (Fig. 1) is a large intracontinental basin located between the Tian Shan to the north, and the Western Kunlun and Altyn Tagh ranges to the south. In its thickest part, it contains up to 16 km of Late Precambrian to Quaternary sediments. This basin underwent multiple phases of tectonic deformation since the Late Precambrian (Desheng et al., 1996). The Tarim craton accreted to the Kazakhstan-Yili terrane in the Late Carboniferous-Early Permian during the final amalgamation of the CAOB and the closure of the South Tian Shan Ocean (Carroll et al., 1995; Chen et al., 1999; Liu et al., 2014; Alexeiev et al., 2015). During that period, the Tarim Basin evolved as a compressive basin with Upper Carboniferous to Lower Permian series consisting of marine limestones, volcanoclastics and continental conglomerates, sandstones and siltstones (Caroll et al., 1995; Lin et al., 2012). Subsequent Early Permian extension then occurred and was associated to the emplacement of a LIP province within the basin (Carroll et al., 1995; Qin et al., 2011; Yu et al., 2011).

During the Mesozoic, the Tarim Basin finally seems to evolve again as a compressive basin in its northern and eastern parts (Desheng et al., 1996), with Triassic, Jurassic and Early Cretaceous depositional systems consisting of alluvial plain to lacustrine environments (Desheng et al., 1996; Hendrix et al., 1992). However, there are no Mesozoic deposits to the south-west of the basin, except along the Pamir-Western Kunlun Range, where Jurassic deposits are interpreted to have been deposited in pull-apart basins (Sobel et al., 1999).

2. 2. 4. The Fergana Basin

The Fergana Basin is an intracontinental basin situated to the west of the Kyrgyz Tian Shan. It is surrounded by the Chatkal and Kurama ranges to the north, the Fergana Range to the east and by the Alai Range to the south (Fig. 1). In its thickest part, it contains around 10 km of Permian to Quaternary sediments.

Following the late Paleozoic building of the ancestral Tian Shan, post-orogenic Upper Permian to Lower Triassic alluvial to lacustrine sediments were deposited (Clarke, 1984; Moisan et al., 2011). The basin was then subsequently inverted leading to a Middle – Late Triassic erosional event (Clarke, 1984; Bande et al., 2015). Renewed subsidence started from the Early Jurassic and led to the accumulation of alluvial to lacustrine deposits during the Jurassic and Early Cretaceous (Clarke, 1984; Jolivet et al., 2017a; De Pelsmaeker et al., 2018).

2. 2. 5. The Yarkand – Fergana Basin

The Yarkand – Fergana Basin is described as a transtensional pull-apart basin located along the south-western termination of the Talas Fergana/Karatau fault (Fig. 1) (Sobel et al., 1999; Allen et al., 2001; Alexeiev et al., 2017; De Pelsmaeker et al., 2018). The sedimentary

thickness progressively decreases away from the fault where up to 5 km of Jurassic sediments were deposited (Sobel et al., 1999; De Pelsmaeker et al., 2018). Lower to Middle Jurassic sediments consist mainly of alluvial, fan delta and deep lake deposits containing coal beds and plant fragments indicating humid conditions (Sobel et al., 1999; De Pelsmaeker et al., 2018). To the south of the basin, in the north-western Tarim region, the Upper Jurassic – Lower Cretaceous transition consists in up to 400 m-thick conglomeratic fluvial channel systems subsequently followed by Lower Cretaceous deposits characterized by fluvial red beds (Sobel et al., 1999).

3. SEDIMENTOLOGICAL ANALYSES

3. 1. METHODS AND AGE CONSTRAINTS

In this study we present new sedimentological data from Upper Triassic to Lower Cretaceous sedimentary units from the south Junggar, north Tarim, Yili and Bayanbulak basins (Fig. 1; see Appendix A for GPS coordinates of analyzed sections). Detailed analyses of field logs (1/1000 scale), sedimentary facies, trace fossils and paleosols were performed on each of the seven sections presented below with the objective of reconstructing the depositional environment evolution through time.

To establish the first order age intervals in the sediment sequences and assess the corresponding formation names (Fig. 2; lithostratigraphy from Hendrix et al., 1992),we relied on geological maps (XBGMR, 1969, 1970, 1973 a, b, 1978 a, b), published ages derived from biostratigraphical analyses and sporopollen assemblages (for more references see Hendrix et al., 1992; Deng et al., 2010) and published lithological descriptions (Hendrix et al., 1992; Eberth et al., 2001; Bian et al., 2010; Deng et al., 2010).

3. 2. FACIES MODEL AND DEPOSITIONAL ENVIRONMENTS

In the seven sections described below, twelve facies assemblages were defined based on lithology and sedimentary structures before being interpreted in terms of depositional processes (Table. 1). Together with those facies, five different pedogenic and alteration features were also identified (Table. 2). All these facies, pedogenic and alteration features were subsequently associated and interpreted in terms of depositional environments (Table. 3). Climatic conditions were inferred from these sedimentological analyses. In total, 10 environments ranging from alluvial fan to lake, evolving in both humid and semi-arid/arid conditions have been defined. 3D diagrams have been constructed to illustrate the general organization of each proposed depositional environment (Table. 3).

However, some morphological variability exists within those environments, especially for the lacustrine delta systems. Indeed, lithologies and sedimentary structures vary depending on the sections and are, for example, characteristic of different flow regimes. For the purpose of this paper we decided to group these more specific morphologies within one general environment associated with a global architecture (i. e. lacustrine delta (LD), Table. 3).

Table. 1: *Summary of the facies characteristics within the Chinese Jurassic Tian Shan and their interpretation in terms of depositional processes*

Facies code	*Lithology*	*Sedimentary structures*	*Inferred depositional processes*
Miscellaneous			
F1	a cm- to dm- thick coal beds	Tabular beds containing plant remains	Peat accumulation
F2	Several cm- to dm- thick white tuffaceous beds	Massive	Subaerial volcanic ash deposition
Calcareous facies			
F3	a cm- to dm- thick siltstones interbedded with a cm- to dm- thick calcareous beds	Massive to flat-laminated siltstone layers alternating with tabular calcareous beds with occasionally medium to strong bioturbation	Deposition from suspension fallout alternating with episodes of calcareous production
Heterolithic facies			
F4	a m- to m- thick siltstones containing cm- to dm- thick fine- to medium-grained sandstones	- Massive or flat laminated siltstones sometimes containing desiccation cracks or bioturbation - Tabular sandstone beds with sharp basal boundaries containing current ripples and sometimes bioturbation	- Deposition from suspension fallout with some emergent events - Tractional current deposition (low energy flows; Miall 1978) with occasional periods of subaqueous biological reworking
F5	heterolithic facies composed of cm- to dm-thick siltstones interbedded with cm- to dm-thick fine to medium (rarely coarse) grained sandstone	Flat laminated siltstone beds alternating with tabular sandstone beds containing current, climbing and/or oscillatory ripples; cm-scale soft sediment deformation structures, slightly to moderately bioturbated	Deposition from suspension fallout alternating with overbanks and waning floods, turbidity currents within a permanent water body (Mulder and Alexander, 2001). Deposition or reworking by waves and biological activity
F6	cm- to dm- thick siltstones alternating with cm- to dm-thick beds of fine- to coarse-grained sandstones	Massive to flat-laminated siltstone beds alternating with sandstone beds either - Tabular containing flat laminations, occasional current and climbing ripples. Occasional plant fragments or - Lenticular and massive with erosional basal boundaries with occasional rip-up mud clasts and plant fragments	Deposition from suspension fallout alternating with overbanks, waning flood currents or from tractional currents under stream flows (Miall, 1978)

Sandstone facies			
F7	Stacked to isolated dm- to m- thick medium to coarse grained sandstones	Tabular to slightly lenticular beds with sharp or low erosional basal boundaries. Trough cross-beddings, flat beddings underlined by rip-up clasts and sometimes with current ripples at the top of the beds. Occasional burrows	3D megaripples or planar beds of tractional currents deposits under subaerial or subaqueous sheet flows and stream flows (Miall, 1978)
F8	a m- to m-thick fine-grained to gravelly sandstones	Slightly to strongly lenticular beds with erosional basal boundaries. Trough cross-stratifications or flat beddings (highlighted by gravels, coal and mud clasts) and current ripples; a dm- to a m- scale fining-up trends	3D megaripples, planar beds of tractional currents deposits under subaerial stream flows (Miall, 1978)
F9	dm- to m- thick, stacked medium-grained to gravelly well-sorted, sandstones	Tabular beds with sharp basal boundaries. Flat-beddings, trough and planar cross stratification, sigmoidal beddings highlighted by gravels, coal and mud clasts and occasional current ripples; a dm- to dm scale dewatering structures and soft sediment deformation	Tractional currents with planar beds, 2D and 3D megaripples under subaqueous sheet flows (Miall, 1978) and with some gravitational events
F10	a m- to m- thick fine- to coarse- grained sandstones, well- to moderately well-sorted	m- to a dcm- high foreset composed of grainfalls and inverse climbing ripple. Horizontal laminations or very low angle mm- scale cross-laminations with inverse climbing ripples. Irregular mm horizontal lamination with adhesion warts and ripples	Aeolian dune and traction deposition by high wind velocity or migration of wind ripples (Hunter 1977). Wind-blown sand to a wet surface (Kocurek and Nielsen, 1986)
Conglomerate facies			

F11	dm- to m- thick clast-supported conglomerates with poorly- to moderately-sorted subangular to subrounded pebbles to boulders alternating with cm to m-thick medium to coarse grained sandstones containing floating gravels	Massive conglomerates with erosive or sharp basal boundaries and occasional pebble imbrications alternating with tabular or lenticular sandstones, structurless or with planar laminations and trough cross-bedding	Hyperconcentrated flows (Svendsen et al., 2003) alternating with 3D megaripple deposits under sheet flows or stream flows (Miall, 1978)
F12	a dm- to m- thick planar couplets of mostly poorly-sorted conglomerates, angular to sub-angular gravels to boulder, and of poorly- to well-sorted sand	Horizontal to sub-horizontal bedded conglomerates and sandstones with erosive or sharp basal boundaries. Sometimes dm to m-thick channelled bed	Sediment-charged flash floods due to either seasonal or irregular rainfalls (e.g., Blair and McPherson, 1994). Occasional sheet flow and stream flow deposits (Miall, 1978)
F13	a m- to pluri m-thick conglomerates with subangular to subrounded pebbles to boulders, poorly-sorted, matrix-supported (sand-rich)	Massive, sometimes with faint horizontal laminations. Erosive or sharp basal boundaries	Gravity flow processes, Debris flows (Postma, 1990; Miall 1996)

335

336 **Table. 2**: *Description and interpretation of pedogenic and alteration features*

Facies code	***Lithology***	***Interpretations***
P1	Closely spaced, disconnected thin vertical root traces, mm in thickness and a few cm-long within siltstones to fine grained sandstones	Paleosols (Retallack, 1988)
P2	Sparse vertical roots, mm wide, a few cm to dm-long within sandstones	Patchy and discontinuous vegetation typical of dry climate conditions (e.g., Hasiotis et al., 2007)
P3	Siltstone and sandstone facies modified by marmorisation processes	Pseudo-hydromorphic palaeovertisoils, wet-dry climate (Kraus, 1999; Klappa, 1980; Hasiotis et al., 2007)
P4	Dispersed to coalescent calcareous nodules, a cm- to several cm in diameter within siltstones to fine grained sandstones	Semi-arid pedogenic processes indicative of seasonality (wet-dry conditions; e.g., Retallack, 1988; Hasiotis et al., 2007)
P5	m- to several m- thick calcareous impregnation/cementation within conglomerates	Long-lasting wet/dry pedogenic processes within semi-arid environment (e.g., Retallack, 1988; 2008)

337 **Table. 3**: *Summary of the characteristics of the associated facies and their interpretations in*

338 *terms of depositional environments.*

Associated facies	***Inferred depositional processes***	***Inferred depositional environment***
AF - F11, F13	Debris flow + hyperconcentrated flows + sheet flows and stream flows	**Alluvial fan environment** (e.g., Blair and McPherson, 1994) 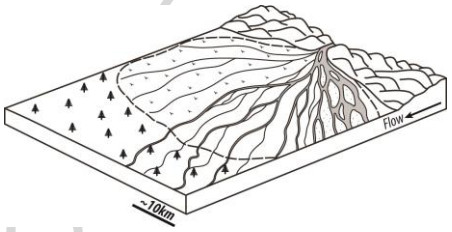
AFa – P2, F11, F12, F13	Flash floods +debris flows + hyperconcentrated flows + occasional sheet flows and stream flows + desiccation cracks and root traces typical of dry climates	**Alluvial fan environment in semi-arid to arid conditions** dominated by ephemeral flows (e.g., Blair and McPherson, 1994; Mather & Hartley 2005) 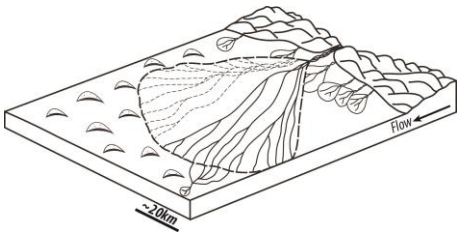
AP1 – F8, F11, (F7), sometimes with coal clasts and plant fragments within F8	Subaerial sheet and stream flows + hyperconcentrated flows	**Proximal alluvial plain environment** with gravelly alluvial deposits, probably characteristic of a low sinuosity bedload-dominated river system (e.g., Miall 1996) 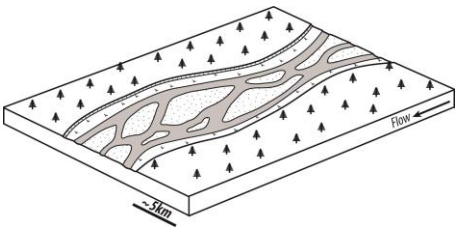

AP1a – P4, F8, F11, (F7)	Same as AP1 but with pedogenic calcareous nodules	**Proximal alluvial plain environment** with gravelly alluvial deposits, probably characteristic of a low sinuosity bedload-dominated river system (e.g., Miall 1996) in **semi-arid conditions** (carbonate nodules: Hasiotis 2006; Hasiotis et al., 2007) 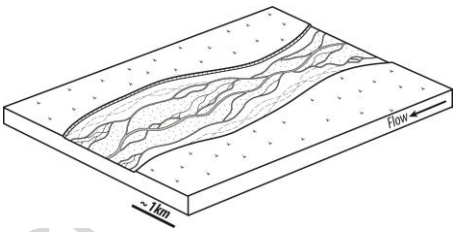
AP2 – P1, P3, F1, F6, F7, F8	Peat accumulation + root traces + suspension fallout + overbank and waning flood currents + subaerial and subaqueous sheet and stream flows	**Distal alluvial plain environment** with sandy alluvial deposits within floodplains and/or swamps 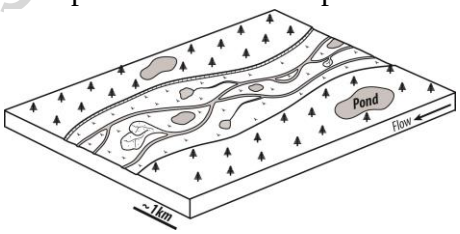
AP2a – P4, F6, F7, F8	Same as AP2 but without peat accumulation and with pedogenic calcareous nodules	**Distal alluvial plain environment** with sandy alluvial deposits within floodplains and/or swamps in **semi-arid conditions** (carbonate nodules: Hasiotis 2006; Hasiotis et al., 2007) 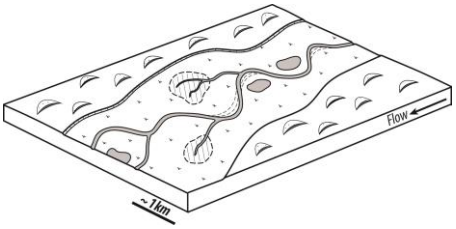
EG – F10	Traction deposition by high velocity wind velocity or migration of wind ripples + wind-blown sand to a wet surface	**Erg deposits** with preservation of large and thick aeolian dunes (up to 50m in thickness) and interdunes deposits

LD – P1, F1, F4, F5, F7, F9	Possible peat accumulation + root traces + overbank or waning floods + subaqueous sheet flows + turbidity currents and suspension fallout within a permanent water body + deposition or reworking by waves + biological reworking	**Lacustrine delta environment** with mouth bars and distal alluvial deposits (ie unconfined flows) within lakes 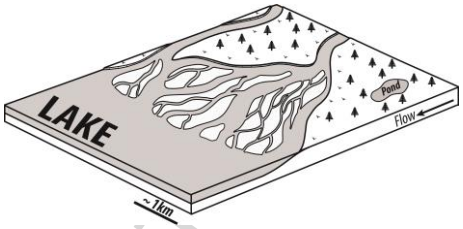
LE1 – F3, F4, F5	Subaqueous suspension fallout + occasional calcareous production + waning floods and turbidity currents within a permanent water body + deposition or reworking by waves + biological reworking	**Lacustrine environment** with some episodes of fluvial input
LE1a – P4, F3, F4, F5, F7	Same as LE1 but with desiccation cracks and pedogenic calcareous nodules	**Shallow or playa lake environment** with frequent emergence (desiccation cracks) and episodes of fluvial input in **semi-arid conditions** (carbonate nodules: Hasiotis 2006; Hasiotis et al., 2007)

3. 3. THE JURASSIC DEPOSITIONAL ENVIRONMENT EVOLUTION OF THE CHINESE TIAN SHAN

3. 3. 1. The south Junggar Basin

3. 3. 1. 1. South Toutunhe section

The South Toutunhe section (Fig. 6) is located in the south Junggar Basin, along the Toutun River on the northern flank of the Tian Shan Range and more precisely to the south of the Toutun dam (Fig. 1; Appendix B for a general overview of the section). The studied ~2000 m-thick section covers Middle Jurassic (Toutunhe Fm), Upper Jurassic (Qigu and Kalaza fms), and Lower Cretaceous (Qingshuihe Fm) deposits (XBGMR, 1978b).

352 The basal part of the logged Toutunhe Fm consists of distal alluvial plain deposits
353 associated to coal beds indicative of rather humid conditions (AP2) (Table. 3), which pass
354 upward, in the last 230 m of the formation to lacustrine delta deposits (LD) (Fig. 6; Appendix
355 B. 1). The transition with the Qigu Fm is progressive with deposits still characteristic of a
356 lacustrine delta environment (LD) in the first 310 m of this formation. The next 90 m consist
357 of distal alluvial plain deposits containing carbonate nodules indicative of semi-arid climate
358 conditions (AP2a; Fig. 6). The Qigu Fm then evolves up section towards lacustrine delta
359 sediments (LD) to finally ends with proximal alluvial plain deposits (AP1). The boundary
360 with the ~190 m-thick Kalaza Fm is sharp and marks a sharp change in depositional
361 environments (Fig. 6; Appendix B. 3). Indeed, the lower part of the Kalaza Fm is composed
362 of a 50 – 70 m-thick unit interpreted as erg deposits (EG) alternating with ~40 m thick units
363 of alluvial fan sediments (AFa) (Appendix B. 4) (for more details see Jolivet et al., 2017a).
364 This erg confirms the aridification trend already observed between the Toutunhe and Qigu
365 formations. The basal part of the Lower Cretaceous Qingshuihe Fm shows a retrogradation
366 towards a lake environment (LE1) (Fig. 6; Appendix B. 5).
367
368 *3. 3. 1. 2. North Toutunhe section*
369
370 The North Toutunhe section (Fig. 7) is also located along the Toutun River, to the
371 north of the Toutun dam (Fig. 1; Appendix C for a general overview of the section) and
372 presents ~1650 m of deposits ranging from Late Jurassic (Qigu and Kalaza fms) to Early
373 Cretaceous (Qingshuihe Fm) in age (XBGMR, 1978b).
374 The first 655 m of the logged Qigu Fm consists of interbedded red siltstones and
375 sandstones interpreted as lacustrine delta deposits (LD) evolving in the last 145 m of the
376 formation towards distal alluvial plain sediments containing carbonate nodules and
377 desiccation cracks indicative of semi-arid conditions (AP2a) (Fig. 7; Appendix C. 1, 2) . As in

the South Toutunhe section, the boundary between the upper Qigu Fm and the Kalaza Fm is sharp and corresponds to an abrupt change in depositional environments (Appendix C. 3). Indeed the Kalaza Fm (~740 m thick) consists of large aeolian dunes (preserved dune sets are up to 50 m in thickness) and interdune deposits characteristic of erg systems (EG) (Fig. 7). The basal part of the Lower Cretaceous Qingshuihe Fm shows a drastic change in environments with the emplacement of sediments indicative of lacustrine delta (LD) followed by lacustrine deposits (LE1) dominated by fine - grained facies.

3. 3. 1. 3. The Manas section

The ~5510 m-thick Manas section (Fig. 8), located in the south Junggar Basin, along the Manas River on the northern flank of the Tian Shan Range (Fig. 1; Appendix D for general pictures of the section) encompasses Upper Triassic, Lower Jurassic (Badaowan and Sangonghe fms), Middle Jurassic (Xishanyao and Toutunhe fms), Upper Jurassic (Qigu and Kalaza fms) and Lower Cretaceous (Qingshuihe Fm) deposits (XBGMR, 1978a; Hendrix et al., 1992; Eberth et al., 2001; Deng et al., 2010).

The upper part of the Triassic succession (only the topmost ~200 m were logged in this work) displays distal alluvial plain (AP2) and lacustrine delta environments (LD) evolving towards alluvial fan systems (AF) (Fig. 8). The first 780 m of the Lower Jurassic series (Badaowan Fm) consists of an alternation of distal alluvial plain (AP2) and alluvial fan (AF) deposits. The latter are dominated by clast-supported conglomerates with sub-rounded pebbles, occasionally associated with coal beds, which suggest rather humid conditions (AF) (Fig. 8; Appendix D. 1). These deposits pass upwards in a retrogradational trend into sediments indicative of a lacustrine delta environment (LD). Above, the top 400 m of the Lower Jurassic series correspond to the Sangonghe Fm, which is characterized by a progradational trend towards a proximal alluvial plain system (AP1) followed by a

retrogradational trend with depositional environments evolving from a proximal to a more distal alluvial plain (AP1, AP2) and finally to a lacustrine delta (LD).

The Middle Jurassic Xishanyao Fm (~1705 m thick; Appendix D. 2) then comprises a poorly exposed basal series (570 m thick) showing a progradational trend from lacustrine delta (LD) to proximal alluvial plain (AP1) deposits. The topmost 1135 m of this formation show a retrogradational trend with environments evolving towards a distal alluvial plain (AP2) and a lacustrine delta (LD) associated with the presence of numerous coal beds indicative of rather humid climate conditions (Fig. 8; Appendix D. 3). At the top of the Middle Jurassic series, the sediments of the Toutunhe Fm are interpreted to represent a distal alluvial plain environment (AP2; Appendix D. 4). Following the Toutunhe Fm, a thick red beds series corresponds to the Upper Jurassic Qigu Fm (Appendix D. 5). The basal 315 m of this formation were interpreted as lacustrine delta deposits (LD) directly followed by ~65 m of distal alluvial plain sediments (AP2) (Fig. 8). The rest of the Qigu Fm is characterized by a retrogradational trend with environments evolving from distal alluvial plain (AP2), to lacustrine delta (LD) and finally to a playa lake (LE1a). In the latter, desiccation cracks and carbonate nodules are indicative of semi-arid conditions. The transition with the Kalaza Fm is sharp with depositional environments passing from a playa lake (LE1a) to an alluvial fan (AFa) systems (Appendix D. 6, 7). The lower part of the Kalaza Fm corresponds to a rather proximal alluvial fan environment characterized by matrix-supported conglomerates associated with desiccation cracks and sparse root traces indicating arid/semi-arid conditions (AFa) (Fig. 8). It passes up section into horizontal to sub-horizontal laminated clast-supported conglomerates characteristic of a more distal alluvial fan environment and deposited under semi-arid conditions. The transition with the basal part of the Lower Cretaceous Qingshuihe Fm is sharp with environments retrograding sharply toward a lacustrine system (LE1).

429 *3. 3. 1. 4. The Wusu section*

430

431 The Wusu section (Fig. 9) is also located on the southern Junggar Basin, to the south
432 of the Wusu City on the northern flank of the Tian Shan Range (Fig. 1; Appendix E for a
433 general overview of the section). Based on the geological map (XBGMR, 1978a), this ~1650
434 m-thick section encompasses Middle (Xishanyao and Toutunhe fms) to Upper Jurassic (Qigu
435 and Kalaza fms) deposits. The lower and upper parts of this sedimentary section (up to the
436 Qigu Fm) have been respectively logged in the west and east of Saili Keti village (Appendix
437 A for GPS coordinates), with a few meters of overlap expected between them.

438 The first 190 m of the Xishanyao Fm correspond to alluvial fan deposits (AF)
439 retrograding sharply towards a ~85 m-thick unit of lacustrine sediments (LE1) (Appendix E.
440 1, 2). This unit marks the onset of a 200 m-thick progradational trend with depositional
441 environments evolving from a lacustrine delta (LD) to more and more proximal alluvial plains
442 (AP2, AP1), followed by an alluvial fan system (AF) (Fig. 9; Appendix E. 3). The upper part
443 of the Xishanyao Fm then consists of alluvial fan (AF) and proximal alluvial plain (AP1)
444 deposits. These proximal alluvial deposits are still present in the lower part of the Toutunhe
445 Fm and pass upward into sediments deposited in a more distal alluvial plain environment
446 (AP2) in a retrogradational trend (Fig. 9; Appendix E. 4, 5). Both the Middle Jurassic
447 Xishanyao and the Toutunhe fms contain several tuffaceous beds (cm to dm thick) indicating
448 volcanic activity as well as numerous coal beds associated with alluvial plain deposits
449 indicating rather humid climate conditions. Above, the lower part of the Upper Jurassic Qigu
450 Fm consists of red siltstones and sandstones displaying root traces and interpreted as proximal
451 alluvial plain (AP1) deposits (Appendix E. 6). The upper Qigu Fm displays alluvial fan
452 deposits (AF) retrograding towards proximal alluvial plain (AP1) to distal alluvial plain
453 (AP2a) deposits containing carbonate nodules indicating semi-arid climatic conditions (Fig.
454 9). The Qigu Fm ends with a sharp boundary marking the transition between the deposits of a

proximal alluvial plain environment (AP1) and the 150 m-thick Kalaza Fm (Fig. 9). The latter is dominated by planar to sub-planar laminated conglomerates (Appendix E. 7) interpreted as an alluvial fan sediments deposited in semi-arid conditions (AFa). Finally, the transition between the Kalaza Fm and the basal part of the Qingshuihe Fm is marked by a rapid retrogradation towards a distal alluvial plain environment (AP2).

3. 3. 2. Intra-mountain basins

3. 3. 2. 1. The Nieleke section

The Nieleke section (Fig. 10) is situated in the Tian Shan Range within the Hexilagen Basin (Fig. 1; Appendix F for a general overview of the section) and covers ~925 m of Middle Jurassic (Toutunhe Fm) deposits (XBGMR, 1978b).

The first 310 m of the section consist mostly of interbedded siltstones and sandstones associated with coal deposits and interpreted to be deposited in a lacustrine delta (LD). Several oxidized paleosols are also visible in the bottom part of this unit (Fig. 10; Appendix F. 1) suggesting warm and humid climatic conditions. The next 410 m show successive retrogradational and progradational trends with depositional environments evolving from a distal alluvial plain (AP2) to a lacustrine delta (LD) and back to a distal alluvial plain (AP2) deposits (Fig. 10; Appendix F. 2). The upper part of the section is characterized by a 50 m-thick unit of stacked, coarse-grained to gravelly sandstone beds interpreted to be lacustrine delta deposits (LD) (Fig. 10). This marks the onset of a progradational trend from a lacustrine delta (LD) to more and more proximal alluvial plain environments (AP2, AP1) (Appendix F. 3).

480 *3. 3. 2. 2. The Bayanbulak section*

481

482 The Bayanbulak section (Fig. 11) is situated in the Tian Shan Range, in the northern
483 part of the Bayanbulak Basin (Fig. 1; Appendix G for a general overview of the section). It
484 presents ~420 m of Middle Jurassic deposits (XBGMR, 1969), which we attribute to the
485 Toutunhe Fm based on their lithology.

486 The lowest ~70 m of sediments of this section indicate a proximal alluvial plain
487 environment (AP1) with several coal deposits. They pass upward into alluvial fan deposits
488 (AF) (Appendix G. 1). The rest of the succession is characterized by an alternation between
489 proximal alluvial plain (AP1) and alluvial fan (AF) deposits (Fig. 11). The last ~20 m of the
490 section are attributed to the Paleogene (XBGMR, 1969; Heilbronn et al., 2015) and comprise
491 red conglomerates impregnated/cemented by limestone (Appendix G. 2, 3) interpreted to be
492 calcrete formed by long-lasting pedogenic processes within semi-arid, seasonal climates (see
493 table 2).

494

495 **3. 3. 3. The north Tarim Basin**

496

497 *3. 3. 3. 1. The Yaha section*

498

499 The Yaha section (Fig. 12) is located in the Kuqa depression, of the north Tarim Basin
500 along the Yaha River on the southern flank of the Tian Shan Range (Fig. 1; Appendix H for a
501 general overview of the section). This ~1525 m-thick section encompasses Lower Jurassic
502 (Yengisar Fm), Middle Jurassic (Kezilenuer and Kalemake fms), Upper Jurassic (Qigu and
503 Kalaza fms), and Lower Cretaceous (Yageliemu Fm) deposits (XBGMR, 1970; Hendrix et al.,
504 1992).

505 The Yengisar Fm (~100 m-thick) consists of stacked, thick bedded gravelly sandstones
506 interpreted as lacustrine delta deposits (LD) (Appendix H. 1, 2). They evolve, at the base of
507 the Kezilenuer Fm, towards distal alluvial plain deposits (AP2) and finally back to lacustrine
508 delta sediments (LD) in the upper part of this formation (the last 325 m) (Fig. 12; Appendix
509 H. 3, 4). The base of the Kalemake Fm (~230 m) still consist of lacustrine delta deposits (LD)
510 retrograding toward lacustrine environments characterized by the presence of calcareous beds
511 with some turbiditic events in the top ~200 m of the formation (Appendix H. 5). Their oxygen
512 and carbon isotope compositions are typical of lacustrine carbonates (Heilbronn et al., 2015).
513 These observations seem to indicate a rather deep lacustrine environment (LE1) in
514 comparison to lake environments encountered in the previous sections. Middle Jurassic units
515 are also associated to numerous coal beds indicating humid climate conditions. The Qigu Fm
516 (~200 m in thickness) is characterized by a thick red-bed series (Appendix H. 6) interpreted as
517 playa lake deposits (LE1a) prograding towards more and more proximal alluvial plain
518 deposits associated to carbonate nodules that indicate semi-arid climate conditions (AP2a,
519 AP1a). Above, the Kalaza Fm is particularly thin (~35 m) in comparison to other sections and
520 consists of alluvial fan deposits (AFa) (Fig. 12; Appendix H. 7). Finally, the lower part of the
521 Lower Cretaceous Yageliemu Fm is characterized by proximal to distal alluvial plain
522 sediments deposited under semi-arid conditions (AP2a, AP1a) (Appendix H. 8). Within the
523 upper part of the section, the sediments evolve towards deposits associated to a more distal
524 lacustrine delta environment (LD).
525
526 **4. JURASSIC PALEOGEOGRAPHICAL EVOLUTION OF THE TIAN SHAN**
527
528 As mentioned above, the present-day geometry of the range results from a series of
529 Meso-Cenozoic reactivations of late Paleozoic tectonic structures (e.g.,Molnar and Taponnier,
530 1975; Hendrix et al., 1992; Sobel et al., 1999; Dumitru et al., 2001; De Grave et al., 2007;

Jolivet et al., 2010). However, the exact pattern of Cenozoic deformation in the Tian Shan Range is still poorly understood. The total Cenozoic shortening is estimated to be 124 ± 30 km at the longitude of Manas (ca. 85,5° E; Chinese Tian Shan) and 203 ± 50 km at the longitude of Kashgar (ca. 76° E; Kyrgyz Tian Shan) (Avouac et al., 1993). Though, this deformation is distributed on a number of faults, the exact kinematics of which being poorly constrained with likely significant strike-slip displacements. In addition, no Mesozoic deformation estimates are available. Due to this lack of kinematic constraints, we decided not to attempt to palinspastically restore the proposed paleogeographic maps.

4. 1. EARLY – EARLY MIDDLE JURASSIC

The Early to early Middle Jurassic paleogeography of the Tian Shan region was characterized by the presence of several sedimentary basins separated by significant reliefs (Fig. 13).

In the northeastern Junggar Basin (Kelameili region), the sedimentation was dominated by alluvial fan and alluvial plain deposits (Eberth et al., 2001; Vincent et al., 2001; Yang et al., 2015), indicating the existence of an eroding relief to the east within the vicinity of the present-day Altai Range. Indeed, Upper Triassic and Lower Jurassic angular unconformities were associated with coarse-grained pulses in the sedimentation suggesting that episodes of deformation and erosion took place in this area (Vincent et al., 2001). This is in agreement with seismic data showing that this region underwent transpressional deformation during Early Jurassic times (Zhao et al., 2014). To the south-east, sedimentation in the Junggar and Turfan basins consisted mainly of alluvial to lacustrine deposits. Widespread perennial lakes and associated lacustrine deltas developed within the central part of both basins while alluvial environments dominated in the areas nearby the reliefs (this study; Hendrix et al., 1992; Eberth et al., 2001; Vincent et al., 2001; Shao et al., 2003; Bian et

al., 2010; Feng et al., 2015; Yang et al., 2015). Paleocurrent measurements together with sedimentological and provenance analyses seem to indicate the presence of a low relief between the Junggar and Turfan basins (the present day Bogda Shan area) (Hendrix et al., 1992; Greene et al., 2001; Shao et al., 2003; Tang et al., 2014). However, the lack of Early Jurassic ages in the low-temperature thermochronology data of the Bogda Shan area indicates the absence of significant tectonic exhumation (Tang et al., 2015). This suggests that the relief was not derived from an Early Jurassic uplift and deformation event, but was probably inherited from the Permian to Triassic topography.

In the western Junggar Basin (Karamay region), several unconformities within the Lower Jurassic series are directly followed by conglomerate deposits (Eberth et al., 2010; Deng et al., 2010; Ma et al., 2014) and indicate that several deformation events also occurred in this area. The presence of alluvial fan and alluvial plain environments (Eberth et al., 2001) together with braided delta prograding eastward into a lake (Feng et al., 2015), point again to the existence of an eroding relief in place of the present day Halaalate mountains which provided sediments to the Junggar Basin.

Along the southern margin of the Junggar Basin, depositional environments consisted of alluvial fans to alluvial plains. The occurrence of numerous coal beds together with plant remnants in the associated series suggests rather humid conditions (this study; Hendrix et al., 1992; Eberth et al., 2001). Even though the Early to early Middle Jurassic sedimentation in that area is mostly regarded as continental, Sha et al. (2011) and Pan et al. (2012) suggested the occurrence of brackish water fauna ("*Waagenoperna*") in the south Junggar Basin indicative of an intermittent connection with the Tethys Sea to the west. However, due to poor preservation, the "*Waagenoperna*", as figured and described from the Badaowan Fm by Sha et al. (2011, 2016) and Pan et al. (2012) shows none of the characteristic generic features situated on the inner side of the shell (Simon Schneider, pers. com.). Moreover, it co-occurs with other bivalves which are clearly freshwater taxa, as stated by Sha et al. (2011) and Pan et

583 al. (2012) themselves. We thus propose that the "*Waagenoperna*" described in the Junggar
584 Basin is most likely a misidentified freshwater bivalve of unknown affinities and that no
585 marine incursion occurred in the southern area of the Junggar Basin during the Early Jurassic
586 epoch.

587 Along the Manas section (Fig. 1 for location; Fig. 8), the unconformity between the
588 Upper Triassic and Lower Jurassic sediments suggests that deformation and erosion events
589 took place at the southern margin of the Junggar Basin during this period (Eberth et al., 2001;
590 Yang et al., 2015). North directed paleocurrent measurements together with provenance data
591 indicate that these sediments were derived from the south, locating a relief in the place of the
592 present day Tian Shan Range (Hendrix et al., 1992; Yang et al., 2013). These observations are
593 in agreement with low-temperature thermochronology data which highlight a Late Triassic -
594 Early Jurassic cooling phase associated with the reactivation of the main Paleozoic structures
595 of the North Tian Shan region (Dumitru et al., 2001; Jolivet et al., 2010).

596 Several intra-mountain basins were also active within the Tian Shan Range during the
597 Early to early Middle Jurassic. The Yili Basin was principally occupied by alluvial plain,
598 lacustrine delta and lacustrine environments with coal deposits suggesting humid conditions.
599 The main depocenter was located in the northern part of the basin (Li et al., 2014). To the
600 south, the Zahosu depression was also active (Li et al., 2015). Coarse grained fan delta
601 deposits prograding towards the north in the Yili Basin (Li et al., 2014) and the sediment
602 grain-size evolving southward from conglomerates to sandstones and siltstones in the Zahosu
603 depression (Li et al., 2015) imply that a physiographic separation existed between the two
604 basins at that time. To the south-east, preserved Lower Jurassic sediments along the northern
605 edge of the Bayanbulak Basin (XBGMR, 1969) suggest that this depression was also active
606 during this period. Finally a Late Triassic – Early Jurassic cooling phase was identified in the
607 low-temperature thermochronology data along the Narat Range between the Bayanbulak and

608 Yili basins. This suggests the presence of an eroding relief separating these basins (Dumitru et
609 al., 2001; Jolivet et al., 2010).

610 To the south-east of the Tian Shan, the Yanqi Basin presents deposits associated to
611 environments evolving from alluvial fan to lacustrine systems (Al-Qaraafi and Guangqing,
612 2013). Sedimentological analyses within both the Turfan and Yanqi basins suggest that they
613 were separated from each other by an eroding relief (Shao et al., 2003; Al-Qaraafi and
614 Guangqing, 2013). However, whether the Yanqi and Tarim basins were connected or
615 separated by a relief during the Early to early Middle Jurassic is unclear due to the lack of
616 data in that region.

617 During this period, the north Tarim Basin was characterized by alluvial fan systems
618 evolving southward to alluvial plain, lacustrine delta and lacustrine environments (Fig. 12).
619 Provenance analyses together with south directed paleocurrents indicate the existence of an
620 eroding relief to the north forming the main source area for the detrital material deposited in
621 this part of the basin (Hendrix et al., 1992; Li and Peng., 2010; Liu et al., 2013; Wang et al.,
622 2015). The very monogenic (quartz) and well-sorted grain size of the lacustrine delta
623 sediments encountered in the Yaha section (Yengisar Fm; Fig. 12) could indicate that these
624 deposits were possibly reworked from an old weathering profile. This statement is in
625 agreement with the provenance data (Liu et al., 2013) which indicate that topography of the
626 source area could have already been partially flattened at that time.

627 To the west of the Tian Shan, in the Fergana Basin, renewed subsidence occurred
628 during the Early Jurassic following the erosion event that characterized the Triassic period in
629 that region (Clarke, 1984). This led to the accumulation of 90-400 m-thick deposits in
630 alluvial, lacustrine fan delta to shallow lacustrine environments, which unconformably
631 overlay the Paleozoic basement (Clarke, 1984; De Pelsmaeker et al., 2018). Numerous coal
632 beds and plant remnants were described in these deposits indicating abundant vegetation and
633 humid climate conditions. At the same time, to the east of the Fergana Basin, ~4000 m of

sediments were deposited within the Yarkand-Fergana Basin (Sobel et al., 1999). This strong sediment accommodation is thought to be induced by strike-slip motion on the Talas Fergana/Karatau fault leading to the formation of an Early – Middle Jurassic pull-apart basin (Sobel et al., 1999; Allen et al., 2001; Alexeiev et al., 2017). Within this Yarkand - Fergana Basin, depositional environments consist mainly of alluvial, fan delta and deep lake systems (Sobel et al., 1999; De Pelsmaeker et al., 2018). Low-temperature thermochronology data also indicate a Late Triassic – Early Jurassic cooling phase within the Kyrgyz Tian Shan area probably induced by the reactivation of Paleozoic structures and basement exhumation (Sobel et al., 2006; De Grave et al., 2007, 2012; Glorie and De Grave, 2016; Nachtergaele et al., 2018).

Several Lower to Middle Jurassic outcrops have also been described by De Pelsmaeker et al. (2018) in the Ming-Kush and south Issyk-Kul basins and similar age deposits were observed in both the Naryn and Aksai basins (VNIGNI and Beicip Franlab, 1992) located within the northern part of the present day Kyrgyz Tian Shan (Fig. 1 for location). Generally, the stratigraphic ages of these sediments reported on the geological maps are Lower Jurassic (e.g., Lasovskiy and Mozolev, 1961), however, no biostratigraphic data are available for these series. Sedimentation mainly consisted of alluvial plain, fan delta and shallow lacustrine deposits. These deposits are often associated with coal-rich layers and plant fragments indicating humid climate conditions although some caliche-type paleosols more typical of semi-arid conditions were also identified in the south Issyk-Kul Basin (De Pelsmaeker et al., 2018; VNIGNI and Beicip Franlab, 1992). Low-temperature thermochronology data support a Middle Triassic - Early Jurassic cooling phase within the basement separating all these basins (e.g., De Grave et al., 2011; Glorie et al., 2011) indicating the presence of eroding reliefs between these intra-mountain basins.

To the north of the Kyrgyz Tian Shan, no Lower Jurassic sediments have been described within the south Chu-Sarysu and Yili-Balkhash basins (VNIGNI and Beicip

660 Franlab, 1992; AGMCA, 2008). We propose that these domains were dominated by sediment
661 by-pass (i. e. lowland areas dominated by soil alteration, low erosion and/or low sedimentary
662 export or by a poor preservation of thin sediment deposits) during the Early – early Middle
663 Jurassic. Similarly, no Jurassic sediments have been deposited in the western part of the
664 Tarim Basin, except for Jurassic series exposed more to the south, along the West Kunlun –
665 Pamir Range (Lee 1985a, b; Sobel et al., 1999; Yang et al., 2017). We thus propose that this
666 domain was also dominated by sediment by-pass during the Early – early Middle Jurassic.
667 Nevertheless, some restricted piedmonts deposits could have existed that were not preserved
668 within the stratigraphic record.
669
670 **4. 2. LATE MIDDLE – EARLY LATE JURASSIC**
671
672 The late Middle to early Late Jurassic paleogeography of the Tian Shan region was
673 mostly characterized by sedimentary basins surrounded by relatively low- relief basement
674 areas (Fig. 14).
675 In the northeastern Junggar Basin (Kelameili region), the late Middle – early Late
676 Jurassic strata consist mainly of alluvial plain to shallow lacustrine deposits (Eberth et al.,
677 2001; Vincent et al., 2001). These environments are more distal compared to the Early
678 Jurassic ones and potentially indicate a lowering or a retreat further to the east of the Early
679 Jurassic relief. However, some local Middle Jurassic unconformities have been identified in
680 this area which suggests recurrent periods of localized deformation and erosion (Eberth et al.,
681 2001; Vincent et al., 2001). To the north-east, in the Junggar and Turfan basins, late Middle –
682 early Late Jurassic deposits reflect alluvial to lacustrine depositional environments (this study;
683 Hendrix et al., 1992; Eberth et al., 2001; Vincent et al., 2001; Shao et al., 2003; Bian et al.,
684 2010; Yang et al., 2015). The paleocurrent measurements, sedimentological analyses and
685 provenance studies indicate the presence of an existing relief between the two basins

686 persisting from the Early Jurassic (Hendrix et al., 1992; Shao et al., 1999, 2003; Tang et al.,
687 2014; Ji et al., 2017). Based on provenance studies, some authors proposed that this area also
688 underwent several uplift episodes during the Middle Jurassic (Tang et al., 2014; Ji et al.,
689 2017). However, the lack of contemporaneous exhumation ages and the occurrence of fine
690 grained sediments in both the Junggar and Turfan basins rather suggest the absence of strong
691 exhumation events in this region (Shao et al., 2003; Tang et al., 2015; Yang et al., 2015).
692 To the west of the Junggar Basin (Karamay region), the sedimentation was dominated by
693 alluvial fan to alluvial plain deposits (Eberth et al., 2001). The presence of a Middle Jurassic
694 unconformity sealed by conglomerates again indicates that deformation persisted in that area
695 during this period (Eberth et al., 2001; Deng et al., 2010).
696 Along the southern margin of the Junggar Basin, the strata exposed in the Wusu
697 section consist mainly of alluvial fan to alluvial plain deposits (Fig. 9). Further east, along the
698 Manas and Toutunhe sections, the sediments are characteristic of more distal environments
699 such as alluvial plain to lacustrine delta (Figs. 6, 7, 8) (this study; Hendrix et al., 1992; Eberth
700 et al., 2001; Deng et al., 2010). North-oriented paleocurrents attest of the presence of an
701 eroding relief to the south (Hendrix et al., 1992). The more distal depositional environments
702 in the Manas region potentially indicate that this relief was lower or located further south than
703 during the Early Jurassic. This trend is in agreement with the low-temperature
704 thermochronology data which associate the Middle Jurassic to a period of low basement
705 cooling rates and thus to a period of flattening of the relief in the North Tian Shan region
706 (Dumitru et al., 2001; Jolivet et al., 2010). In the southern margin of the Junggar Basin, the
707 late Middle Jurassic deposits contain numerous coal beds (Figs. 6, 7, 8) (this study; Hendrix et
708 al., 1992; Eberth et al., 2001; Deng et al., 2010). The occurrence of these coal beds indicates
709 that rather humid conditions persisted during that period. This coal disappears in the early
710 Late Jurassic deposits, while extensive calcareous paleosols indicative of semi-arid conditions
711 developed (This study; Hendrix et al., 1992; Eberth et al., 2001; Vincent et al., 2001; Deng et

al., 2010 Jolivet et al., 2017a). Several volcanic tuff layers and syn-sedimentary volcanic zircons have also been described in the Middle Jurassic series along the southern margin of the Junggar Basin (Wusu and Manas sections, Bogda Shan) indicating a volcanic activity within the north Tian Shan region during that period (Fig. 9; Yang et al., 2013; Simonov et al., 2015; Ji et al., 2017). However, the eruption center has not yet been located.

The Middle Jurassic sediment in the Yili Basin consists of alluvial to lacustrine deposits (Fig. 10; Li et al., 2014). Due to the absence of coarse grained sediments and to the presence of extensive coal beds in the southern part of the basin as well as in the Zahosu depression immediately to the south (Li et al 2014; Li et al., 2015), we suggest that no erosive domain separated these two basins during that period. However, the occurrence of alluvial fan to proximal alluvial plain deposits in the northern part of the Bayanbulak Basin (Fig. 11) implies the existence of a nearby eroding relief. Moreover, low-temperature thermochronology data indicate a Middle Jurassic period of slow cooling in the Narat region interpreted as a period of slow erosion (Dumitru et al., 2001; Jolivet et al., 2010). We thus propose that the relief established along the Narat fault during the Late Paleozoic – Early Jurassic was not entirely flattened by Middle Jurassic and therefore, that it still constituted a physiographic separation between the Bayanbulak and Yili basins.

To the south-east of the Tian Shan, no data are available for the Middle – Late Jurassic strata of the Yanqi Basin. However, sedimentological analyses within the Turfan Basin indicate the presence of an eroding relief separating the Turfan Basin from the Tarim Basin (Shao et al., 2003).

Along the Yaha section in the north Tarim Basin, the Middle Jurassic strata were deposited in alluvial plain to lacustrine environments (Fig. 12). South-directed paleocurrents and provenance analyses also indicate the presence of an eroding relief to the north (Hendrix et al., 1992; Li and Peng., 2010; Liu et al., 2013; Wang et al., 2015). However, the more distal depositional environments compared to the Early Jurassic ones suggest a lowering or a

738 northward retreat of the relief with a widening of the basin. This is also supported by detrital
739 zircon U-Pb data showing a widening of the sediment source area during the Middle Jurassic
740 (Liu et al., 2013).

741 To the west of the Tian Shan, the Middle Jurassic series in the Fergana Basin consist
742 of 100-300 m-thick alluvial to lacustrine deposits (Clarke, 1984; De Pelsmaeker et al., 2018).
743 Coal beds and plant fragments are abundant within these sediments and indicate humid
744 conditions (De Pelsmaeker et al., 2018). To the east of the Fergana Basin, the Yarkand-
745 Fergana Basin was still subsiding due to strike-slip motion along the Talas Fergana/Karatau
746 fault and it accommodated ~600–1550 m of Middle Jurassic sediments (Sobel et al., 1999;
747 Allen et al., 2001; Alexeiev et al., 2017). The facies of the latter indicate the occurrence of
748 alluvial plain, lacustrine delta and lacustrine depositional environments (Sobel et al., 1999; De
749 Pelsmaeker et al., 2018). Like in the Chinese Tian Shan, low-temperature thermochronology
750 data indicate low cooling rates during the Middle Jurassic within the Kyrgyz Tian Shan. This
751 was interpreted as a period of slow erosion leading to progressive planation of the basement
752 areas (De Grave et al., 2007, 2013; Macaulay et al., 2014; Glorie and De Grave, 2016).
753 Meanwhile, in the Ming-Kush, south Issyk-Kul, Naryn and Aksai basins, a Middle Jurassic to
754 Eocene hiatus in sedimentation has been identified (VNIGNI and Beicip Franlab, 1992;
755 Burbank et al., 1999; De Pelsmaeker et al., 2018).

756 Further north, no Middle - Late Jurassic sediments were described within the south
757 Chu-Sarysu and Yili-Balkhash basins (VNIGNI and Beicip Franlab, 1992; AGMCA, 2008).
758 We propose that these domains were still dominated by sediment by-pass during this period.
759 Similarly to the Early Jurassic period, the western Tarim Basin seems also dominated by
760 sediment by-pass during the Middle - Late Jurassic (Lee 1985a, b). Nevertheless, some
761 restricted piedmonts deposits could again have existed that were not preserved within the
762 stratigraphic record.

763

764 **4. 3. LATE JURASSIC - EARLY CRETACEOUS TRANSITION**

765

766 In the Tian Shan region, the Late Jurassic - Early Cretaceous transition corresponds to
767 a drastic paleogeographic change in comparison to the Early and Middle Jurassic periods (Fig.
768 15). In the Junggar and Turfan basins, the sedimentation was dominated by alluvial fan to
769 alluvial plain deposits (Hendrix et al., 1992; Shao et al., 1999; Eberth et al., 2001; Vincent et
770 al., 2001; Bian et al., 2010; Jolivet et al., 2017a). Low-temperature thermochronology data
771 indicate a Jurassic - Early Cretaceous fast cooling event in the present day Bogda Shan area
772 implying that this region underwent deformation and uplift during this period (Tang et al.,
773 2015).

774 To the north-east and north-west of the Junggar Basin, in the Kelameili and Karamay
775 regions (Fig. 15), the Upper Jurassic - Lower Cretaceous deposits are associated with alluvial
776 fans and alluvial plain environments (Eberth et al., 2001; Vincent et al., 2001; Jolivet et al.,
777 2017a). Angular unconformities at the base of the alluvial fans sediments (corresponding to
778 the Kalaza Fm) have been identified in both regions and are, in the Kelameili area, associated
779 with incised paleo-valleys (Eberth et al., 2001). They imply uplift and relief building in these
780 areas, in agreement with the seismic data indicating that transpressive deformation occurred
781 within the eastern and western part of the Junggar Basin during the Jurassic (Zhao et al.,
782 2014; Yu et al., 2016). Such a tectonic setting could have led to widespread deformation
783 leading to the generation of a relief within the Junggar Basin.

784 Indeed, a NE-SW-orientated erosional area, the Chemo uplift, started to develop
785 within the central part of the Junggar Basin during the Middle Jurassic and reached its peak
786 stage during the Late Jurassic - Early Cretaceous (Lianhua et al., 2009; Yang et al., 2015; Gao
787 et al., 2017). Erosion of this topographic high provided terrigenous material that was shed into
788 the adjacent, still subsiding areas (Lianhua et al., 2009; Yang et al., 2015; Gao et al., 2017).

789 Based on seismic data, Lianhua et al. (2009) estimated that the amplitude of this paleorelief
790 could have reached 740 m during its peak development stage.

791 Along the southern margin of the Junggar Basin, the sedimentation consisted mainly
792 of several meters to hundred meters-thick alluvial fan deposits typical of semi-arid to arid
793 climate conditions (Figs. 6, 8, 9) (this study; Jolivet et al., 2017a). Indeed, aeolian deposits are
794 present in the Kelameili and Toutunhe regions (Fig. 1 for location). Along the south Toutunhe
795 section, they are interbedded with ephemeral alluvial fan deposits (Fig. 6) and evolved
796 northward to erg deposits with large dunes and interdunes (Fig. 7). The occurrence of these
797 thick aeolian deposits indicate that this region was under semi-arid to arid climate conditions
798 during the Late Jurassic - Early Cretaceous (this study; Eberth et al., 2001; Vincent et al.,
799 2001; Jolivet et al., 2017a).

800 As in the north of the Junggar Basin, angular unconformities have been identified at
801 the base or within the Kalaza Fm (Hutubi and North Toutunhe sections) (this study; Jolivet et
802 al., 2017a). Moreover, provenance analyses demonstrate that recycling of Mesozoic sediments
803 took place in this area. These observations imply that some tectonic movements and rock
804 uplift also occurred during the Late Jurassic - Early Cretaceous within the North Tian Shan
805 foothills (Yang et al., 2013). However, low-temperature thermochronology data on basement
806 rocks from the central Tian Shan do not identify any evidence of tectonic movements during
807 this period and show that exhumation was in fact controlled by slow erosion since the Middle
808 Jurassic (Dumitru et al., 2001; Jolivet et al., 2010). Accordingly, we propose that small
809 amplitude tectonic movements occurred within the North Tian Shan Range and its piedmont,
810 leading to limited relief building during the Late Jurassic - Early Cretaceous.

811 Within the Tian Shan Range, both Yili and Bayanbulak basins do not contain Upper
812 Jurassic – Lower Cretaceous sediments (AGMCA, 2008). Following an Late Jurassic – Early
813 Cretaceous unconformity, a ~40 m-thick weathered layer formed within the Yili Basin,
814 overlain by Upper Cretaceous sediments and indicating rather stable conditions for a long

period of time (VNIGNI and Beicip Franlab, 1992). Therefore, we propose that this domain was dominated by sediment by-pass during the Late Jurassic – Early Cretaceous. To the south, low-temperature thermochronology data indicate slow cooling, hence low erosion within the Narat Range. This suggests a continuous flattening of the topography during this period (Dumitru et al., 2001; Jolivet et al., 2010). In the Bayanbulak Basin, Eocene (?) strata rest unconformably on the Middle Jurassic series again implying that the basin was dominated by sediment by-pass and/or erosion during the Late Jurassic - Early Cretaceous.

To the south-east of the Tian Shan, the relation between the Yanqi and the Tarim basins is not clear. No Upper Jurassic – Lower Cretaceous sediments were described within the Yanqi Basin (AGMCA, 2008; Huang et al., 2015). We therefore propose that this region was dominated by sediment by-pass during this period.

In the northern part of the Tarim Basin, the Late Jurassic – Early Cretaceous sedimentation was characterized by relatively thin alluvial fan deposits (in comparison to the Junggar Basin) evolving southward towards alluvial plain deposits (Fig. 15). Provenance and petrographic analyses point to a sediment source from the South Tian Shan Range, altogether with local recycling of Mesozoic sediments indicating a southward migration of the eroding topography (Li et al., 2004; Li and Peng, 2010).

To the west, the Late Jurassic - Early Cretaceous sedimentation in the Fergana Basin consisted of alluvial fan and alluvial plain deposits (Fig. 15). In the northern part of the basin (Tash-Komyr section; Fig. 1), the transition between the Jurassic and the Cretaceous is marked by an erosional unconformity directly followed by > 110 m-thick alluvial fan deposits (De Pelsmaeker et al., 2018). This suggests that some tectonic movements occurred during that period. To the south (Jetim-Dobo section; Fig. 1) the sedimentation consists of alluvial plain deposits containing calcareous paleosols, and indicating semi-arid climate conditions (De Pelsmaeker et al., 2018).

Meanwhile to the east, alluvial fan and proximal alluvial plain systems developed in the western and southern parts of the Yarkand–Fergana Basin (Sobel et al., 1999; De Pelsmaeker et al., 2018). Provenance studies on Late Jurassic – Early Cretaceous samples indicate potential recycling of older Jurassic sediments and smaller drainage area compared to the Early – Middle Jurassic paleogeography (De Pelsmaeker et al., 2018). Together, these data imply a Late Jurassic – Early Cretaceous inversion of the Yarkand-Fergana Basin. This renewed tectonic activity is further supported by low-temperature thermochronology data which identify a Late Jurassic –Early Cretaceous cooling event in the Kyrgyz Tian Shan Range suggesting a localized relief building (De Grave et al., 2007, 2012, 2013; Glorie and De Grave., 2016; Nachtergaele et al., 2018).

No Upper Jurassic – Lower Cretaceous sediments were described within the Chu-Sarysu, Yili–Balkash and west Tarim basins (Lee 1985a, b; VNIGNI and Beicip Franlab, 1992; AGMCA, 2008). We therefore propose that these domains were still dominated by sediment by pass during this period even though some restricted piedmont deposits could have existed and not subsequently preserved within the stratigraphic record.

5. DISCUSSION

5. 1. TOPOGRAPHIC AND CLIMATIC EVOLUTION OF THE TIAN SHAN

The Jurassic topographic evolution of the Tian Shan was dominated by the progressive planation of a late Paleozoic to early Mesozoic relief, locally interrupted by discreet topographic rejuvenations (Fig. 16) (e.g., this study, Dumitru et al., 2001; Jolivet et al., 2010; Li and Peng, 2010; Liu et al., 2013; Macaulay et al., 2014). In both the north and south Tian Shan foothills, a progressive transition can be observed from Early Jurassic coarse-grained sediments associated with proximal alluvial environments, to finer-grained deposits

characteristic of distal alluvial to lacustrine systems during the Middle Jurassic (this study; Hendrix et al., 1992; Eberth et al., 2001; Bian et al., 2010). This highlights the progressive decrease of the Tian Shan relief. During the Early to Middle Jurassic, the sedimentation, in the basins surrounding the range and in the intra-mountain depressions, was characterized by alluvial to lacustrine deposits containing numerous coal beds and plant fragments indicating humid climate conditions (Fig. 16; this study; Hendrix et al., 1992; Sobel et al., 1999; Eberth et al., 2001; Bian et al., 2010; De Pelsmaeker et al., 2018). Finally, the Middle Jurassic period was also characterized by volcanic activity within the north Tian Shan region (this study; Yang et al., 2013; Simonov et al., 2015; Ji et al., 2017). During the early Late Jurassic, the Tian Shan relief was still decreasing, with contemporaneous fine-grained sediments deposited in distal alluvial to lacustrine environments. However, this period was marked by a change in climate conditions, recorded all over the Tian Shan area by the disappearance of the humid conditions marked by coal layers and the extensive formation of calcareous paleosols, indicative of semi-arid conditions (this study; Hendrix et al., 1992; Eberth et al., 2001; Vincent et al., 2001; De Pelsmaeker et al., 2018). This Late Jurassic aridification affected most of Central Asia and was also identified in the West Siberian Basin (e.g., Hendrix et al., 1992; Le Heron et al., 2008) and within the Turan domain where sedimentation partly consisted on thick evaporite units (Brunet et al., 2017).

The Late Jurassic – Early Cretaceous transition was marked by a tectonic reactivation leading to localized relief building within the Tian Shan and coarse-grained proximal alluvial deposits surrounding the range (Fig. 16) (; De Grave et al., 2007, 2012, 2013; Tang et al., 2015; Glorie and De Grave., 2016; Nachtergaele et al., 2018). Meanwhile, the Yili and Bayanbulak basins were dominated by sediment by-pass and/or limited erosion. Contemporaneous, limited relief building is also suggested in the Altai (Eberth et al., 2001; Yuan et al., 2006). The Late Jurassic – Early Cretaceous transition was further characterized by the climax of the aridification trend which was prevailing since the early Late Jurassic. In

892 the Junggar Basin, this peak in aridity has been associated to the deposition of alluvial fans
893 together with large - scale aeolian dunes (Jolivet et al., 2017a).
894
895 **5. 2. AN EARLY - MIDDLE JURASSIC KINEMATIC FRAMEWORK DRIVEN BY**
896 **FAR-FIELD TECTONICS**
897
898 The Jurassic tectonic and topographic evolution of the Tian Shan region is thought to
899 be mostly controlled by compressive or transpressive events at continental scale (Allen et al.,
900 1991; Hendrix et al., 1992; Sobel et al., 1999; Vincent et al., 2001; Allen et al., 2001; Yang et
901 al., 2015). Thus, Late Triassic-Early Jurassic evidences of deformation in the area are often
902 related to the Qiangtang collision along the southern margin of Eurasia to the south, which
903 ended at that time (Kapp et al., 2007; Roger et al., 2010). However, no major collision
904 episode has been reported along this Eurasian margin between the Qiangtang collision and the
905 Early Cretaceous Lhasa collision (Kapp et al., 2007; Roger et al., 2010). The absence of
906 significant collision suggests that other kinematic events occurred during the Jurassic, leading
907 to tectonic activity in the Tian Shan region. To the south, in the Tibet area, no major Jurassic
908 geodynamic event has been described (Roger et al., 2004, 2010; Reid et al., 2005). To the
909 north-east, the timing of the final closure of the Mongol-Okhotsk Ocean remains poorly
910 constrained. It is thought to occur during the Late Jurassic-Early Cretaceous time (e.g.,Zorin,
911 1999; Donskaya et al. 2013; Daoudene et al., 2017) and was probably not associated with
912 strong compressive deformation (Fig. 17. A) but rather with distributed extension affecting a
913 thin, abnormally warm crust (Daoudene et al., 2017; Jolivet et al., 2017b).
914 As mentioned above, in the Tian Shan region, east of the Talas Fergana/Karatau fault,
915 the first order geometry of the Jurassic sediments preserved within the Tarim and Junggar
916 basins is characterized by depocenters located along the Tian Shan Range (Fig. 17. B) (Lee,
917 1985; Hendrix et al., 1992; Bian et al., 2010; Yang et al., 2015). Moreover, recurrent periods

of localized and limited Jurassic deformation associated with thrust faults have been reported within the two basins (e.g.,Eberth et al., 2001; Vincent et al., 2001; Liu et al., 2006; Wang et al., 2012; Zhao et al., 2014; Chen et al., 2015; Ma et al., 2015; Yang et al., 2015). These observations indicate that the Jurassic Junggar and Tarim basins were compressive basins and that the Tian Shan region was under compressional setting at that time (Allen et al., 1991; Hendrix et al., 1992; Yang et al., 2015). Nonetheless, the Early-Middle Jurassic period was mainly characterized by the progressive planation of the Tian Shan relief established during the late Paleozoic – early Mesozoic (Dumitru et al., 2001; Jolivet et al., 2010; Glorie and De Grave, 2016). This implies that no major compressive tectonic event leading to an extensive relief building occurred in that area. The attested recurrent tectonic activity, together with the absence of a major relief build-up during this period, suggest strike-slip fault kinematics with limited vertical motion rather than true compressional tectonics. This idea is supported by seismic data interpretations that also indicate a Jurassic transpressional deformation in the Junggar Basin (Liu et al., 2006; Wang et al., 2012; Yu et al., 2016), which is potentially related to the Jurassic- Early Cretaceous rotation of the Junggar block (Lianhua et al., 2009; Yu et al., 2016). Jurassic to Cretaceous strike-slip tectonics has also been described in the eastern part of the Tarim Basin (Wang et al., 2012) as well as extensional faults (Yang et al., 2017).

In the Tian Shan area, several NW-SE and E-W oriented lithospheric faults (e.g.,the Talas Fergana fault, the Nikolaev line, the North Tian Shan fault and numerous smaller ones) accommodated late Paleozoic block rotations (Bazhenov et al., 1999; Van Der Voo et al., 2006 and references therein). Similarly, we propose that these structures could have been reactivated during the Jurassic accommodating the rotation of several blocks localized in the Tian Shan region. Such motion would favor the development of localized, small scale relief along these main faults. Early Jurassic reactivation along the Talas Fergana/Karatau fault has indeed been identified by kinematic analysis conducted on the south Turgay Basin and by

944 geochronological studies (Rolland et al., 2013; Alexeiev et al., 2017).Along the southern edge
945 of the Tarim Basin, geochronology data indicate that strike-slip motion of the Altyn Tagh
946 fault occurred during Middle Jurassic times (Sobel et al., 2001; Liu et al., 2007). However, the
947 exact kinematic of these strike-slip motion as well as the direction of rotation of the blocks
948 localized in the Tian Shan region is still unclear. Indeed, Jurassic clockwise or anticlockwise
949 rotation of the Junggar Basin has been proposed in the literature (for example respectively in
950 Lianhua et al., 2009 and Yu et al., 2016). Similarly, both Jurassic dextral and sinistral motion
951 along the Altyn Tagh fault have been suggested (Sobel et al., 1999; Liu et al., 2007). Finally,
952 post early Permian sinistral strike-slip motion has been identified along the Nikolaev line in
953 Kyrgyztan (Bazhenov and Mikolaichuk, 2004) but it is not clear if this kinematic prevailed
954 during the Jurassic.

955 West of the Talas Fergana/Karatau fault,compressional events of regional significance
956 occurred throughout the Caspian, Turan and south Kazakh domains during the Late Triassic
957 leading to the inversion of numerous basins in this area (Otto, 1997; Thomas et al., 1999).
958 Following this compressional phase, a widespread late Early to Middle Jurassic extension
959 associated to back-arc development driven by the northward subduction of the Neo-Tethys
960 oceans affected these regions (Zonenshain and Le Pichon 1986; Nikishin et al. 1998; Thomas
961 et al., 1999; Brunet et al., 2003, 2017; Robert et al., 2014; Mordvintsev et al., 2017). This
962 extension reactivated mainly NW-SE orientated Paleozoic structures as normal faults. In turn,
963 these normal faults induced localized subsidence leading to the emplacement of elongated
964 NW-SE depocenters in the Amu-Darya and Kopet Dagh basins (Fig. 17) (e.g., Robert et al.,
965 2014; Brunet et al., 2017; Mordvintsev et al., 2017). Further east, Triassic – Middle Jurassic
966 extension has also been reported in the western part of the Afghan - Tajik Basin (Brookfield
967 and Hashmat, 2001).

968 Accordingly, the Talas Fergana/Karatau fault seems to be a major NW-SE structure
969 separating the Tian Shan domain to the east, dominated by possible strike slip tectonics and

970 block rotations and the Turan and southwest Kazakh domains to the west, dominated by
971 extension. Along this fault, several basins formed during the Early-Middle Jurassic (Fig. 17).
972 To the north, the South Turgay Basin is characterized by a series of N to NW orientated
973 grabens and half grabens, separated by basement highs and filled by up to 2.5 km of Lower to
974 Middle Jurassic fluvio-lacustrine sediments (Moseley and Tsimmer, 2000; Allen et al., 2001;
975 Shi et al., 2016; Alexeiev et al., 2017). Within the central part of the Talas Fergana/Karatau
976 fault, the Leontiev Graben is an elongate basin containing up to 1.5 km of Jurassic fluvial and
977 lacustrine sediments (Sobel et al., 1999; Allen et al., 2001). Finally, at the south-eastern
978 termination of the fault, the Yarkand-Fergana Basin consists of thick (c. a. 5 km) Lower to
979 Middle Jurassic series of continental deposits (Sobel et al., 1999; De Pelsmaeker et al., 2018).
980 Several studies propose that these basins formed in response to dextral strike-slip motion
981 along the Talas Fergana/Karatau fault. This would induce the opening of the South Turgay
982 Basin as a trailing imbricate fan and the opening of both the Leontiev and Yarkand-Fergana
983 basins, either as dextral transtensional structures at right-stepping jogs in the fault system
984 (e.g., Allen et al., 2001; Alexeiev et al., 2017) or as pull-apart basins (Sobel et al., 1999). This
985 kinematic model has been mainly based on geometrical analysis of seismic data conducted on
986 the Turgay system (Alexeiev et al., 2017). These authors suggest that consequent Jurassic
987 dextral strike-slip motion occurred along the Talas Fergana/Karatau fault, and its maximum
988 offset was estimated by Alexeiev et al., (2017) to reach 70 km. On the other hand, Burtman
989 (1980) considered Jurassic slip as insignificant along this fault in the Kyrgyztan region.
990 Finally, the driving mechanism leading to such dextral motion along the Talas
991 Fergana/Karatau fault during the Early to Middle Jurassic period is yet to be fully understood.
992 Indeed, the precise onset age of formation of these basins is unclear. In the Leontiev Basin,
993 Lower Jurassic sediments have a pre Toarcian age based on palynological and geochemical
994 studies (Schnyder et al.,2016) while no clear stratigraphic ages are available for the south
995 Turgay and Yarkand Fergana basins. Geochronological data indicate that the Talas

Fergana/Karatau fault was already active close to the Triassic - Jurassic transition in the Kyrgyz region (Rolland et al., 2013). The only coeval geodynamic event known in this region that could cause such dynamic is the Qiangtang collision which ended during the Late Triassic-Early Jurassic (Kapp et al., 2007). Therefore we propose that the early Early Jurassic dextral motion along this fault could have been induced by far-field effects of the final stage of the Qiangtang collision. However, it is difficult to understand how such a far-field induced compressional regime could have led to the opening of the Yarkand-Fergana Basin. Indeed, Sobel et al. (1999) proposed the existence of a strike-slip fault system located in the Kunlun area during that same period, allowing the formation of a Jurassic transtensional basin encompassing both the Yarkand-Fergana and the western Tarim Jurassic deposits. However, seismic data obtained within the western margin of the Tarim Basin neither show the presence of a Jurassic depot-center nor the presence of any fault parallel to the Talas Fergana/Karatau one in this area (Fig. 17) (Yang et al., 2017). This implies that both of these systems were disconnected from each other at that time. Moreover, opening of these basins continued during the late Early to Middle Jurassic (Sobel et al., 1999; Moseley et al., 2000; Allen et al., 2001; Alexeiev et al., 2017). During this period, no major collisional event has been identified along the Eurasian margin implying that another kinematic event induced the tectonic activity observed along the Talas Fergana/Karatau fault. As mentioned previously, simultaneous widespread extension affected the whole Caspian-Turan domains to the west. We propose that this subduction related extension could also have affected the Talas Fergana/Karatau region leading to continuous opening of the South Turgay, Leontiev and Yarkand Fergana basins during the late Early-Middle Jurassic period.

Therefore, we propose that the early Early Jurassic evolution of the Tian Shan region was driven by the far-field effects of the Qiangtang collision final stage. However, recurrent tectonic activity persisted throughout the Tian Shan region during the Early – Middle Jurassic and such dynamic cannot be explained by this collision. The only regional geodynamic event

affecting Central Asia during this period is the subduction of the Neotethys oceans which led to extension throughout the Caspian, Turan and south Kazakh domains (Zonenshain and Le Pichon 1986; Nikishin et al. 1998; Thomas et al., 1999; Brunet et al., 2003, 2017; Robert et al., 2014; Mordvintsev et al., 2017). We therefore assume that the extensional stress-field induced by the Neo-Tethys subduction also played a major role in driving the late Early to early Middle Jurassic tectonic and topographic evolution of the Tian Shan region. The far-field extension could have led to continuous opening of the basins previously formed along the Talas-Fergana Karatau fault while the rest of the Tian Shan was still possibly dominated by strike slip tectonics accommodated by the reactivation of the major NW-SE and E-W Paleozoic structures located within the range.

5. 3. A LATE MIDDLE TO EARLY LATE JURASSIC PERIOD OF RELATIVE TECTONIC QUIESCENCE

As explained above, the Jurassic topographic evolution of the Tian Shan Range was dominated by the progressive planation of a late Paleozoic to early Mesozoic relief. By Late Jurassic, almost all of the Tian Shan relief was thus flattened. Accordingly, even if a tectonic activity still occurred during the late Middle – early Late Jurassic, leading to the building of the Chemo uplift in the western part of the Junggar Basin for example (Lianhua et al., 2009; Yang et al., 2015; Gao et al., 2017), it stayed moderate and localized on the major tectonic structures. Meanwhile, west of the Talas Fergana/Karatau fault, this period marked the onset of a post rift phase dominated by thermal subsidence following extension in the Caspian – Turan – Kazakh domains (Thomas et al., 1999; Brunet et al., 2017; Mordvintev et al., 2017). Thermal subsidence also occurred in the South Turgay and Fergana basins (Clarke, 1984; Moseley and Tsimmer, 2000; Alexeiev et al., 2017).

5. 4. A LATE JURASSIC – EARLY CRETACEOUS EVOLUTIONCONTROLLED BY FAR-FIELD COLLISION AND CLIMATE

The Late Jurassic - Early Cretaceous transition corresponds to a period of renewed transpression and localized uplift in the Tian Shan area (this study; Hendrix et al., 1992; Eberth et al., 2001; Vincent et al., 2001; De Grave et al., 2007, 2012, 2013; Yang et al., 2015; Tang et al., 2015; Glorie and De Grave., 2016; Nachtergaele et al., 2018). Throughout the region, this period is marked by a sharp change in depositional environments with the emplacement of alluvial fan systems in the adjacent Junggar, Turfan, Tarim and Fergana basins. Along the Junggar Basin margins, the presence of angular unconformities at the base of conglomerate deposits indicates that tectonic movements occurred during this period (Hendrix et al., 1992; Eberth et al., 2001; Vincent et al., 2001). Meanwhile, the Chemo-uplift reached its peak stage leading to the formation of a widespread paleorelief within the basin (Lianhua et al., 2009; Yang et al., 2015; Gao et al., 2017). Similarly, in the Fergana Basin, the presence of an angular unconformity sealed by alluvial fan systems at the Jurassic-Cretaceous transition suggests that some tectonic movements occurred (De Pelsmaeker et al., 2018). Finally, Late Jurassic-Early Cretaceous compression has also been identified along the Talas Fergana/Karatau fault, since tectonic inversion and deformation have been described in the South Turgay (Yin et al., 2012), Leontiev (Allen et al., 2001) and Yarkand-Fergana basins (De Pelsmaeker et al., 2018). However, if episodes of deformations have been reported in the Tian Shan region, numerous large-scale, pre-orogenic planation surfaces have been preserved throughout the Tian Shan Range (e.g., Burbank et al., 1999; De Grave et al., 2011; Jolivet et al., 2010; Jolivet, 2017). In the western Tian Shan, Upper Cretaceous strata overlying perfectly flat surfaces imply that no high relief existed in this region during the Early Cretaceous. Meanwhile, low temperature thermochronology data identified localized Late Jurassic –Early Cretaceous cooling event in the Kyrgyz Tian Shan Range suggesting only

restricted relief building (De Grave et al., 2007, 2012, 2013; Glorie et al., 2011; Glorie and De Grave., 2016; Nachtergaele et al., 2018). However, despite, the lack of strong relief build up, this period is characterized by the emplacement of extensive alluvial fan systems in the basins surrounding the range (Fig. 15). Their development could be also strongly controlled by the contemporaneous climate aridification affecting this region (Jolivet at al., 2017a).

To the west of the Tian Shan area, a Late Jurassic – Early Cretaceous phase of tectonic deformation associated to the accretion of the Helmand Block also affected the Caspian – Turan –Kazakh domains and led to the inversion of the southern basins of Central Iran and Central Afghanistan (Brunet et al., 2017). This deformation event also induced uplift within the Amu-Darya Basin (Brunet et al., 2017) and up to the North Ustyurt Basin (Otto, 1997).

Based on the concordant ages of these events, we suggest that the Late Jurassic – Early Cretaceous tectonic activity and the renewed localized relief building observed in the Tian Shan area was mainly related to the accretion of the Helmand Block to the south-west, and possibly to the onset of accretion of the Lhasa Block along the southwestern margin of Eurasia. This could also explain why stronger relief building occurred in the western part of the Tian Shan compared to its eastern part.

6. CONCLUSIONS:

Using both detailed field analysis conducted on the Chinese Tian Shan region and previously published data we reconstructed the Jurassic paleogeographical evolution of the Tian Shan region.

Following a Late Triassic – Early Jurassic period of relief build-up, the Early to early Middle Jurassic topographic evolution of the Tian Shan Range was dominated by the progressive planation of this previously established relief, locally interrupted by discreet topographic rejuvenations. Throughout the region, the contemporaneous sedimentation was

1100 characterized by alluvial to lacustrine deposits settled under rather humid conditions.
1101 Sediment by-pass dominated to the north-west and south-west of the range, in the Chu-
1102 Sarysu, Yili-Balkhash and west Tarim basins. The Early to early Middle Jurassic was also
1103 marked by recurrent limited deformation events recorded within the basins surrounding the
1104 range and associated with both strike-slip and compressive tectonics. These episodes of
1105 deformation cannot be explained by the Qiangtang collision but could instead, be associated
1106 to the coeval subduction-related extension affecting the Caspian - Turan domains to the west
1107 of the Tian Shan area. During the late Middle to early Late Jurassic, the planation of the
1108 Paleozoic – early Mesozoic Tian Shan Range continued with contemporaneous fine-grained
1109 sediments being deposited in distal alluvial to lacustrine environments throughout the area,
1110 except to the north-west and south-west where sediment by-pass still prevailed. During that
1111 period, a drastic climate change occurred across the entire Tian Shan region, shifting from
1112 humid conditions during the late Middle Jurassic to more semi-arid conditions during the Late
1113 Jurassic. At that time, relatively few evidences of deformation exist in the Tian Shan. Further
1114 west, the tectonic evolution is marked by the onset of a post-rift phase dominated by thermal
1115 subsidence following the extension in the Caspian - Turan domains, and up to the South
1116 Turgay and Fergana basins.

1117 By Late Jurassic, almost all of the Tian Shan relief was flattened. The Late Jurassic –
1118 Early Cretaceous transition was then marked by a tectonic reactivation leading to localized
1119 relief building in the Tian Shan and to the deposit of coarse-grained proximal alluvial
1120 sediments. Contemporaneously, the sediment by-pass and erosion extended within and around
1121 the range. In addition, the Late Jurassic – Early Cretaceous transition was characterized by the
1122 climax of the aridification trend prevailing since the early Late Jurassic. This aridification
1123 trend also played a major role in the Late Jurassic - Early Cretaceous paleogeography of the
1124 Tian Shan. At that time, renewed deformation and uplift occurred in the Tian Shan area from
1125 west to east, leading to the inversion of the Yarkand–Fergana Basin and to the formation of

localized relief builds up. We propose that this renewed transpressive deformation phase was mainly related to the coeval accretion of the Helmand Block to the south-west, and possibly to the onset of the accretion of the Lhasa Block along the southwestern margin of Eurasia.

AKNOWLEDGMENTS

This work was supported by the Darius program. The work of Laurie Barrier for this publication is the IPGP contribution #3933. We want to thank S. Schneider for his expertise on the bivalves of the Badoawan Fm, S. Vincent for constructive discussions and anonymous reviewers for these constructive comments which improved the original version of the manuscript.

REFERENCES

Alexeiev D.V., Biske Yu.S., Wang Bo, Djenchuraeva A.V., Getman O.F., Aristov V.A., Kröner A., Liu H.S., Zhong L.L., 2015. Tectono-stratigraphic framework and Palaeozoic evolution of the Chinese South Tianshan. Geotectonics 49 (2), 93–122

Alexeiev, D.V., Bykadorov, V.A., Volozh, Yu.A., Sapozhnikov, R.B., 2017. Kinematic analysis of Jurassic grabens of Southern Turgai and the role of the Mesozoic stage in the evolution of the Karatau–Talas–Ferghana strike-slip fault, Southern Kazakhstan and Tian Shan. Geotectonics, 51 (2), 105–120.

Alexeiev, D. V., Cook, H. E., Djenchuraeva, A. V., Mikolaichuk, A. V., 2017b. The stratigraphic, sedimentological and structural evolution of the southern margin of the Kazakhstan continent in the Tien Shan Range during the Devonian to Permian. In: Brunet, M.F., McCann, T. Sobel, E. R. (Eds.), Geological Evolution of Central Asian Basins and the Western Tien Shan Range. Geological Society, London, Special Publications, 427.

1151 Allegre, C. O., Courtillot, V., Tapponnier, P., Hirn, A., Mattauer, M., Coulon, C., ... and Burg,
1152 J. P., 1984. Structure and evolution of the Himalaya–Tibet orogenic belt. Nature, 307(5946),
1153 17.

1154 Allen, M. B., and Natal'in, B. A., 1995. Junggar, Turfan and Alakol basins as Late Permian
1155 to? Early Triassic extensional structures in a sinistral shear zone in the Altaid orogenic
1156 collage, Central Asia. Journal of the Geological Society, 152 (2), 327-338.

1157 Allen, M.B., Windley, B.F., Chi, Z., Zhong-Yan, Z., Guang-Rei, W., 1991. Basin evolution
1158 within and adjacent to the Tien Shan Range, NW China. Journal of Geological Society,
1159 London, 148, 369-378.

1160 Allen, M.B., Alsop, G.I., Zhemchuzhnikov, V.G., 2001. Dome and basin refolding and
1161 transpressive inversion along the Karatau fault System, southern Kazakstan. Journal of the
1162 Geological Society of London, 158, 83–95.

1163 Al-Qaraafi, F. A., and Guangqing, Y., 2013. Sand Body Description for Upper Sangonghe
1164 Formation (Early Jurassic), Baolang Oilfield, Yanqi Basin Northwest China. International
1165 Journal of Chemical Engineering and Applications, 4 (1), 26.

1166 Ashraf, A. R., Sun, Y., Sun, G., Uhl, D., Mosbrugger, V., Li, J., Herrmann, M., 2010. Triassic
1167 and Jurassic palaeoclimate development in the Junggar Basin, Xinjiang, Northwest China - a
1168 review and additional lithological data. Palaeobiodiversity and Palaeoenvironments, 90 (3),
1169 187-201.

1170 Atlas of Geological Maps of Central Asia and Adjacent Areas (AGMCA). Geological Map 1:
1171 2 500 000, Beijing: Geological Publishing House, 2008.

1172 Avouac, J. P., Tapponnier, P., Bai, M., You, H., Wang, G., 1993. Active Thrusting and
1173 Folding Along the Northern Tien Shan and Late Cenozoic Rotation of the Tarim Relative to
1174 Dzungaria and Kazakhstan. Journal of Geophysical. Research, 98**,** 6755–6804.

1175 Bande, A., Radjabov, S., Sobel, E. R., Sim, T., 2015. Cenozoic palaeoenvironmental and
1176 tectonic controls on the evolution of the northern Fergana Basin. Geological Society London,
1177 Special Publications, 427.

1178 Bazhenov M.L., Burtman V.S., Dvorova A.V., 1999. Permian paleomagnetism of the Tien
1179 Shan fold belt, Central Asia: post-collisional rotations and deformation. Tectonophysics 312,
1180 303-329.

1181 Bazhenov M.L. and Mikolaichuk A.V., 2004. Structural evolution of Central Asia to the north
1182 of Tibet: a synthesis of paleomagnetic and geological data. Geotectonics 38 (5), 379-393.

1183 Bian, W., Hornung, J., Liu, Z., Wang, P., Hinderer, M., 2010. Sedimentary and
1184 palaeoenvironmental evolution of the Junggar Basin, Xinjiang, Northwest China.
1185 Palaeobiology Palaeoenvironment, 90, 175–186.

1186 Blair, T. C. and McPherson, J. G., 1994. Alluvial fans and their natural distinction from rivers
1187 based on morphology, hydraulic processes, sedimentary processes and facies assemblages.
1188 Journal of Sedimentary Research, 64, 450–489.

1189 Brookfield, M. E., and Hashmat, A., 2001. The geology and petroleum potential of the North
1190 Afghan platform and adjacent areas (northern Afghanistan, with parts of southern
1191 Turkmenistan, Uzbekistan and Tajikistan). Earth-Science Reviews, 55(1), 41-71.

1192 Brunet, M. F., Korotaev, M. V., Ershov, A. V., Nikishin, A. M., 2003. The South Caspian
1193 Basin: a review of its evolution from subsidence modelling. Sedimentary Geology, 156 (1),
1194 119-148.

1195 Brunet, M. F., Ershov, A. V., Korotaev, M. V., Melikhov, V. N., Barrier, E., Mordvintsev, D.
1196 O., Sidorova, I. P., 2017. Late Palaeozoic and Mesozoic evolution of the Amu Darya Basin
1197 (Turkmenistan, Uzbekistan). Geological Society, London, Special Publications, 427 (1), 89-
1198 144.

1199 Burbank, D. W., McLean, J. K., Bullen, M., Abdrakhmatov, K. Y., Miller, M. M., 1999.
1200 Partitioning of intermontane basins by thrust-related folding, Tien Shan, Kyrgyzstan. Basin
1201 Research, 11(1), 75-92.

1202 Burtman, V. S. (1980). Faults of middle Asia. American Journal of Science, 280 (8), 725-744.

1203 Buslov, M. M., Fujiwara, Y., Iwata, K., and Semakov, N. N., 2004. Late paleozoic-early
1204 Mesozoic geodynamics of Central Asia. Gondwana Research, 7(3), 791-808.

1205 Carroll, A. R., Yunhai, L., Graham, S. A., Xuchang, X., Hendrix, M. S., Jinchi, C., McKnight,
1206 C. L., 1990. Junggar basin, northwest China: trapped Late Paleozoic ocean. Tectonophysics,
1207 181 (1), 1-14.

1208 Carroll, A. R., Graham, S. A., Hendrix, M. S., Ying, D., Zhou, D., 1995. Late Paleozoic
1209 tectonic amalgamation of northwestern China: sedimentary record of the northern Tarim,
1210 northwestern Turpan, and southern Junggar basins. Geological Society of America Bulletin,
1211 107 (5), 571-594.

1212 Charvet, J., Shu, L., Laurent-Charvet, S., Wang, B., Faure, M., Cluzel, D., Chen, Y., De Jong,
1213 K., 2011, Palaeozoic tectonic evolution of the Tianshan belt, NW China: Science China Earth
1214 Sciences, 54 (2), 166-184.

1215 Charvet, J., Shu, L. S., Laurent-Charvet, S., 2007. Paleozoic structural and geodynamic
1216 evolution of eastern Tianshan (NW China): welding of the Tarim and Junggar plates.
1217 Episodes Journal of International Geoscience, 30 (3), 162-186.

1218 Chen, C., Lu, H., Jia, D., Cai, D., Wu, S., 1999. Closing history of the southern Tianshan
1219 oceanic basin, western China: an oblique collisional orogeny. Tectonophysics, 302, 23–40.

1220 Clarke, J.W., 1984. Geology and possible uranium deposits of the Fergana region of Soviet
1221 Central Asia: United States Geological Survey Open-File Report, 84-513.

1222 Cogné, J. P., Kravchinsky, V. A., Halim, N., Hankard, F., 2005. Late Jurassic-Early
1223 Cretaceous closure of the Mongol-Okhotsk Ocean demonstrated by new Mesozoic
1224 palaeomagnetic results from the Trans-Baikal area (SE Siberia). Geophysical Journal
1225 International, 163(2), 813-832.

1226 Daoudene, Y., Gapais, D., Ledru, P., Cocherie, A., Hocquet, S., Donskaya, T. V., 2009. The
1227 Ereendavaa Range (north-eastern Mongolia): an additional argument for Mesozoic extension
1228 throughout eastern Asia. International Journal of Earth Sciences, 98 (6), 1381-1393.

1229 Daoudene, Y., Gapais, D., Cogné, J. P., Ruffet, G., 2017. Late Jurassic–Early Cretaceous
1230 continental extension in northeast Asia–Relationships to plate kinematics. Bulletin de la
1231 Société géologique de France, 188 (1-2), 1-16.

1232 De Grave, J., Buslov, M.M., Van den haute, P., 2007. Distant effects of India-Eurasia
1233 convergence and Mesozoic intracontinental deformation in Central Asia: Constraints from
1234 apatite fission-track thermochronology. Journal of Asian Earth Sciences, 29, 188-204.

1235 De Grave, J., Glorie, S., Buslov, M. M., Izmer, A., Fournier-Carrie, A., Batalev, V. Y.,
1236 Vanhaecke, F., Elburg, M., Van den haute, P., 2011. The thermo-tectonic history of the Song-
1237 Kul plateau, Kyrgyz Tien Shan: constraints by apatite and titanite thermochronometry and
1238 zircon U/Pb dating. Gondwana Research, 20, 4, 745-763

1239 De Grave, J., Glorie, S., Ryabinin, A., Zhimulev, F. Izmer, A., Buslov, M.M., Elburg, M.,
1240 Vanhaeke, F., Van den haute, P., 2012. Late Palaeozoic and Meso-Cenozoic tectonic

evolution of the Southern Kyrgyz Tien Shan: constraints from multi-method thermochronology in the Trans-Alai, Turkestan-Alai Section and the Southeastern Ferghana Basin. Journal of Asian Earth Sciences, 44, 149-168.

De Grave, J., Glorie, S., Buslov, M. M., Stockli, D. F., McWilliams, M. O., Batalev, V. Y., 2013. Thermo-tectonic history of the Issyk-Kul basement (Kyrgyz northern Tien Shan, Central asia). Gondwana Research, 23 (3), 998-1020.

Deng, S., Yuanzhzen, L., Ru, F., Yanhong, P., Xiansheng, C., Guobin, F., Qifei, W., Huazhang, P., Yanbin, S., Yaqiong, W., Haichun, Z., Chengkai, J., Wenzhe, D., Linhao, F., 2010. The Jurassic System of Northern Xinjiang, China. University of Science and Technology of China Press, 279 pp.

Dengfa, H., Xinfa, C., Kuang, J., Lu, Z., Yong, T., Deguang, L., 2008. Development and genetic mechanism of Chepaizi-Mosuowan uplift in Junggar Basin, China. Earth Science Frontiers, 15 (4), 42-55.

De Pelsmaeker, E., Jolivet, M., Laborde, A., Poujol, M., Robin, C., Zhimulev, F. I., Nachtergaele, S., Glorie, S., De Clercq, S., Batalev, V. Y., De Grave, J., 2018. Source-to-sink dynamics in the Kyrgyz Tien Shan from the Jurassic to the Paleogene: Insights from sedimentological and detrital zircon U-Pb analyses. Gondwana Research, 54, 180-204.

Desheng, L., Digang, L., Chengzao, J., Gang, W., Qizhi, W., Dengfa, H., 1996. Hydrocarbon accumulations in the Tarim basin, China. AAPG bulletin, 80 (10), 1587-1603.

Donskaya, T. V., Windley, B. F., Mazukabzov, A. M., Kröner, A., Sklyarov, E. V., Gladkochub, D. P., ... and Hegner, E., 2008. Age and evolution of late Mesozoic metamorphic core complexes in southern Siberia and northern Mongolia. Journal of the Geological Society, 165 (1), 405-421.

Donskaya, T. V., Gladkochub, D. P., Mazukabzov, A. M., Ivanov, A. V., 2013. Late Paleozoic–Mesozoic subduction-related magmatism at the southern margin of the Siberian continent and the 150 million-year history of the Mongol-Okhotsk Ocean. Journal of Asian Earth Sciences, 62, 79-97.

Dumitru, T. A., Zhou, D., Chang, E. Z., Graham, S. A., Hendrix, M. S., Sobel, E. R., Carroll, A. R., 2001. Uplift, exhumation, and deformation in the Chinese Tian Shan: Memoirs-Geological Society of America 114, 71-100.

Eberth, D.A., Brinkman, D.B., Chen, P.-J., Yuan, F.-T., Wu, S.-Z., Li, G., Cheng, X.-S., 2001. Sequence stratigraphy, paleoclimate patterns, and vertebrate fossil preservation in Jurassic-Cretaceous strata of the Junggar Basin, Xinjiang Autonomous Region, People's Republic of China. Canadian Journal of Earth Sciences, 38(12), 1627-1644.

Enkin, R. J., Courtillot, V., Leloup, P., Yang, Z., Xing, L., Zhang, J., Zhuang, Z., 1992. The paleomagnetic record of uppermost Permian, Lower Triassic rocks from the south China block. Geophysical research letters, 19(21), 2147-2150.

Fedorenko, O.A., Miletenko, N.V. (Coordinators) 2002. Atlas of the lithology-paleogeographical, structural, palinspastic and geo-environmental maps of Central Eurasia. Center for geoinformation support of the military forces of Kazakhstan Republic, Almaty.

Feng, Y., Jiang, S., Wang, C., 2015. Sequence stratigraphy, sedimentary systems and petroleum plays in a low-accommodation basin: Middle to upper members of the Lower Jurassic Sangonghe Formation, Central Junggar Basin, Northwestern China. Journal of Asian Earth Sciences, 85-103.

Gao, J., Li, M., Xiao, X., Tang, Y., He, G., 1998. Paleozoic tectonic evolution of the Tianshan orogen, northwestern China. Tectonophysics, 287, 213–231.

1287 Gao, C., Ji, Y., Ren, Y., Zhou, Y., Jin, J., Zhang, L., Li, Z., Zhou, Y., Wu, H., 2017.
1288 Geomorphology and sedimentary sequence evolution during the buried stage of paleo-uplift in
1289 the Lower Cretaceous Qingshuihe Formation, Junggar Basin, northwestern China:
1290 Implications for reservoir lithofacies and hydrocarbon distribution. Marine and Petroleum
1291 Geology, 86, 1224-1251.

1292 Glorie, S., De Grave, J., Buslov, M. M., Zhimulev, F. I., Stockli, D. F., Batalev, V. Y., Izmer,
1293 A., Van den Haute, P., Vanhaecke, F., Elburg, M. A., 2011. Tectonic history of the Kyrgyz
1294 South Tien Shan (Atbashi-Inylchek) suture zone: The role of inherited structures during
1295 deformation-propagation. Tectonics, 30, 6.

1296 Glorie, S. and De Grave, J., 2016. Exhuming the Meso-Cenozoic Kyrgyz Tienshan and
1297 Siberian Altai-Sayan: A review based on low-temperature thermochronology. Geoscience
1298 Frontiers, 7, 155-170.

1299 Graham, S. A., Hendrix, M. S., Johnson, C. L., Badamgarav, D., Badarch, G., Amory, J., ...
1300 and Hacker, B. R. ,2001. Sedimentary record and tectonic implications of Mesozoic rifting in
1301 southeast Mongolia. Geological Society of America Bulletin, 113 (12), 1560-1579.

1302 Greene, T. J., Carroll, A. R., Hendrix, M. S., Graham, S. A., Wartes, M. A., Abbink, O. A.,
1303 2001. Sedimentary record of Mesozoic deformation and inception of the Turpan-Hami basin,
1304 northwest China. MEMOIRS-GEOLOGICAL SOCIETY OF AMERICA, 317-340.

1305 Hasiotis, S. T., 2006. Continental Trace Fossils. Society of Economic Paleontologists and
1306 Mineralogists (SEPM), Short Courses, 51.

1307 Hasiotis, S. T., Kraus, M. J., Demko, T. M., 2007. Climatic controls on continental track
1308 fossils. In: Miller, W. (Eds.) Trace Fossils Concepts, Problems, Prospects. Elsevier, Berlin,
1309 172–195.

1310 Heilbronn, G., Boulvais, P., Marchand, E., Robin, C., Bourquin, S., Barrier, L., Jia, Y., Fu, B.,
1311 Jolivet, M., 2015. Stable isotope characterization of pedogenic and lacustrine carbonates from
1312 the Chinese Tian Shan: constraints on the Mesozoic–Lower Cenozoic palaeoenvironmental
1313 evolution. Chemie der Erde-Geochemistry, *75* (1), 133-141.

1314 Hendrix, M. S., Graham, S. A., Carroll, A., Sobel, E., McKnight, C., Schulein, B., Wang, Z.,
1315 1992. Sedimentary record and climatic implications of recurrent deformation in the Tian
1316 Shan: evidence from Mesozoic strata of the north Tarim, south Dzungar, and Turpan basin,
1317 northwest China: Geological Society of America Bulletin, 104, 53–79.

1318 Huang, W. L., Yang, X. P., Li, A., Pierce, I. K., Thompson, J. A., Angster, S. J., Zhang, L.,
1319 2015. Late Pleistocene shortening rate on the northern margin of the Yanqi Basin,
1320 southeastern Tian Shan, NW China. Journal of Asian Earth Sciences, 112, 11-24.

1321 Hunter, R. E., 1977. Basic types of stratification in small eolian dunes. Sedimentology, 24,
1322 361–387.

1323 Jia, Y., Fu, B., Jolivet, M., Zheng, S., 2015. Cenozoic tectono-geomorphological growth of
1324 the SW Chinese Tian Shan: Insight from AFT and detrital zircon U-Pb data. Journal of Asian
1325 Earth Sciences, 111, 395-413.

1326 Ji, H., Tao, H., Wang, Q., Qiu, Z., Ma, D., Qiu, J., Liao, P., 2017. Early to Middle Jurassic
1327 tectonic evolution of the Bogda Mountains, Northwest China: Evidence from sedimentology
1328 and detrital zircon geochronology. Journal of Asian Earth Sciences.

1329 Johnson, C. L., 2004. Polyphase evolution of the East Gobi basin: sedimentary and structural
1330 records of Mesozoic–Cenozoic intraplate deformation in Mongolia. Basin Research, 16 (1),
1331 79-99.

1332 Jolivet, M., Dominguez, S., Charreau, J., Chen, Y., Li, Y., Wang, Q., 2010. Mesozoic and
1333 Cenozoic tectonic history of the Central Chinese Tian Shan: reactivated tectonic structures
1334 and active deformation: Tectonics, 29, TC 6019.

1335 Jolivet, M., Bourquin, S., Heilbronn, G., Robin, C., Barrier, C., Dabard, M.-P., Jia, Y., De
1336 Pelsmaeker, E., Fu, B., 2017a. The Upper Jurassic–Lower Cretaceous alluvial-fan deposits of
1337 the Kalaza Formation (Central Asia): tectonic pulse or increased aridity? In: Brunet, M.F.,
1338 McCann, T. Sobel, E. R. (Eds.), Geological Evolution of Central Asian Basins and the
1339 Western Tien Shan Range. Geological Society, London, Special Publications, 427.

1340 Jolivet, M., Arzhannikova, A., Frolov, A., Arzhannikov, S., Kulagina, N., Akulova, V.,
1341 Vassallo, R., 2017b. Late Jurassic-Early Cretaceous paleoenvironmental evolution of the
1342 Transbaikal basins (SE Siberia): implications for the Mongol-Okhotsk orogeny. Bulletin de la
1343 Société géologique de France, 188(1-2), 1-22.

1344 Jolivet, M., 2017c. Mesozoic tectonic and topographic evolution of Central Asia and Tibet: a
1345 preliminary synthesis. Geological Society, London, Special Publications, 427 (1), 19-55.

1346 Kapp, P., DeCelles, P. G., Gehrels, G. E., Heizler, M., Ding, L., 2007. Geological records of
1347 the Lhasa-Qiangtang and Indo-Asian collisions in the Nima area of central Tibet. Geological
1348 Society of America Bulletin, 119 (7-8), 917-933.

1349 Klappa, C.F., 1980. Rhizolites in terrestrial carbonates: classification, recognition, genesis and
1350 significance. Sedimentology, 27, 613–627.

1351 Kocureck, G. and Nielson, J. 1986. Conditions favourable for the formation of warm-climate
1352 aeolian sand sheets. Sedimentology, 33, 795–816.

1353 Kraus, M.J., 1999. Paleosols in clastic sedimentary rocks: their geologic applications. Earth
1354 Science Reviews, 47, 41–70.

1355 Lasovskiy A. G., Mozolev L. N., 1961. Geology map of USSR, sheet K 43-XXI, scale 1:200
1356 000, Northern Tian-Shan series.

1357 Laurent-Charvet, S., Charvet, J., Shu, L., Ma, R., Lu, H., 2002. Palaeozoic late collisional
1358 strike-slip deformations in Tianshan and Altay, Eastern Xinjiang, NW China. Terra Nova, 14
1359 (4), 249-256.

1360 Lee, K. Y., 1985a, Geology of the petroleum and coal deposits in the Junggar (Zhungaer)
1361 basin, Xinjiang Uygur Zizhiqu, northwest China: U.S. Geological Survey Open-File Report
1362 85-0230, p. 53.

1363 Lee, K. Y., 1985b, Geology of the Tarim basin with special emphasis on petroleum deposits,
1364 Xinjiang Uygur Zizhiqu, northwest China: U.S. Geological Survey Open-File Report 85-616,
1365 p. 55.

1366 Le Heron, D. P., Buslov, M. M., Davies, C., Richards, K., Safonova, I., 2008. Evolution of
1367 Mesozoic fluvial systems along the SE flank of the West Siberian Basin, Russia. Sedimentary
1368 Geology, 208 (1-2), 45-60.

1369 Lianhua, H., Jinghong, W., Kuang, L., Zhang, G., Lei, L. I. U., Kuang, J., 2009. Provenance
1370 sediments and its exploration significance—A case from member 1 of Qingshuihe formation
1371 of Lower Cretaceous in Junggar Basin. Earth Science Frontiers, 16 (6), 337-348.

1372 Li, Z., Song, W., Peng, S., Wang, D., Zhang, Z., 2004. Mesozoic–Cenozoic tectonic
1373 relationships between the Kuqa subbasin and Tian Shan, northwest China: constraints from
1374 depositional records. Sedimentary Geology, 172 (3), 223-249.

1375 Li, Z., Peng, S., 2010. Detrital zircon geochronology and its provenance implications:
1376 responses to Jurassic through Neogene basin-range interactions along northern margin of the
1377 Tarim Basin, Northwest China. Basin Research, 22, 126-138.

1378 Li, B., Zhuang, X., Li, J., Zhao, S., 2014. Geological controls on coal quality of the Yili
1379 Basin, Xinjiang Northwest China. International Journal of Coal Geology, 131, 186-199.

1380 Li, D., He, D., Tang, Y., Wu, X., Lian, Y., Yang, Y., 2015. Dynamic processes from plate
1381 subduction to intracontinental deformation: Insights from the tectono-sedimentary evolution
1382 of the Zhaosu–Tekesi Depression in the southwestern Chinese Tianshan. Journal of Asian
1383 Earth Sciences, 113, 728-747.

1384 Lin, B., Zhang, X., Xu, X., Yuan, J., Neng, Y., Zhu, J., 2015. Features and effects of
1385 basement faults on deposition in the Tarim Basin. Earth-Science Reviews, 145, 43-55.

1386 Lin, C., Yang, H., Liu, J., Rui, Z., Cai, Z., Zhu, Y., 2012. Distribution and erosion of the
1387 Paleozoic tectonic unconformities in the Tarim Basin, Northwest China: significance for the
1388 evolution of paleo-uplifts and tectonic geography during deformation. Journal of Asian Earth
1389 Sciences, 46, 1-19.

1390 Liu, D., Jolivet, M., Yang, W., Zhang, Z., Cheng, F., Bei, Z., Guo, Z., 2013. Latest Paleozoic–
1391 Early Mesozoic basin–range interactions in South Tian Shan (northwest China) and their
1392 tectonic significance: Constraints from detrital zircon U–Pb ages. Tectonophysics, 599, 197-
1393 213.

1394 Liu, D., Guo, Z., Jolivet, M., Cheng, F., Song, Y., Zhang, Z., 2014. Petrology and
1395 geochemistry of Early Permian volcanic rocks in South Tian Shan, NW China: implications
1396 for the tectonic evolution and Phanerozoic continental growth. International Journal of Earth
1397 Sciences, 103 (3), 737-756.

1398 Liu D., Cheng F., Guo Zh., Jolivet M., Song Y., 2015. Lahar facies of the latest Paleozoic
1399 Arbasay Formation: Geomorphological characters and paleoenvironment reconstruction of
1400 Northern Tian Shan, NW China. Journal of Asian Earth Sciences, 113, 282-292.

1401 Liu, Y. J., Neubauer, F., Genser, J., Ge, X. H., Takasu, A., Yuan, S. H., Chang, L. H., Li, W.
1402 M., 2007. Geochronology of the initiation and displacement of the Altyn Strike-Slip Fault,
1403 western China. Journal of Asian Earth Sciences, 29 (2-3), 243-252.

1404 Ma, D., He, D., Li, D., Tang, J., Liu, Z., 2015. Kinematics of syn-tectonic unconformities and
1405 implications for the tectonic evolution of the Hala'alat Mountains at the northwestern margin
1406 of the Junggar Basin, Central Asian Orogenic Belt. Geoscience Frontiers, 6 (2), 247-264.

1407 Macaulay, E. A., Sobel, E. R., Mikolaichuk, A., Kohn, B., Stuart, F. M., 2014. Cenozoic
1408 deformation and exhumation history of the Central Kyrgyz Tien Shan. Tectonics, 33 (2), 135-
1409 165.

1410 Mattauer, M., Malavieille, J., Calassou, S., Lancelot, J., Roger, F., Hao, Z. W., ... and Hou, L.
1411 W., 1992. The Songpan-Garze Triassic belt of west Sechuan and eastern Tibet: A decollement
1412 fold belt on passive margin. Comptes rendu de l'Académie des sciences. Serie II, 314 (6),
1413 619-626.

1414 Matte, P., Tapponnier, P., Arnaud, N., Bourjot, L., Avouac, J. P., Vidal, P., Qing, L.,
1415 Yusheng, P., Yi, W., 1996. Tectonics of Western Tibet, between the Tarim and the Indus.
1416 Earth and Planetary Science Letters, 142 (3-4), 311-330.

1417 Metcalfe, I., 2013. Gondwana dispersion and Asian accretion: tectonic and palaeogeographic
1418 evolution of eastern Tethys. Journal of Asian Earth Sciences, 66, 1-33.

1419 Miall, A. D., 1978. Lithofacies types and vertical profile models in braided river deposits: a
1420 summary. In: Miall, A. D. (Eds.) Fluvial Sedimentology. Canadian Society Petroleum
1421 Geology, Memoirs, 5, 597–604.

1422 Miall, A. D., 1996. The Geology of Fluvial Deposits. Springer, Berlin, 582 p.

1423 Moisan, P., Voigt, S., Pott, C., Buchwitz, M., Schneider, J. W., Kerp, H., 2011. Cycadalean
1424 and bennettitalean foliage from the Triassic Madygen Lagerstätte (SW Kyrgyzstan, central
1425 Asia). Review of Palaeobotany and Palynology, 164 (1), 93-108.

1426 Molnar, P., Tapponnier, P., 1975. Cenozoic tectonics of Asia: effects of a continental
1427 collision: features of recent continental tectonics in Asia can be interpreted as results of the
1428 India-Eurasia collision. Science, 189, 419–426.

1429 Mordvintsev, D., Barrier, E., Brunet, M. F., Blanpied, C., Sidorova, I., 2017. Structure and
1430 evolution of the Bukhara-Khiva region during the Mesozoic: the northern margin of the Amu-
1431 Darya Basin (southern Uzbekistan). Geological Society, London, Special Publications, 427,
1432 SP427-16.

1433 Moseley, B. A., and Tsimmer, V. A., 2000. Evolution and hydrocarbon habitat of the South
1434 Turgay Basin, Kazakhstan. Petroleum Geoscience, 6 (2), 125-136.

1435 Mulder, T., and Alexander, J., 2001. The physical character of subaqueous sedimentary
1436 density flows and their deposits. Sedimentology, 48 (2), 269-299.

1437 Nachtergaele, S., De Pelsmaeker, E., Glorie, S., Zhimulev, F., Jolivet, M., Danišík, M.,
1438 Buslov, M.M., De Grave, J., 2018. Meso-Cenozoic tectonic evolution of the Talas-Fergana
1439 region of the Kyrgyz Tien Shan revealed by low-temperature basement and detrital
1440 thermochronology, Geoscience Frontiers, doi: 10.1016/j.gsf.2017.11.007.

1441 Nikishin, A. M., Cloetingh, S. A. P. L., Brunet, M. F., Stephenson, R. A., Bolotov, S. N.,
1442 Ershov, A. V., 1998. Scythian platform, Caucasus and Black Sea region: Mesozoic–Cenozoic
1443 tectonic history and dynamics. Peri-Tethys Memoir, 3, 163-176.

1444 Novikov, I. S., 2013. Reconstructing the stages of orogeny around the Junggar basin from the
1445 lithostratigraphy of Late Paleozoic, Mesozoic, and Cenozoic sediments. Russian Geology and
1446 Geophysics, 54(2), 138-152.

1447 Otto, S. C., 1997. Mesozoic-Cenozoic history of deformation and petroleum systems in
1448 sedimentary basins of Central Asia; implications of collisions on the Eurasian margin.
1449 Petroleum Geoscience, 3 (4), 327-341.

1450 Pan, Y., Sha, J., Wang, Y., Zhang, X., Yao, X., Peng, B., Rao, X., 2012. The brackish-water
1451 bivalve *Waagenoperna* from the Lower Jurassic Badaowan Formation of the Junggar Basin
1452 and its palaeoenvironmental and palaeogeographic significance. Geoscience Frontiers, 4, 95–
1453 103

1454 Postma, G., 1990. Depositional architecture and facies of river and fan deltas: a synthesis. In:
1455 Collela, A., Prior, D. B. (Eds.), Coarse-grained deltas. International Association of
1456 Sedimentologists, Special Publications, 10, 13-27.

1457 Qin, K., Su, B. X., Sakyi, P. A., Tang, D. M., Li, X. H., Sun, H., Xiao, Q. H., Liu, P. P., 2011.
1458 SIMS zircon U-Pb geochronology and Sr-Nd isotopes of Ni-Cu-Bearing Mafic-Ultramafic
1459 Intrusions in Eastern Tianshan and Beishan in correlation with flood basalts in Tarim Basin
1460 (NW China): Constraints on a ca. 280 Ma mantle plume. American Journal of Sciences 311,
1461 237–260.

1462 Qiu, N. S., Zha, M.,Wang, X. L., Yang, H. B., 2005. Tectono-thermal evolution of the
1463 Junggar Basin, NW China: constraints from Ro and apatite fission track modelling, Petrol.
1464 Geosci., 11, 361–372.

1465 Reid, A.J., Wilson, C.J.L., Liu, S., 2005. Structural evidence for the Permo-Triassic tectonic
1466 evolution of the Yidun arc, eastern Tibetan plateau. Journal of Structural Geology 27, 119–
1467 137.

1468 Retallack, G. J., 1997. A Colour Guide to Paleosols. John Wiley and Sons, Chichester,
1469 England.

1470 Retallack, G.J., 1988. Field recognition of palaeosols. In: Reinhardt, J., Sigleo,W.R. (Eds.),
1471 Palaeosols and Weathering through Geologic Time; Principles and Applications: Geological
1472 Society of America Special Papers, 216, 1–20.

1473 Ritts, B. D., Berry, A. K., Johnson, C. L., Darby, B. J., Davis, G. A., 2010. Early Cretaceous
1474 supradetachment basins in the Hohhot metamorphic core complex, Inner Mongolia, China.
1475 Basin Research, 22 (1), 45-60.

1476 Robert, A. M., Letouzey, J., Kavoosi, M. A., Sherkati, S., Müller, C., Vergés, J., Aghababaei,
1477 A., 2014. Structural evolution of the Kopeh Dagh fold-and-thrust belt (NE Iran) and
1478 interactions with the South Caspian Sea Basin and Amu Darya Basin. Marine and Petroleum
1479 Geology, 57, 68-87.

1480 Roger, F., Malavieille, J., Leloup, P.H., Calassou, S., Xu, Z., 2004. Timing of granite
1481 emplacement and cooling in the Songpan-Garzê fold belt (eastern Tibetan plateau) with
1482 tectonic implications. Journal of Asian Earth Sciences 22, 465–481.

1483 Roger, F., Jolivet, M., and Malavieille, J., 2010. The tectonic evolution of the Songpan Garze
1484 (North Tibet) and adjacent areas from Proterozoic to Present: a synthesis. Journal of Asian
1485 Earth Sciences, 39, 254-269.

1486 Roger, F., Jolivet, M., Cattin, R., Malavieille, J., 2011. Mesozoic-Cenozoic tectonothermal
1487 evolution of the eastern part of the Tibetan Plateau (Songpan-Garzê, Longmen Shan area):

1488 insights from thermochronological data and simple thermal modelling. Geological Society,
1489 London, Special Publications, 353(1), 9-25.

1490 Rolland, Y., Alexeiev, D., Kroner, A., Corsini, M., Loury, C., Monie, P., 2013. Late
1491 Palaeozoic to Mesozoic kinematic history of the Talas–Ferghana strike-slip fault (Kyrgyz
1492 West Tianshan) as revealed by 40Ar/39Ar dating of syn-kinematic white mica. Journal of
1493 Asian Earth Sciences, 67–68, 76–92.

1494 Schnyder, J., Pons, D., Yans, J., Tramoy, R., Abdulanova, S., 2016. Integrated stratigraphy of
1495 a continental Pliensbachian–Toarcian Boundary (Lower Jurassic) section at Taskomirsay,
1496 Leontiev Graben, southwest Kazakhstan. Geological Society, London, Special
1497 Publications, 427, SP427-15.

1498 Sengör, A.M.C., 1979. Tethys and its implications. Nature, 279 (14), 14.

1499 Sengör, A.M.C., Natal'in, B.A., Burtman, V.S., 1993. Evolution of the Altaid Tectonic
1500 Collage and Paleozoic Crustal Growth in Eurasia. Nature, 364 (6435), 299-307.

1501 Sengör, A. M. C., 1996. Paleotectonics of Asia: fragments of a synthesis. The tectonic
1502 evolution of Asia, 486-640.

1503 Sha, J., Vajda, V., Pan, Y., Larsson, L., Yao, X., Zhang, X., Wang, Y., Cheng, X., Jiang, B.,
1504 Deng, S., Chen, S., Peng, B., 2011. Stratigraphy of the Triassic–Jurassic boundary
1505 successions of the southern margin of the Junggar Basin, northwestern China. Acta Geologica
1506 Sinica, 85, 421-436.

1507 Sha, J., Wang, Y., Pan, Y., Yao, X., Rao, X., Cai, H., Zhang, X., 2016. Temporal and spatial
1508 distribution patterns of the marine–brackish-water bivalve *Waagenoperna* in China and its
1509 implications for climate and palaeogeography through the Triassic–Jurassic transition.
1510 Palaeogeography, Palaeoclimatology, Palaeoecology, 464, 43–50.

1511 Shao, L., Stattegger, K., Li, W., Haupt, B. J., 1999. Depositional style and subsidence history
1512 of the Turpan Basin (NW China). Sedimentary Geology, 128, 155–169.

1513 Shao, L., Zhang, P., Hilton, J., Gayer, R., Wang, Y., Zhao, C., Luo, Zh., 2003.
1514 Palaeoenvironments and Palaeogeography of the Lower and lower Middle Jurassic coal
1515 measures in the Turpan-Hami oil-prone coal basin, northwestern China. American
1516 Association of Petroleum Geology Bulletin, 87, 335–355.

1517 Shi, J., Jin, Z., Fan, T., Liu, Q., Zhang, F., Fan, X., 2016. Sequence development, depositional
1518 filling evolution, and prospect forecast in northern Aryskum Depression of South Turgay
1519 Basin, Kazakstan. Energy Exploration & Exploitation, 34 (4), 621-642.

1520 Sobel, E. R., 1999. Basin analysis of the Jurassic-Lower Cretaceous southwest Tarim Basin,
1521 northwest China. Geological Society of America Bulletin, 111 (5), 709-724.

1522 Sobel, E. R., Arnaud, N., Jolivet, M., Ritts, B. D., Brunei, M., 2001. Jurassic to Cenozoic
1523 exhumation history of theAltyn Tagh range, northwest China, constrained by 40Ar/39Ar and
1524 apatite fission track thermochronology. Paleozoic and Mesozoic tectonic evolution of central
1525 and eastern Asia, 194, 247.

1526 Sobel, E. R., Oskin, M., Burbank, D., Mikolaichuk, A., 2006. Exhumation of basement-cored
1527 uplifts: Example of the Kyrgyz Range quantified with apatite fission track thermochronology.
1528 Tectonics, 25 (2).

1529 Svendsen, J., Stollhofen, H., Krapf, C. B. E. Stanistreet, I. G., 2003. Mass and
1530 hyperconcentrated flow deposits record dune damming and catastrophic breakthrough of
1531 ephemeral rivers, Skeleton Coast Erg, Namibia. Sedimentary Geology, 160, 7–31.

1532 Tang, W., Zhang, Z., Li, J., Li, K., Chen, Y., Guo, Z., 2014. Late Paleozoic to Jurassic
1533 tectonic evolution of the Bogda area (northwest China): Evidence from detrital zircon U–Pb
1534 geochronology. Tectonophysics, 626, 144-156.

1535 Tang, W., Zhang, Z., Li, J., Li, K., Luo, Z., Chen, Y., 2015. Mesozoic and Cenozoic uplift
1536 and exhumation of the Bogda Mountain, NW China: Evidence from apatite fission track
1537 analysis. Geoscience Frontiers, 6 (4), 617-625.

1538 Tapponnier, P., Zhiqin, X., Roger, F., Meyer, B., Arnaud, N., Wittlinger, G., Jingsui, Y.,
1539 2001. Oblique stepwise rise and growth of the Tibet Plateau. science, 294(5547), 1671-1677.

1540 Thomas, J. C., Cobbold, P. R., Shein, V. S., Le Douaran, S., 1999. Sedimentary record of late
1541 Paleozoic to Recent tectonism in central Asia—analysis of subsurface data from the Turan
1542 and south Kazak domains. Tectonophysics, 313 (3), 243-263.

1543 Van der Voo, R., Levashova, N.M., Skrinnik, L.I., Kara, T.V., Bazhenov, M.L., 2006. Late
1544 orogenic, large-scale rotations in the Tien Shan and adjacent mobile belts in Kyrgyzstan and
1545 Kazakhstan. Tectonophysics 426, 335-360.

1546 Vincent, S. J. and Allen, M. B., 2001. Sedimentary record of Mesozoic intracontinental
1547 deformation in the eastern Junggar Basin, north-west China: response to orogeny at the Asian
1548 margin. In: Hendrix, M. S., Davis, G. A. (Eds) Palaeozoic and Mesozoic Tectonic Evolution
1549 of Central and Eastern Asia: from Continental Assembly to Intracontinental Deformation.
1550 Geological Society of America, Memoirs, 194, 341–360.

1551 VNIGNI and Beicip Franlab., 1992. Petroleum potential of Central Asia, 2 volumes, Beicip
1552 Franlab, Rueil-Malmaison, France.

1553 Wang B., Faure M., Cluzel D., Shu L.S., Charvet J., Meffre S., 2006. Late Paleozoic tectonic
1554 evolution of the northern West Tian Shan, NW China. Geodynamica Acta, 19 (3-4), 237-247.

1555 Wang, B., Chen, Y., Zhan, S., Shu, L., Faure, M., Cluzel, D., Charvet, J., Laurent-Charvet, S.,
1556 2007a. Primary Carboniferous and Permian paleomagnetic results from the Yili Block (NW
1557 China) and their implications on the geodynamic evolution of Chinese Tianshan Belt. Earth
1558 and Planetary Science Letters 263, 288–308.

1559 Wang, B., Shu, L. S., Cluzel, D., Faure, M., Charvet, J., 2007b. Geochemical constraints on
1560 Carboniferous volcanic rocks of the Yili Block (Xinjiang, NW China): Implication for the
1561 tectonic evolution of Western Tianshan. Journal of Asian Earth Sciences 29, 148–159.

1562 Wang B., Cluzel D., Shu L.S., Faure M., Charvet J., Chen Y., Meffre S., De Jong K., 2009.
1563 Evolution of calc-alkaline to alkaline magmatism through Carboniferous convergence to
1564 Permian transcurrent tectonics, western Chinese Tianshan. International Journal of Earth
1565 Science, 98, 1275-1298.

1566 Wang, M., Zhang, J., Liu, K., 2015. Continuous denudation and pediplanation of the Chinese
1567 Western Tianshan orogen during Triassic to Middle Jurassic: Integrated evidence from detrital
1568 zircon age and heavy mineral chemical data. Journal of Asian Earth Sciences, 113 (1), 310-
1569 324.

1570 Wang, S. L., Shu, L. S., Zhu, W. B., Xu, M. J., Lu, H. F., Xiao, Z. Y., Luo, J-C., Zhu, C. J.,
1571 2012. Mesozoic faults in the NE Tarim (western China) and the implications on collisions in
1572 the southern Eurasian margin. Journal of Asian Earth Sciences, 56, 191-199.

1573 Wartes, M.A, Carroll, A.R., Greene, T.D., 2002. Permian sedimentary record of the Turpan-
1574 Hami basin and adjacent regions, northwest China: Constraints on postamalgamation tectonic
1575 evolution. Geological Society of America Bulletin, 114 (2), 131-152.

1576 Watson, M. P., Hayward, A. B., Parkinson, D. N., Zhang, Z. M., 1987. Plate tectonic history,
1577 basin development and petroleum source rock deposition onshore China. Marine and
1578 Petroleum Geology, 4 (3), 205-225.

1579 Wilhem, C., Windley, B. F., Stampfli, G. M., 2012. The Altaids of Central Asia: a tectonic
1580 and evolutionary innovative review. Earth-Science Reviews, 113 (3), 303-341.

1581 Windley, B.F., Alexeiev, D., Xiao, W., Kröner, A., Badarch, G., 2007. Tectonic models for
1582 the accretion of the Central Asion Orogenic Belt. Journal of the Geological Society of
1583 London, 164, 31-47.

1584 Xia, L., Xu, X., Li, X., Ma, Z., Xia, Z., 2012. Reassessment of petrogenesis of Carboniferous–
1585 Early Permian rift-related volcanic rocks in the Chinese Tianshan and its neighboring areas.
1586 Geoscience Frontiers, 3 (4), 445-471.

1587 Xinjiang Bureau of Geology and Mineral Resources (XBGMR), Geological maps of the
1588 Bayanbulak area, scale 1:200,000, Geol. Publ. House, Beijing (1969).

1589 Xinjiang Bureau of Geology and Mineral Resources (XBGMR), Geological maps of the Yaha
1590 area, scale 1:200,000, Geol. Publ. House, Beijing (1970).

1591 Xinjiang Bureau of Geology and Mineral Resources (XBGMR), Geological maps of the
1592 Wusu area, scale 1:200,000, Geol. Publ. House, Beijing (1973a).

1593 Xinjiang Bureau of Geology and Mineral Resources (XBGMR), Geological maps of the
1594 eastern Yili area, scale 1:200,000, Geol. Publ. House, Beijing (1973b).

1595 Xinjiang Bureau of Geology and Mineral Resources (XBGMR), Geological maps of the
1596 Manas area, scale 1:200,000, Geol. Publ. House, Beijing (1978a).

1597 Xinjiang Bureau of Geology and Mineral Resources (XBGMR), Geological maps of the
1598 Urumqi area, scale 1:200,000, Geol. Publ. House, Beijing (1978b)

1599 Yang, W., Jolivet, M., Dupont-Nivet, G., Guo, Z., Zhang, Z., Zhang, Z., 2013. Source to sink
1600 relations between the Tian Shan and Junggar Basin (northwest China) from Late Palaeozoic to
1601 Quaternary: evidence from detrital U-Pb zircon geochronology. Basin Research, 25, 219–240.

1602 Yang, Y.-T., Song, C.-C., He, S., 2015. Jurassic tectonostratigraphic evolution of the Junggar
1603 basin, NW China: A record of Mesozoic intraplate deformation in Central Asia. Tectonics, 34,
1604 86-115.

1605 Yang, Y. T., Guo, Z. X., Luo, Y. J., 2017. Middle-Late Jurassic tectonostratigraphic evolution
1606 of Central Asia, implications for the collision of the Karakoram-Lhasa Block with Asia.
1607 Earth-Science Reviews, 166, 83-110.

1608 Yin, A., 2010. Cenozoic tectonic evolution of Asia: A preliminary synthesis. Tectonophysics,
1609 488 (1-4), 293-325.

1610 Yu, X., Yang, S. F., Chen, H. L., Chen, Z. Q., Li, Z. L., Batt, G. E., Li, Y. Q., 2011. Permian
1611 flood basalts from the Tarim Basin, Northwest China: SHRIMP zircon U–Pb dating and
1612 geochemical characteristics. Gondwana Research 20, 485–497.

1613 Yu, Y., Wang, X., Rao, G., Wang, R., 2016. Mesozoic reactivated transpressional structures
1614 and multi-stage tectonic deformation along the Hong-Che fault zone in the northwestern
1615 Junggar Basin, NW China. Tectonophysics, 679, 156-168.

1616 Yuan, W., Carter, A., Dong, J., Bao, Z., An, Y., Guo, Z., 2006. Mesozoic–Tertiary
1617 exhumation history of the Altai Mountains, northern Xinjiang, China: new constraints from
1618 apatite fission track data. Tectonophysics, 412 (3), 183-193.

Zhang, Z., Guo, Z., Han, Z., 1998. Geochemistry and geological significance of the mid-Jurassic volcanic rocks in Dunhuang Basin. ACTA SCIENTIARUM NATURALIUM-UNIVERSITATIS PEKINENSIS, 34, 72-79.

Zhao, S., Li, S., Liu, X., Suo, Y., Dai, L., Lou, D., Sun, W., Li, T., Wang, X., Yang, Z., 2014. Intracontinental orogenic transition: Insights from structures of the eastern Junggar Basin between the Altay and Tianshan orogens. Journal of Asian Earth Sciences, 88, 137-148.

Zonenshain, L. P., and Pichon, X., 1986. Deep basins of the Black Sea and Caspian Sea as remnants of Mesozoic back-arc basins. Tectonophysics, 123 (1-4), 181-211.

Zorin, Y. A., 1999. Geodynamics of the western part of the Mongolia–Okhotsk collisional belt, Trans-Baikal region (Russia) and Mongolia. Tectonophysics, 306 (1), 33-56.

FIGURES CAPTIONS:

Fig. 1. General topography and tectonic framework of the Tian Shan region. The locations of the sedimentological sections are indicated by red stars and white circles: T-K, Tash-Kumir; J-D, Jetim-Dobo; Te, Terek; Ku, Kuzigongsu; M-K, Ming-Kush; K-S, Kadji-Sai; J-O, Jeti-Oguz; Ya, Yaha; Ba, Bayanbulak; Ni, Nieleke; Wu, Wusu; Ma, Manas; To, Toutunhe (north and south); Ai, Aiwergou; Ke, Kerjan; Ta, Taoshuyan; Ke, Kelameili; Ka, Karamay. TFF, Talas-Fergana fault; DNF = Dzhalair – Naiman Fault; NTSF, North Tian Shan fault. Y-F B, Yarkand-Fergana Basin; Bay. B., Bayanulak Basin.

Fig. 2. Synthesis of the chronostratigraphic charts available for the Jurassic to Early Cretaceous series in the Junggar, Tarim and Fergana basins.

1641 Fig. 3. Pictures illustrating the various Jurassic sedimentary facies of the Tian Shan region.
1642 See Table. 1 for the facies codes and descriptions. Pictures of facies respectively from: F1,
1643 Toutunhe Fm (Wusu section); F2, Xishanyao Fm (Wusu section); F3, Kalemake Fm (Yaha
1644 section); F4, F7 Qigu Fm, (Yaha and South Toutunhe sections); F5, Kalemake Fm (Yaha
1645 section); F6, Kezilenuer Fm (Yaha section)

1646 Fig. 4. Pictures illustrating the various Jurassic sedimentary facies of the Tian Shan region.
1647 See Table. 1 for the facies codes and descriptions. Pictures of facies respectively from: F7,
1648 Qigu Fm (Yaha section), F8, Qigu Fm (South Toutunhe section) F9, respectively from
1649 Yengisar Fm (Yaha section), Toutunhe Fm (Nieleke section); F4, F10, Kalaza Fm (South
1650 Toutunhe section); F11, Kalaza Fm (Yaha section); F12, Kalaza Fm (Manas section); F13,
1651 Xishanyao Fm (Wusu section).

1652 Fig. 5. Pictures illustrating the various Jurassic pedogenic and alteration features encountered
1653 within the Tian Shan region. See Table. 2 for facies codes and descriptions. Pictures of
1654 pedogenic features respectively from: P1, Yengisar Fm (Yaha section); P2, Kalaza Fm
1655 (Manas section), P3, Qigu Fm (Wusu section); P4, Qigu Fm (Wusu and Yaha sections); P5
1656 (Bayanbulak section)

1657 Fig. 6. Sedimentary log of the South Toutunhe section in the south Junggar Basin. Associated
1658 facies assemblages and their interpretation in term of depositional environments as in Table.
1659 3.

1660 Fig. 6 bis. Graphical caption presenting the various symbols used in Figs 6-12.

1661 Fig. 7. Sedimentary log of the North Toutunhe section in the south Junggar Basin. Symbols as
1662 in Fig. 6. Associated facies assemblages and their interpretation in term of depositional
1663 environments as in Table. 3.

Fig. 8. Sedimentary log of the Manas section in the south Junggar Basin. Symbols as in Fig. 6. Associated facies assemblages and their interpretation in term of depositional environments as in Table. 3.

Fig. 9. Sedimentary log of the Wusu section in the south Junggar Basin. Symbols as in Fig. 6. Associated facies assemblages and their interpretation in term of depositional environments as in Table. 3.

Fig. 10. Sedimentary log of the Nieleke section in the Yili Basin. Symbols as in Fig. 6. Associated facies assemblages and their interpretation in term of depositional environments as in Table. 3.

Fig. 11. Sedimentary log of the Bayanbulak section in the Bayanbulak Basin. Symbols as in Fig. 6. Associated facies assemblages and their interpretation in term of depositional environments as in Table. 3.

Fig. 12. Sedimentary log of the Yaha section in the north Tarim Basin. Symbols as in Fig. 6. Associated facies assemblages and their interpretation in term of depositional environments as in Table. 3.

Fig. 13. Early – early Middle Jurassic paleogeography of the Tian Shan region atop of the present-day topography; AB: Aksai Basin; BB: Bayanbulak Basin; FB: Fergana Basin; IB: Issyk-Kul Basin; MB: Ming Kush Basin; NB: Naryn Basin; TB: Turfan Basin; YB: Yili Basin; YFB; Yarkand-Fergana Basin; ZB: Zahosu Basin.

Fig. 14. Late Middle – early Late Jurassic paleogeography of the Tian Shan region atop of the present-day topography; AB: Aksai Basin; BB: Bayanbulak Basin; FB: Fergana Basin; IB: Issyk-Kul Basin; MB: Ming Kush Basin; NB: Naryn Basin; TB: Turfan Basin; YB: Yili Basin; YFB; Yarkand-Fergana Basin; ZB: Zahosu Basin.

Fig. 15. Late Jurassic – Early Cretaceous paleogeography of the Tian Shan region atop of the present-day topography; AB: Aksai Basin; BB: Bayanbulak Basin; FB: Fergana Basin; IB: Issyk-Kul Basin; MB: Ming Kush Basin; NB: Naryn Basin; TB: Turfan Basin; YB: Yili Basin; YFB; Yarkand-Fergana Basin; ZB: Zahosu Basin.

Fig. 16. Synthetic chart of the Tian Shan region: stratigraphic record, thermochronology (Thermo.), topography, climate and geodynamic events.

Fig. 17. A. Late Early to Middle Jurassic paleogeography of the Asian continent (modified from Jolivet, 2017c); EU, European Craton; CIB, GCB; Great Caucasian Basin; SCB, South Caspian Basin; Central Iran Blocks; LH, Lhasa Block; QI, Qiangtang Block; SG, Songpan-Garzê prism; Q, Qaidam Block; Mon, Mongolian Block; NC, North China Block; SC, South China Block; IND, Indochina Block; SIB, Sibumasu Block; WB, West Burma Block; TFF, Talas Fergana fault. B. Late Early to Middle Jurassic kinematic framework of the west Central Asia region. Regional Jurassic basins and main depocenters were derived from these studies; Lee (1985a, b); Thomas et al., (1999); Sobel et al., (1999); Fedorenko and Miletenko. (2002); Alexeiev et al., (2017). Tectonic structures were compiled from VNIGNI and Beicip Franlab., (1992); Thomas et al., (1999); Wang et al., (2012); Robert et al., (2014); Yang et al., (2015); Brunet et al., (2017). The location and the geometry of the subduction zone were derived from Brunet et al., (2017). ST: South Turgay Basin; LT: Leontiev Basin; YF: Yarkand Fergana Basin; B: Bayanbulak Basin; T: Turfan Basin; TFF: Talas Fergana/Karatau fault; NTSF: North Tian Shan fault; ATF: Altyn Tagh fault; 1, Paleotethys suture; 2, Turkestan suture; 3, Jinsha suture; 4, Kunlun suture.

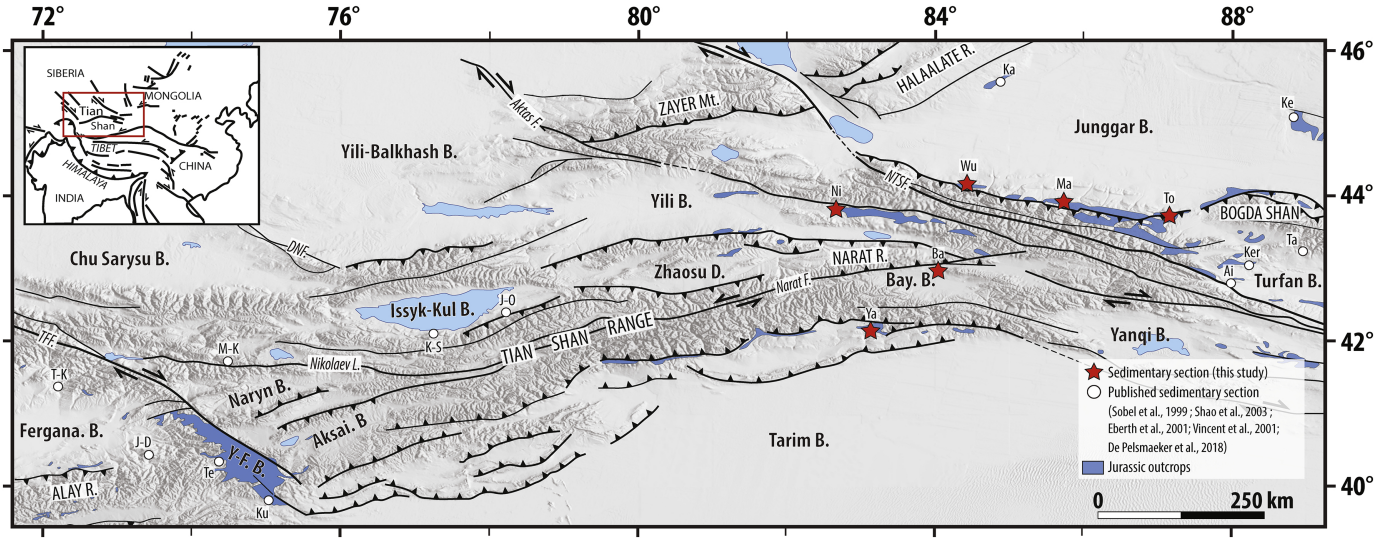
72°
76°
80°
84°
88°
46°
44°
42°
40°
SIBERIA
MONGOLIA
Tian
Shan
TIBET
HIMALAYA
CHINA
INDIA
Yili-Balkhash B.
Chu Sarysu B.
Issyk-Kul B.
Fergana. B.
ALAY R.
Naryn B.
Aksai. B
Y-F. B.
Tarim B.
Yanqi B.
Turfan B.
Bay. B.
Zhaosu D.
Yili B.
Junggar B.
BOGDA SHAN
ZAYER Mt.
HALAALATE R.
NARAT R.
TIAN—SHAN—RANGE
Aktash F.
DNF
TFF
Nikolaev L.
Narat F.
NTSF
Ka
Ke
Wu
Ma
To
Ni
Ba
Ya
Ta
Ker
Ai
M-K
T-K
K-S
J-O
J-D
Te
Ku
Sedimentary section (this study)
Published sedimentary section
(Sobel et al., 1999 ; Shao et al., 2003 ; Eberth et al., 2001; Vincent et al., 2001; De Pelsmaeker et al., 2018)
Jurassic outcrops
0
250 km

Figure 1

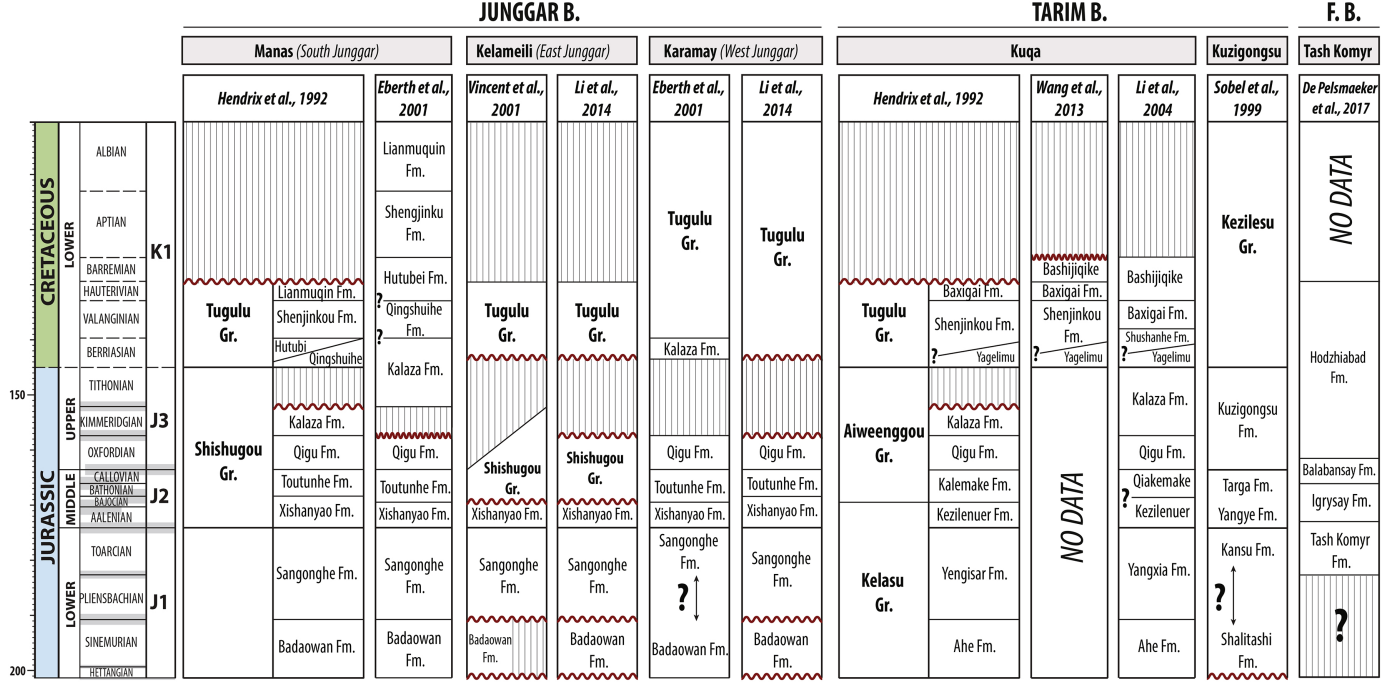
JUNGGAR B.
TARIM B.
F. B.
Manas (South Junggar)
Kelameili (East Junggar)
Karamay (West Junggar)
Kuqa
Kuzigongsu
Tash Komyr
Hendrix et al., 1992
Eberth et al., 2001
Vincent et al., 2001
Li et al., 2014
Hendrix et al., 1992
Wang et al., 2013
Li et al., 2004
Sobel et al., 1999
De Pelsmaeker et al., 2017
CRETACEOUS
JURASSIC
LOWER
UPPER
MIDDLE
LOWER
ALBIAN
APTIAN
BARREMIAN
HAUTERIVIAN
VALANGINIAN
BERRIASIAN
TITHONIAN
KIMMERIDGIAN
OXFORDIAN
CALLOVIAN
BATHONIAN
BAJOCIAN
AALENIAN
TOARCIAN
PLIENSBACHIAN
SINEMURIAN
HETTANGIAN
K1
J3
J2
J1
150
200
Tugulu Gr.
Lianmuqin Fm.
Shenjinkou Fm.
Hutubi
Qingshuihe
Shishugou Gr.
Kalaza Fm.
Qigu Fm.
Toutunhe Fm.
Xishanyao Fm.
Sangonghe Fm.
Badaowan Fm.
Lianmuquin Fm.
Shengjinku Fm.
Hutubei Fm.
Qingshuihe Fm.
Kalaza Fm.
Qigu Fm.
Toutunhe Fm.
Xishanyao Fm.
Sangonghe Fm.
Badaowan Fm.
Tugulu Gr.
Shishugou Gr.
Xishanyao Fm.
Sangonghe Fm.
Badaowan Fm.
Badaowan Fm.
Tugulu Gr.
Shishugou Gr.
Xishanyao Fm.
Sangonghe Fm.
Badaowan Fm.
Tugulu Gr.
Kalaza Fm.
Qigu Fm.
Toutunhe Fm.
Xishanyao Fm.
Sangonghe Fm.
?
Badaowan Fm.
Tugulu Gr.
Qigu Fm.
Toutunhe Fm.
Xishanyao Fm.
Sangonghe Fm.
Badaowan Fm.
Tugulu Gr.
Baxigai Fm.
Shenjinkou Fm.
?
Yagelimu
Aiweenggou Gr.
Kalaza Fm.
Qigu Fm.
Kalemake Fm.
Kezilenuer Fm.
Kelasu Gr.
Yengisar Fm.
Ahe Fm.
Bashijiqike
Baxigai Fm.
Shenjinkou Fm.
?
Yagelimu
NO DATA
Bashijiqike
Baxigai Fm.
Shushanhe Fm.
?
Yagelimu
Kalaza Fm.
Qigu Fm.
Qiakemake
?
Kezilenuer
Yangxia Fm.
Ahe Fm.
Kezilesu Gr.
Kuzigongsu Fm.
Targa Fm.
Yangye Fm.
Kansu Fm.
?
Shalitashi Fm.
NO DATA
Hodzhiabad Fm.
Balabansay Fm.
Igrysay Fm.
Tash Komyr Fm.
?

Figure 2

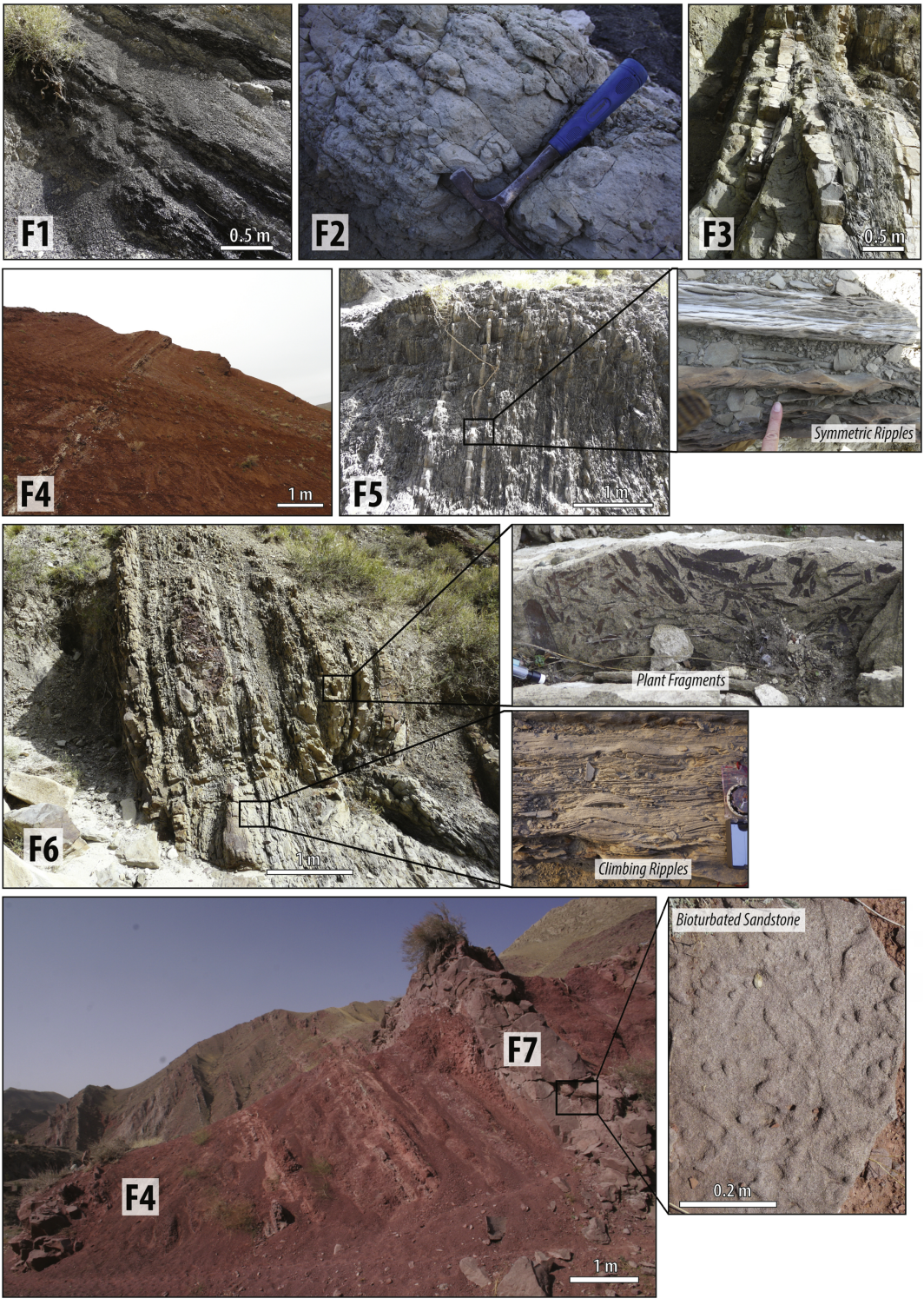
F1
0.5 m
F2
F3
0.5 m
F4
1 m
F5
1 m
Symmetric Ripples
F6
1 m
Plant Fragments
Climbing Ripples
F7
F4
1 m
Bioturbated Sandstone
0.2 m

Figure 3

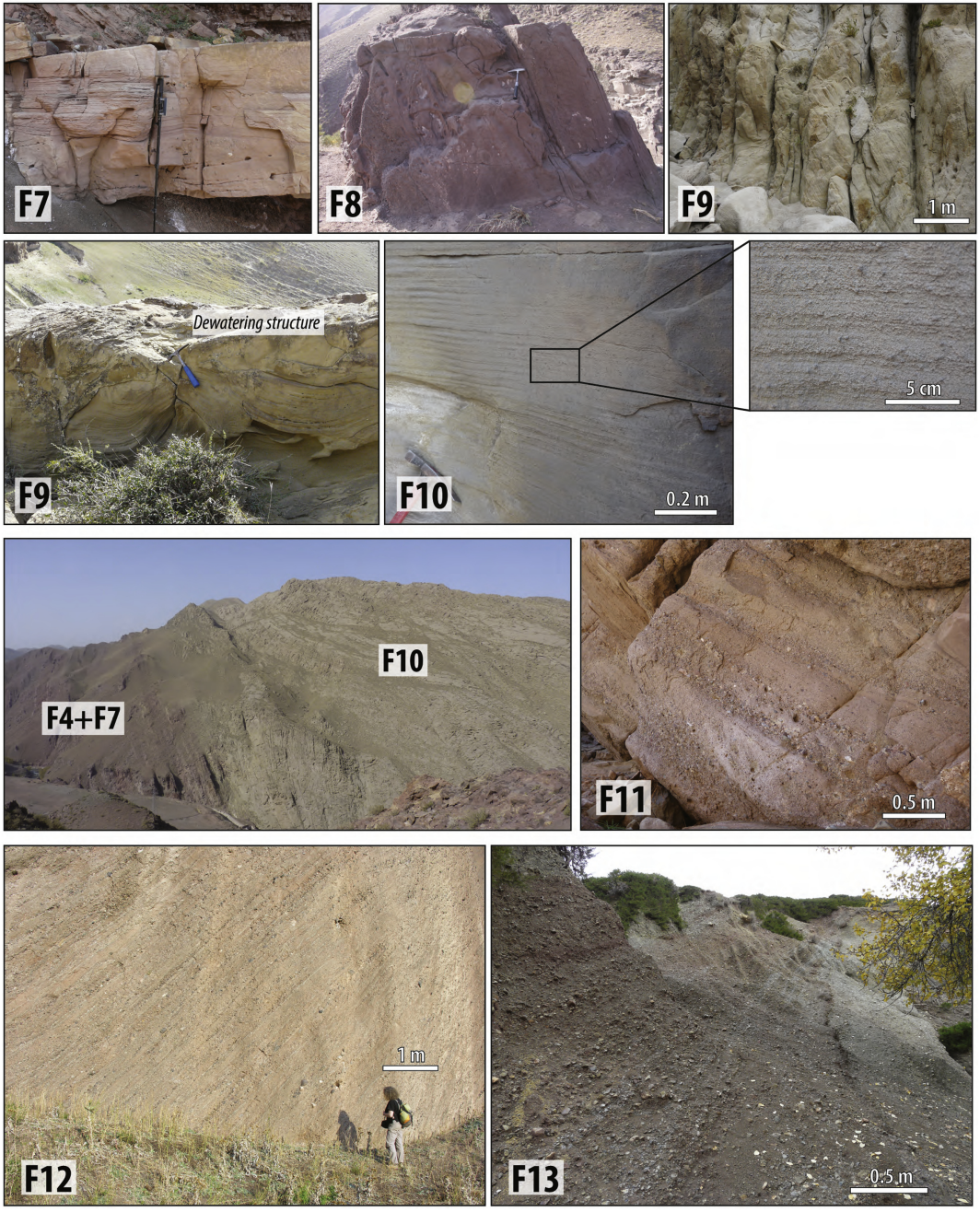
F7
F8
F9
1 m
Dewatering structure
F9
F10
0.2 m
5 cm
F4+F7
F10
F11
0.5 m
F12
1 m
F13
0.5 m

Figure 4

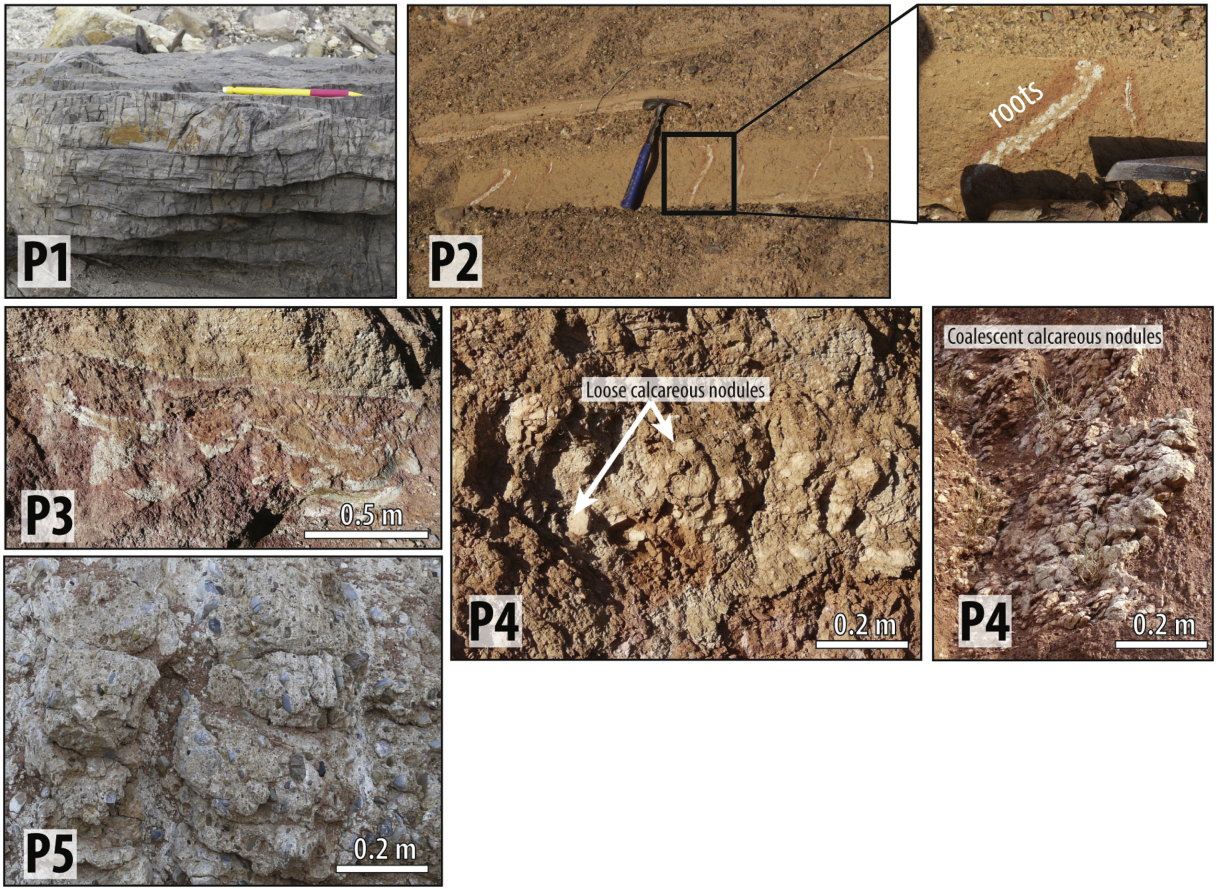
P1
P2
roots
P3
0.5 m
Loose calcareous nodules
P4
0.2 m
Coalescent calcareous nodules
P4
0.2 m
P5
0.2 m

Figure 5

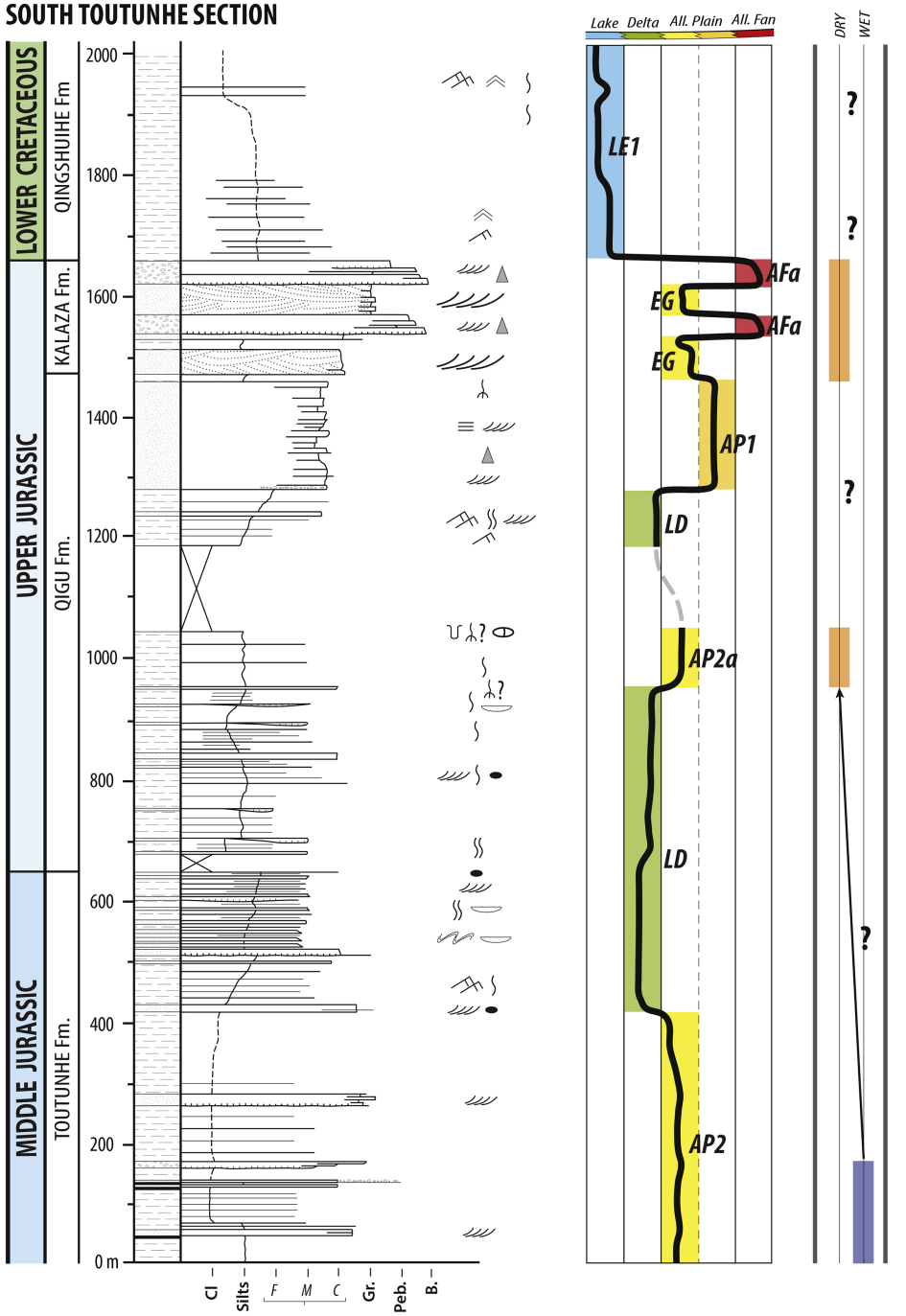

BEDDINGS

- Current ripples
- Climbing ripples
- 2D megaripples
- 3D megaripples
- flat laminations
- Wave features
- Aeolian 3D megaripples

BIOTURBATIONS

- Horizontal burrows
- Vertical burrows
- Pervasive Bioturbation (intensity)
- Shell remains?

SYMBOLS

- Plant fragments
- Root traces
- Rip-up clasts
- Lenses or channels
- Amalgamated lenses / channels
- Normal grading
- Flute cast
- Dessication cracks
- Slumps
- Tuffs
- Carbonated nodules
- Dewatering structures

LITHOLOGY

- Conglomerate
- Sandstone
- Aeolian sandstone
- Siltstone
- Siltstone (grey/black)
- Coal-rich layer

BASAL BOUNDARIES

- Slightly erosional basal boundary
- Strongly erosional basal boundary

Figure 6

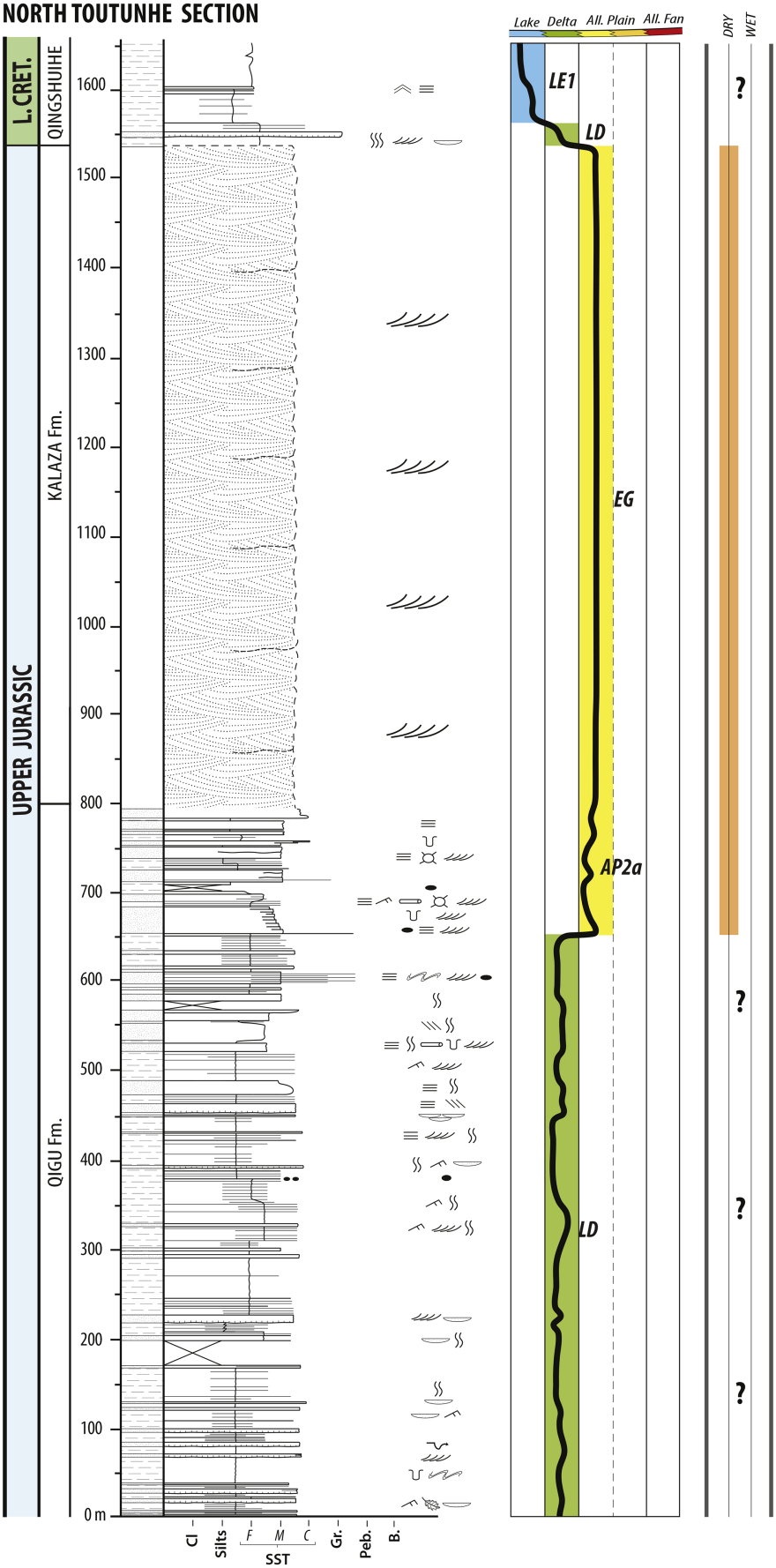
NORTH TOUTUNHE SECTION
L. CRET.
QINGSHUIHE
UPPER JURASSIC
KALAZA Fm.
QIGU Fm.
1600
1500
1400
1300
1200
1100
1000
900
800
700
600
500
400
300
200
100
0 m
Cl
Silts
F
M
C
SST
Gr.
Peb.
B.
Lake
Delta
All. Plain
All. Fan
LE1
LD
EG
AP2a
LD
DRY
WET
?
?
?
?

Figure 7

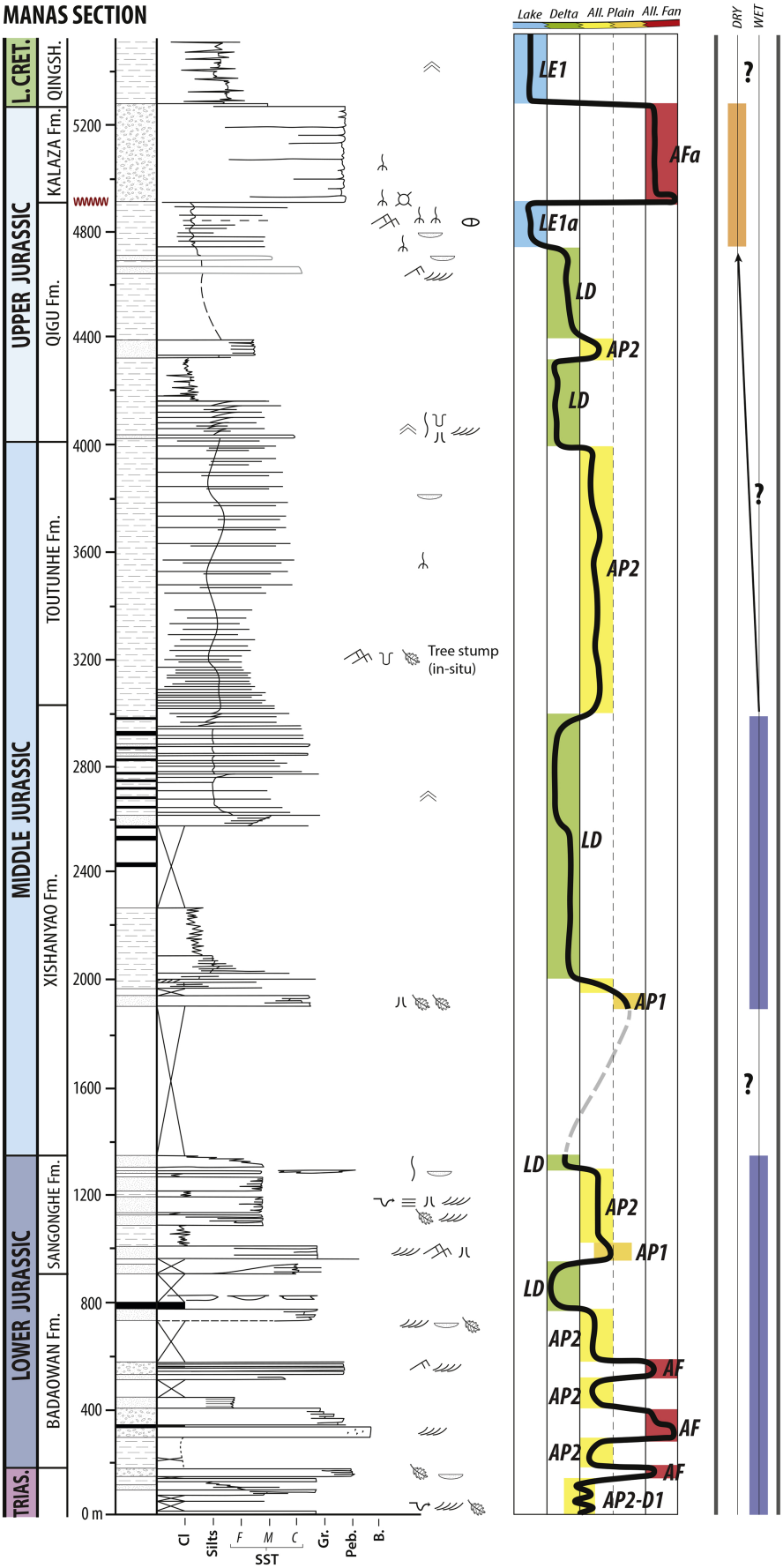
MANAS SECTION
L. CRET.
UPPER JURASSIC
MIDDLE JURASSIC
LOWER JURASSIC
TRIAS.
QINGSH.
KALAZA Fm.
QIGU Fm.
TOUTUNHE Fm.
XISHANYAO Fm.
SANGONGHE Fm.
BADAOWAN Fm.
5200
4800
4400
4000
3600
3200
2800
2400
2000
1600
1200
800
400
0 m
Tree stump
(in-situ)
Cl
Silts
F
M
C
SST
Gr.
Peb.
B.
Lake
Delta
All. Plain
All. Fan
LE1
AFa
LE1a
LD
AP2
LD
AP2
LD
AP1
LD
AP2
AP1
LD
AP2
AF
AP2
AF
AP2
AF
AP2-D1
DRY
WET
?
?
?

Figure 8

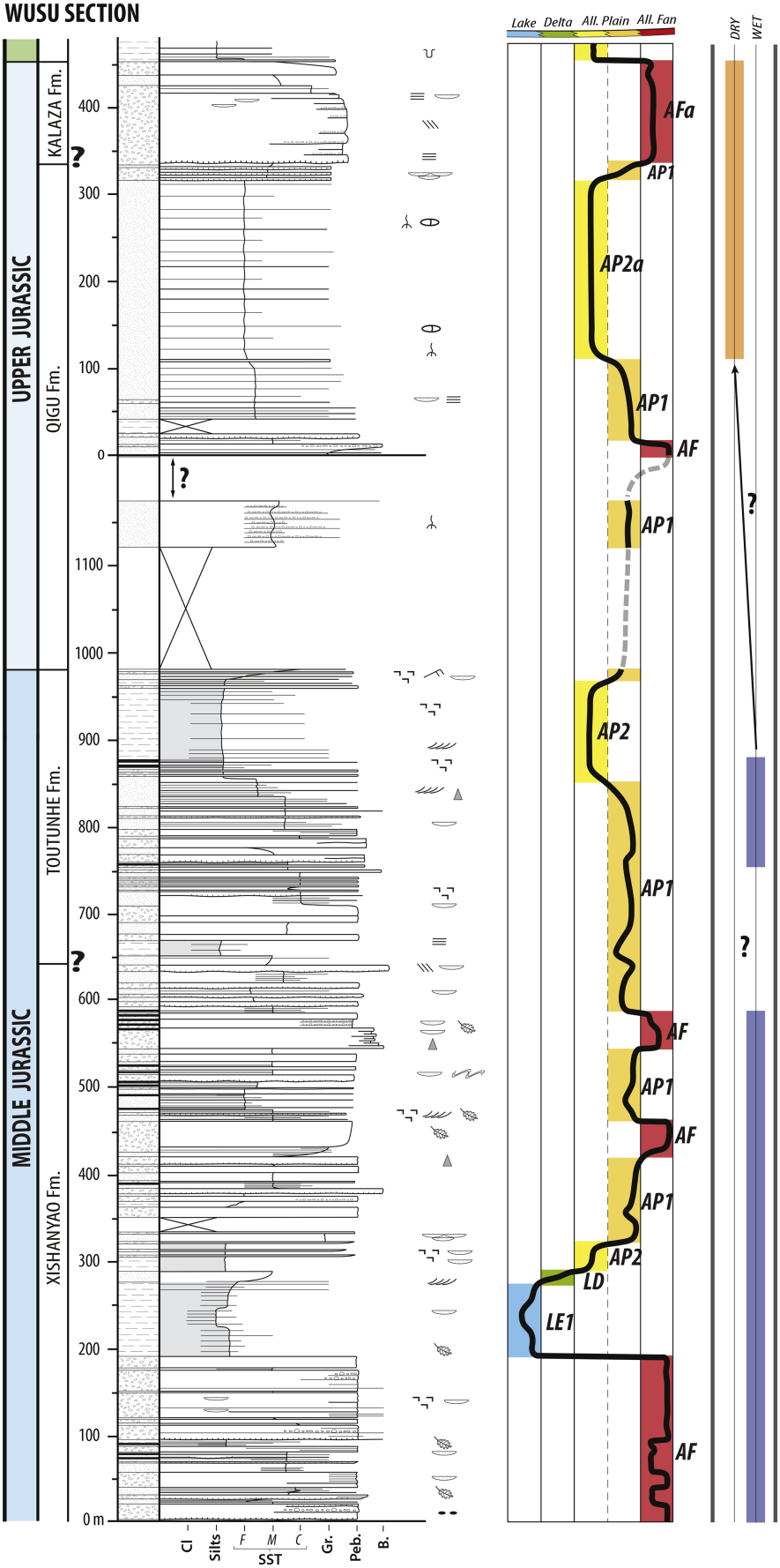
WUSU SECTION
UPPER JURASSIC
MIDDLE JURASSIC
KALAZA Fm.
QIGU Fm.
TOUTUNHE Fm.
XISHANYAO Fm.
0 m
100
200
300
400
?
0
?
1000
1100
900
800
700
?
600
500
400
300
200
100
Cl
Silts
F
M
C
SST
Gr.
Peb.
B.
Lake
Delta
All. Plain
All. Fan
AFa
AP1
AP2a
AP1
AF
AP1
AP2
AP1
AF
AP1
AF
AP1
AP2
LD
LE1
AF
DRY
WET
?
?

Figure 9

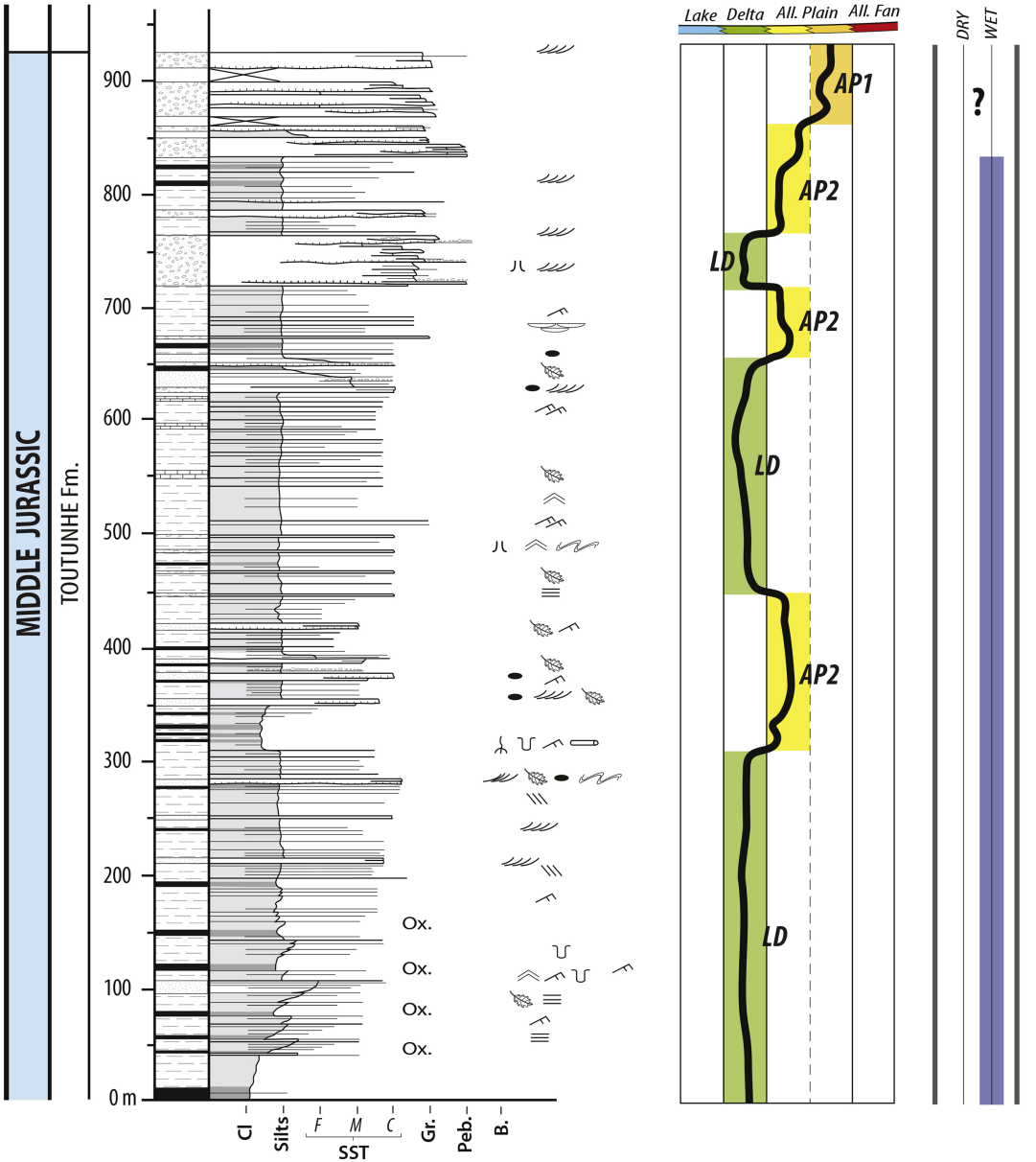
NIELEKE SECTION
MIDDLE JURASSIC
TOUTUNHE Fm.
900
800
700
600
500
400
300
200
100
0 m
Ox.
Ox.
Ox.
Ox.
Cl
Silts
F
M
C
SST
Gr.
Peb.
B.
Lake
Delta
All. Plain
All. Fan
AP1
AP2
LD
AP2
LD
AP2
LD
DRY
WET
?

Figure 10

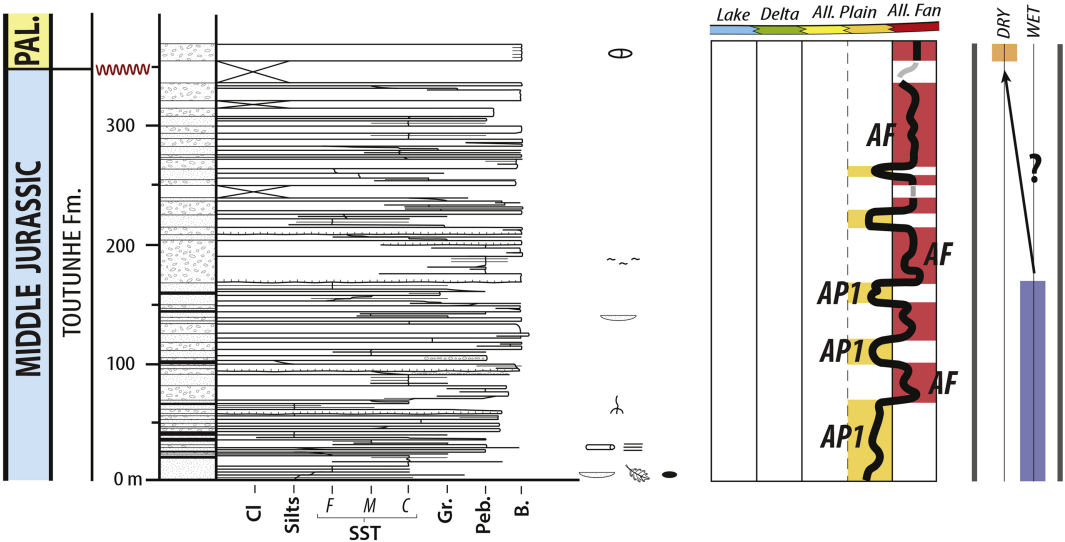
BAYANBULAK SECTION
PAL.
MIDDLE JURASSIC
TOUTUNHE Fm.
300
200
100
0 m
Cl
Silts
F
M
C
SST
Gr.
Peb.
B.
Lake
Delta
All. Plain
All. Fan
AF
AF
AP1
AP1
AF
AP1
DRY
WET
?

Figure 11

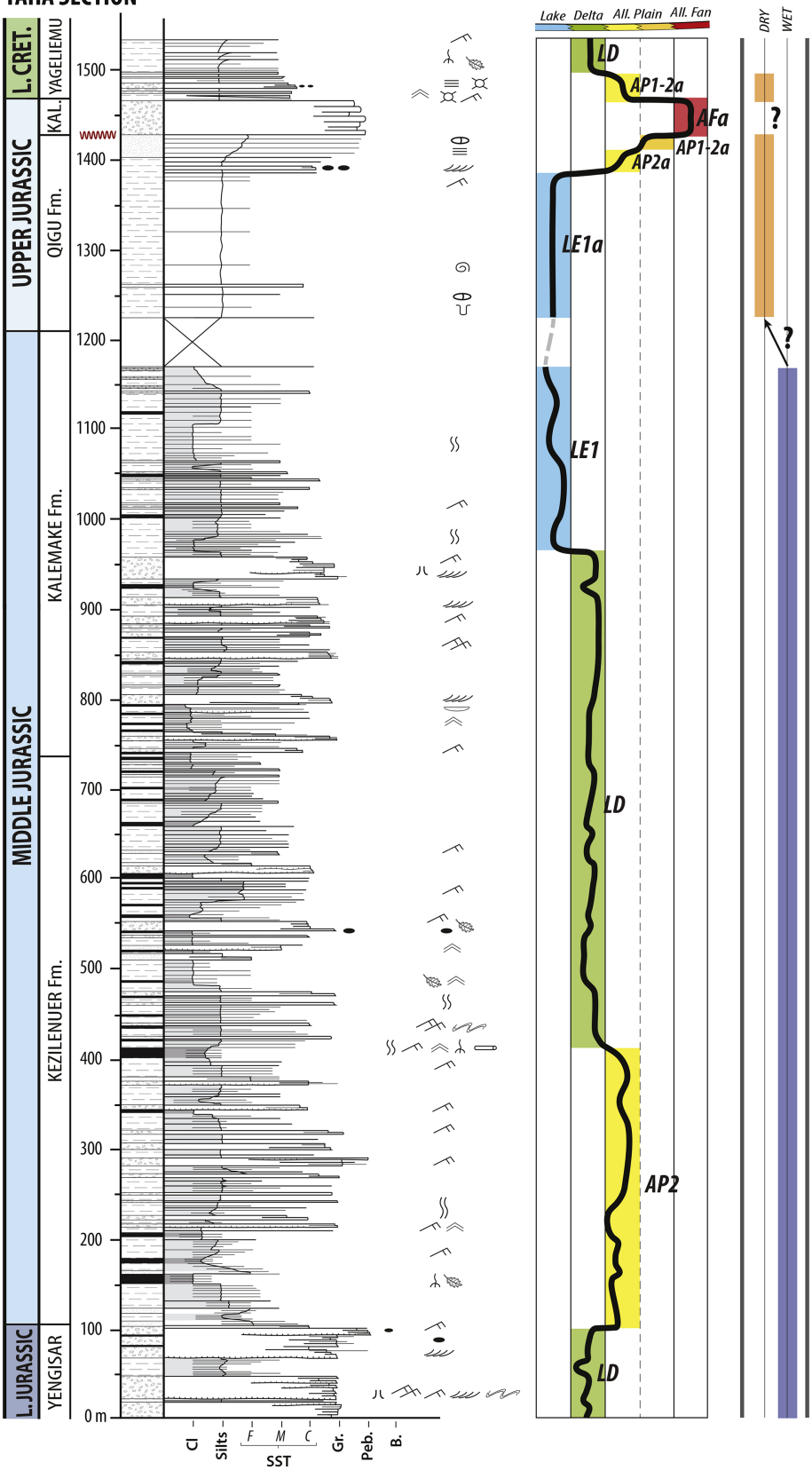
YAHA SECTION
L. CRET.
UPPER JURASSIC
MIDDLE JURASSIC
L. JURASSIC
YAGELIEMU
KAL.
QIGU Fm.
KALEMAKE Fm.
KEZILENUER Fm.
YENGISAR
1500
1400
1300
1200
1100
1000
900
800
700
600
500
400
300
200
100
0 m
Cl
Silts
F M C
SST
Gr.
Peb.
B.
Lake Delta All. Plain All. Fan
LD
AP1-2a
AFa
AP1-2a
AP2a
LE1a
LE1
LD
AP2
LD
DRY
WET
?
?

Figure 12

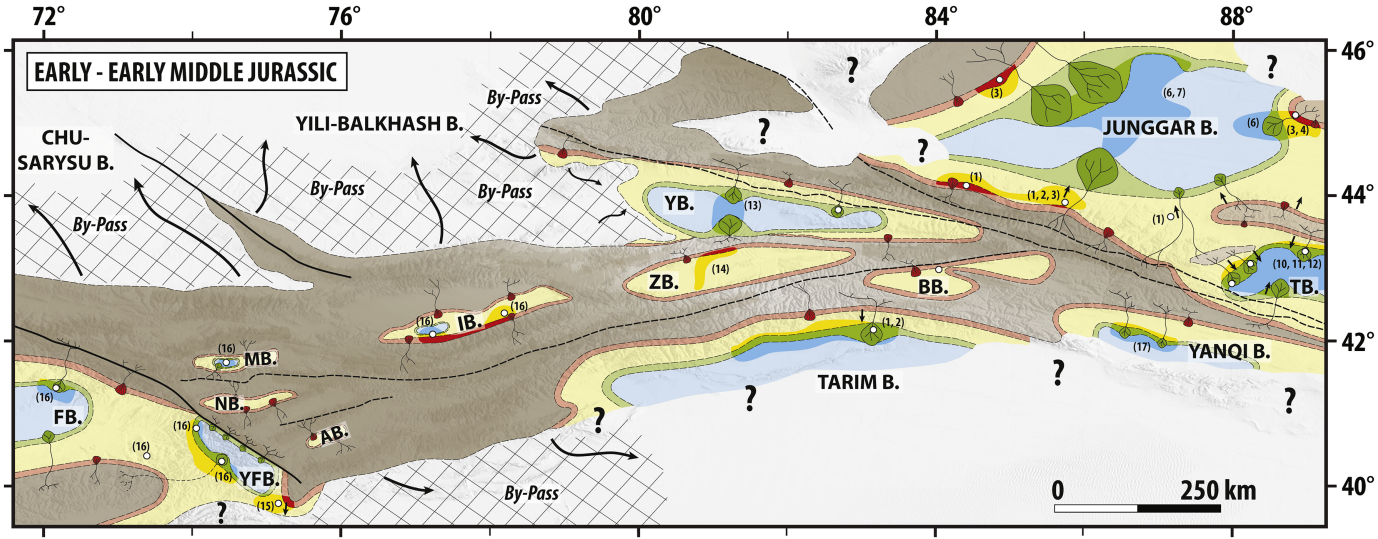

(1) This study ; (2) Hendrix et al., 1992; (3) Eberth et al., 2001; (4) Vincent et al., 2001; (5) Jolivet et al., 2017; (6) Feng et al., 2015; (7) Yang et al., 2015; (8) Lianhua et al., 2009; (9) Gao et al., 2017; (10) Shao et al., 1999; (11) Greene et al., 2001; (12) Shao et al., 2003; (13) Li et al., 2014; (14) Li et al., 2015; (15) Sobel et al., 1999; (16) De Pelsmaeker et al., 2018; (17) Al-Qaraafi and Guangqing, 2013

Environments

Constraint
- \+ *Alluvial fan*
- \+ *Alluvial plain*
- \+ *Lacustrine delta*
- \+ *Lake*

Aeolian dunes

Amplitude
- \+ *Relief*

By-pass area

Volcanism

Structures

Inferred active fault

Fault (undetermined)

Sedimentary section

Potential sediment transport direction

Paleocurrents

Figure 13

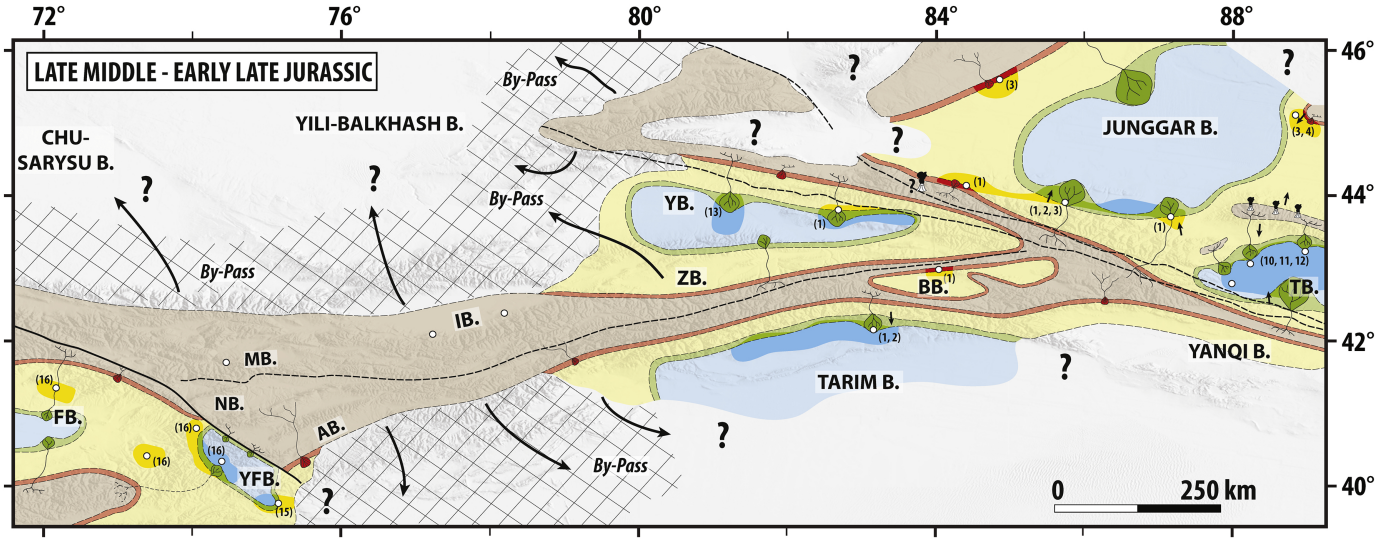

(1) This study ; (2) Hendrix et al., 1992; (3) Eberth et al., 2001; (4) Vincent et al., 2001; (5) Jolivet et al., 2017; (6) Feng et al., 2015; (7) Yang et al., 2015; (8) Lianhua et al., 2009; (9) Gao et al., 2017; (10) Shao et al., 1999; (11) Greene et al., 2001; (12) Shao et al., 2003; (13) Li et al., 2014; (14) Li et al., 2015; (15) Sobel et al., 1999; (16) De Pelsmaeker et al., 2018; (17) Al-Qaraafi and Guangqing, 2013

Environments

Constraint
- \+ Alluvial fan
- \+ Alluvial plain
- \+ Lacustrine delta
- \+ Lake
- Aeolian dunes

Amplitude
- \+ Relief
- By-pass area
- Volcanism

Structures

- Inferred active fault
- Fault (undetermined)
- Sedimentary section
- Potential sediment transport direction
- Paleocurrents

Figure 14

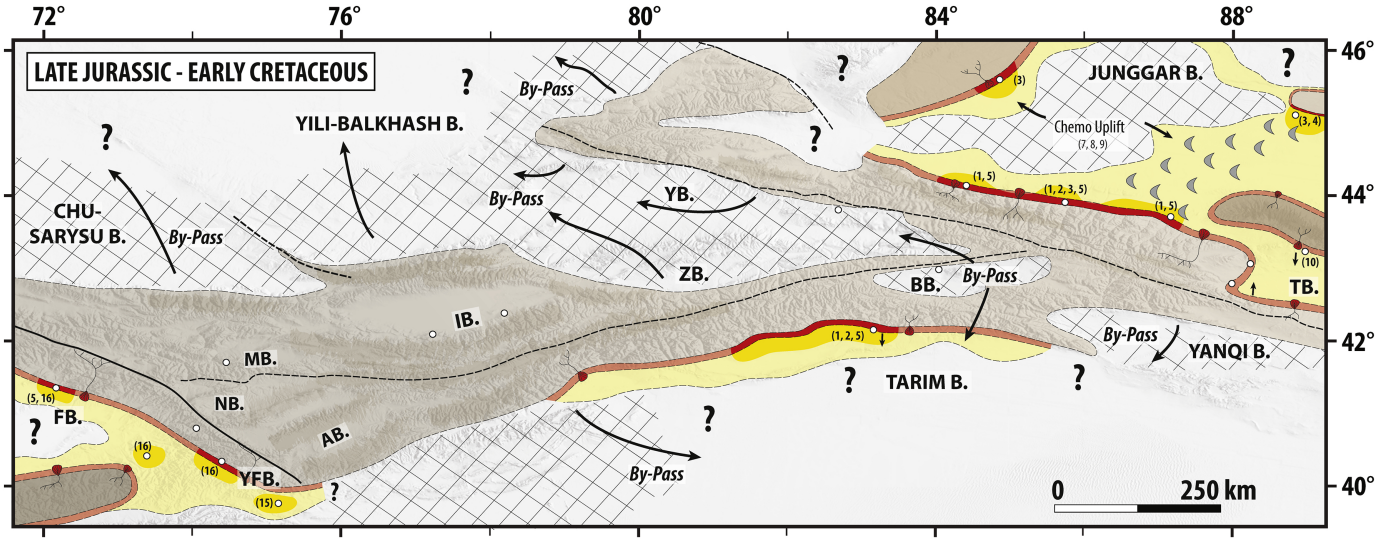

(1) This study ; (2) Hendrix et al., 1992; (3) Eberth et al., 2001; (4) Vincent et al., 2001; (5) Jolivet et al., 2017; (6) Feng et al., 2015; (7) Yang et al., 2015; (8) Lianhua et al., 2009; (9) Gao et al., 2017; (10) Shao et al., 1999; (11) Greene et al., 2001; (12) Shao et al., 2003; (13) Li et al., 2014; (14) Li et al., 2015; (15) Sobel et al., 1999; (16) De Pelsmaeker et al., 2018; (17) Al-Qaraafi and Guangqing, 2013

Environments

Constraint
- \+ Alluvial fan
- \+ Alluvial plain
- \+ Lacustrine delta
- \+ Lake
- Aeolian dunes

Amplitude
- \+ Relief
- By-pass area
- Volcanism

Structures

- Inferred active fault
- Fault (undetermined)
- Sedimentary section
- Potential sediment transport direction
- Paleocurrents

Figure 15

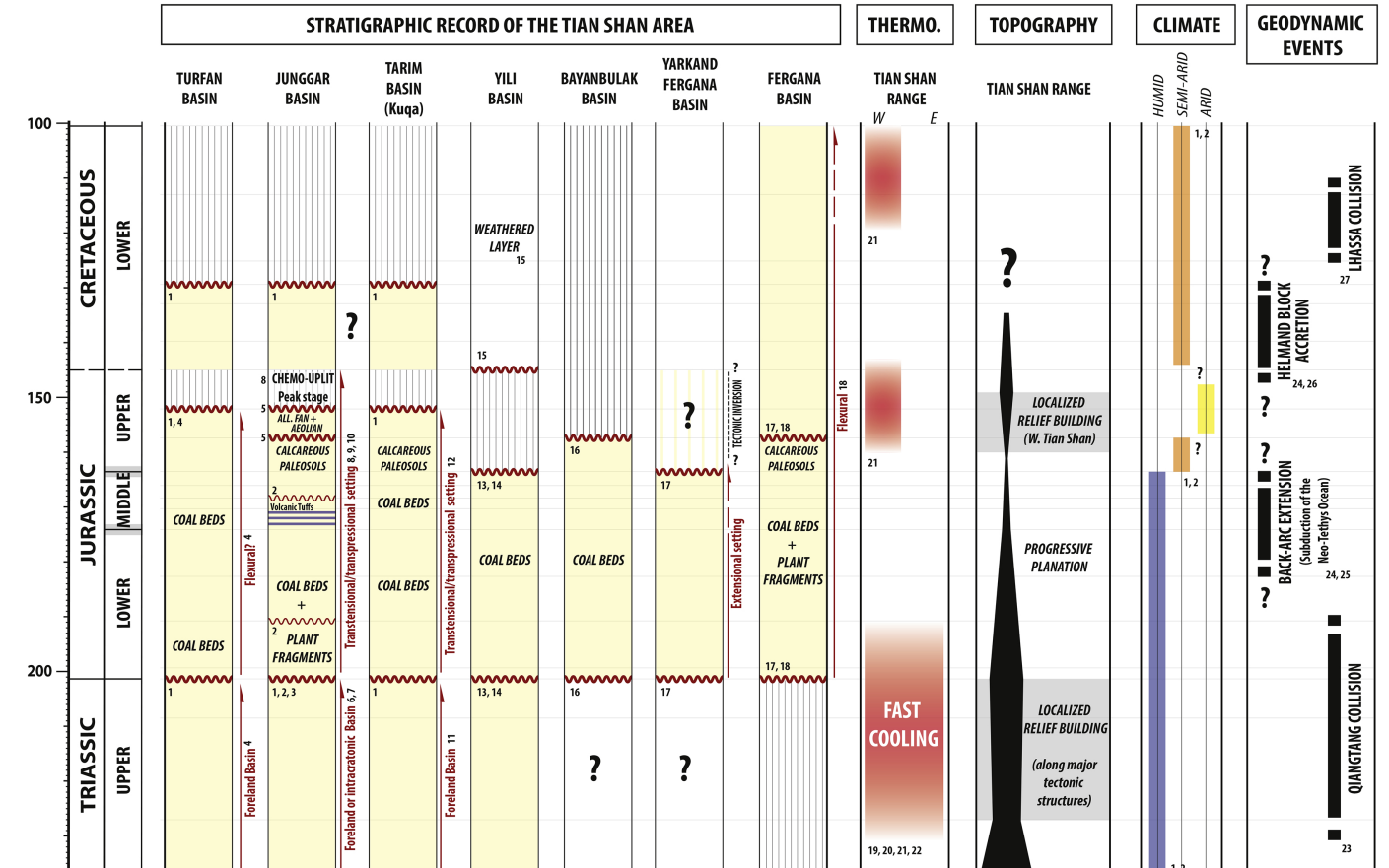

1) Hendrix et al., 1992
2) Eberth et al., 2001
3) Vincent et al., 2001
4) Shao et al., 1999
5) Yang et al., 2015
6) Bian et al., 2010
7) Yang et al., 2013
8) Lianhua et al., 2009
9) Wang et al., 2013
10) Yu et al., 2016
11) Desheng et al., 1996
12) Wang et al., 2012
13) Li et al., 2014
14) Li et al., 2015
15) VNIGNI and Beicip Franlab, 1992
16) XBGMR, 1969
17) De Pelsmaeker et al., 2017
18) Clarke, 1984
19) Dumitru et al., 2001
20) Jolivet et al., 2010
21) Glorie and De Grave, 2016
22) Macaulay et al., 2014
23) Roger et al., 2010
24) Brunet et al., 2017
25) Zonenshain and Le Pichon, 1986
26) Thomas et al., 1999
27) Kapp et al., 2007

Figure 16

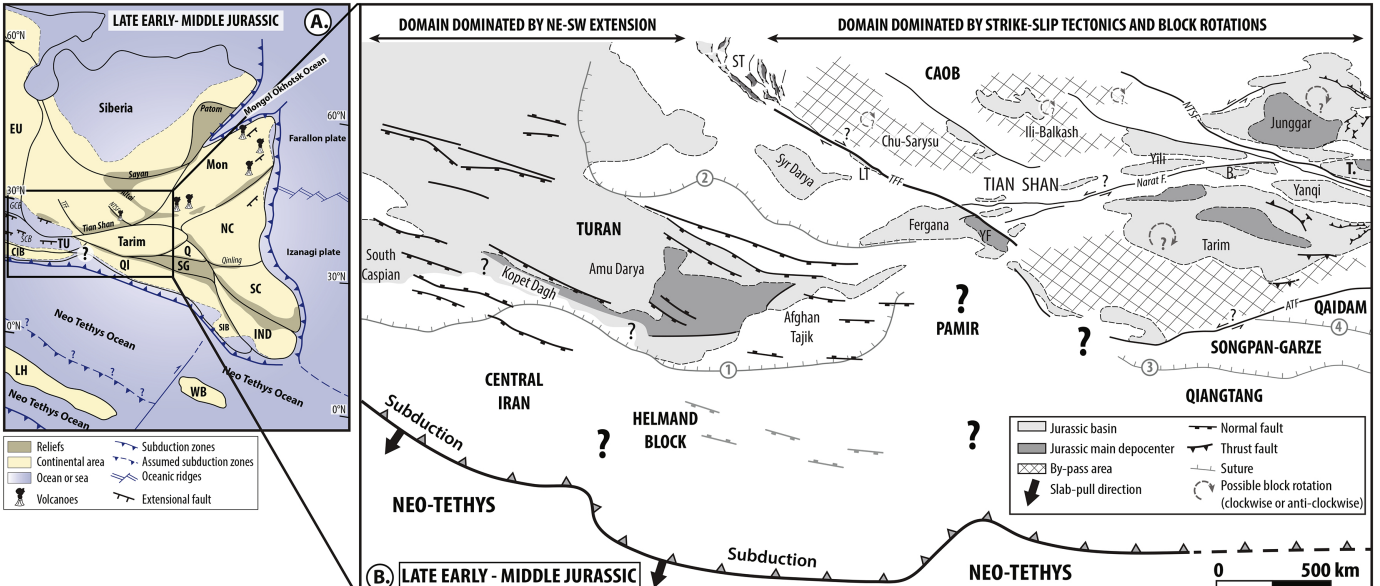
A.
LATE EARLY- MIDDLE JURASSIC
60°N
30°N
0°N
EU
Siberia
Putom
Mongol Okhotsk Ocean
Farallon plate
Sayan
Altay
Mon
Tian Shan
GCB
CIB
TU
Tarim
NC
Q
Qilian
QI
SG
Izanagi plate
SC
SIB
IND
Neo Tethys Ocean
LH
WB
Reliefs
Continental area
Ocean or sea
Volcanoes
Subduction zones
Assumed subduction zones
Oceanic ridges
Extensional fault
DOMAIN DOMINATED BY NE-SW EXTENSION
DOMAIN DOMINATED BY STRIKE-SLIP TECTONICS AND BLOCK ROTATIONS
ST
CAOB
Chu-Sarysu
Ili-Balkash
Junggar
Syr Darya
LT
TFF
TIAN SHAN
Yili
B.
T.
Yanqi
Narat F.
Fergana
YF
Tarim
TURAN
Amu Darya
South Caspian
Kopet Dagh
Afghan Tajik
PAMIR
ATF
QAIDAM
SONGPAN-GARZE
QIANGTANG
CENTRAL IRAN
HELMAND BLOCK
Subduction
NEO-TETHYS
Subduction
NEO-TETHYS
B.
LATE EARLY - MIDDLE JURASSIC
Jurassic basin
Jurassic main depocenter
By-pass area
Slab-pull direction
Normal fault
Thrust fault
Suture
Possible block rotation (clockwise or anti-clockwise)
0
500 km

Figure 17